NUMERICAL AND EXPERIMENTAL INVESTIGATION ON THE EFFECT OF TURBOPROP ENGINE EXHAUST GAS IMPINGEMENT ON PROPELLER AND AIRCRAFT SURFACES

Thesis

Submitted in partial fulfilment of the requirements for the degree of

DOCTOR OF PHILOSOPHY

by

VINAY C A

DEPARTMENT OF MECHANICAL ENGINEERING

NATIONAL INSTITUTE OF TECHNOLOGY KARNATAKA,

SURATHKAL, MANGALORE -575025

July 2023

NUMERICAL AND EXPERIMENTAL INVESTIGATION ON THE EFFECT OF TURBOPROP ENGINE EXHAUST GAS IMPINGEMENT ON PROPELLER AND AIRCRAFT SURFACES

Thesis

Submitted in partial fulfilment of the requirements for the degree of

DOCTOR OF PHILOSOPHY

by

VINAY C A

(197ME509)

Under the guidance of

Dr. KUMAR G. N.

DEPARTMENT OF MECHANICAL ENGINEERING

NATIONAL INSTITUTE OF TECHNOLOGY KARNATAKA,

SURATHKAL, MANGALORE -575025

July 2023

DECLARATION

I hereby *declare* that the Research Thesis entitled "**Numerical and experimental investigation on the effect of turboprop engine exhaust gas impingement on propeller and aircraft surfaces**" which is being submitted to the National Institute of Technology Karnataka, Surathkal in partial fulfillment of the requirements for the award of the Degree of **Doctor of Philosophy** in "Department of Mechanical Engineering" is a *bonafide report of the research work carried out by me*. The material contained in this Research Thesis has not been submitted to any University or Institution for the award of any degree.

Registration Number : 197526ME509

Name : VINAY C A

Signature :

Department of Mechanical Engineering

Place: NITK-Surathkal

Date:

CERTIFICATE

This is to *certify* that the Research Thesis entitled "**Numerical and experimental investigation on the effect of turboprop engine exhaust gas impingement on propeller and aircraft surfaces**" submitted by **Vinay C A, (Register Number: 197526ME509)** as the record of the research work carried out by him, *is accepted as the Research Thesis submission* in partial fulfillment of the requirements for the award of the degree of Doctor of Philosophy.

Dr. Kumar G. N.
(Research Guide)

Date:

Chairman-DRPC
Date:

Dedicated to my

Beloved Wife Late Smt. Aruna Kumari M

&

Teachers

Whose Love and Support

Sustained Me Throughout

ACKNOWLEDGEMENT

I would like to express my heartfelt gratitude and respect to my research supervisor and the backbone of my entire research, **Dr. Kumar G. N.**, Associate Professor, Department of Mechanical Engineering, NITK Surathkal, for his uninterrupted support and guidance throughout my research. It is my privilege to have a Guru like him who gave me the freedom to work with routine check and proper instructions to shape the project. I thank him for his motivations and for prompting me at the right time to improve my research awareness, even during the difficult times of Covid-19. I am grateful to him for allowing me to overcome several challenges and difficulties that arose during the research process including emotional support during my nightmare situations of Covid-19. I would also sincerely thank **Dr. Prasad Krishna**, the Director, NITK Surathkal, and **Dr. Abhay Pashilkar,** Director, CSIR-National Aerospace Laboratories, Bengaluru, for providing adequate facilities to carry out my doctoral research.

I sincerely pay my gratitude to the Research Progress Assessment Committee members, including **Dr. G S Dwarakish** (Professor, Department of Water Resources and Ocean Engineering) and **Dr. Gnanasekaran N** (Assistant Professor, Department of Mechanical Engineering), for their beneficial suggestions and productive remarks that helped improve my research. My heartfelt gratitude goes to **Dr. Ravikiran Kadoli**, Professor and Head, Department of Mechanical Engineering, NITK Surathkal, **Dr. Giridhara Babu Y**, Sr. Principal Scientist, CSIR-National Aerospace Laboratories, Bengaluru for their consistent support and encouragement throughout my research work.

I must express my gratitude to the team behind my doctoral research, **Mrs. Shruthi P, Mr. Shashidhara V, Mr. Jayagopal S, Mr. Kalyana Sundaram, Mrs. Kshama S, Dr. Dilip B Alone, Mr. Chidananda M S, Mr. Bhaskar Chakravarthy, Mr. Vineet Kumar, Mr. Sathish R Rohidekar, Mr. Jitendra J Jadhav,** for their valuable support and advice. I must acknowledge the help and assistance I got from my fellow research scholars, **Mr. Jayashish Pandey, Mr. Dinesh M H** and **Mr. Kishorebabu Bhumula**. The doctoral research would not have been completed smoothly without the emotional support of my loved ones, particularly my wife, **Late Mrs. Aruna Kumari M** who was my strength. **Aditi V** and **Harshitha V** 's smiles and naughty pranks always relieved my tiredness and fatigue. I'd also like to express my gratitude to my parents, **Mrs. Pushpalatha N** and **Mr. Anand C K**, for their blessings and encouragement. I'd like to thank my wife's parents, **Mrs. Kamala B** and **Mr. Mudliaha H T**, for their support of my family during these trying times. I must express my gratitude to our entire family.

ABSTRACT

Typically, commuter/transport category aircraft are powered by turboprop engines due to the benefit of fuel efficiency and high power-to-weight ratio. These aircraft are normally configured in either pusher or tractor versions based on the position of the powerplant (engine-propeller). Generally, in turbofan or turbojet engines managing hot engine exhaust is not critical as the exhaust plume is totally overboard of the aircraft. However, in turboprops, exhaust plume management gains importance as the plume gases exit at an angle or perpendicular to the engine axis, crossing the propeller (pusher) plane and airframe surfaces. This becomes especially critical in reverse thrust operations, with a composite propeller. This requires an exhaust nozzle or stub to duct the engine exhaust hot gases out. The design of these exhaust stub is dictated primarily by the structural and aero-thermal requirements, such as aircraft's configuration, drag contribution, exhaust jet thrust, and engine performance.

Exhaust stubs are designed to meet pusher configuration aircraft requirements. The stubs are designed to minimize the impingement of the hot plume gases on the propeller and airframe surface without significantly affecting the benefit of jet thrust. The critical geometrical parameters of stubs are exit area, turning angle, plume trajectory etc. A fluid-thermal-structure coupling analysis is performed to understand the thermal effects of the engine exhaust jet flow on the thermo-mechanical behaviour of pusher-configured light transport aircraft propellers and affected structural components. The steady-state thermal flow field of the aircraft with both forward and reverse thrust in which propeller blade angle vary, were analysed for various forward velocities. Further, investigated a three-dimensional analysis of flow around the nacelle-airframe and the effect of exhaust flue gas impingement on the propeller blade surface. Based on the results from this analysis, the designed exhaust duct was integrated into the aircraft. Experimental evaluations were carried out on the prototype aircraft for ground static and flight trials to validate the numerical findings. During the experiment, propeller blade and fuselage surface temperature were measured. The experiments show that the numerical analysis carried out is in good agreement with the measured results. Further, it is observed that the estimated temperatures on the propeller blade surface are within the allowable limit as prescribed by the original equipment manufacturer. The confidence gained from this numerical study and its experimental validation, facilitates a numerical approach that can be adopted for new developmental activities such as configuration change studies and new aircraft designs where the experimental data are unavailable.

Subsequently, the numerical studies were extended to design and develop new exhaust stubs for tractor-configuration aircraft fitted with the same engines having twin exhaust ports per engine. The new tractor aircraft chosen is a twin-engine airplane with its powerplant mounted in the high wing configuration. Even though the tractor configuration propeller is not in the critical path, the finding from the studies were extended for the design of a light weight composite airframe. The airframe design team used such numerical results to select skin material for the fuselage, wing, nacelle, plexiglass passenger window, flap design, and geometry. The use of thermal barrier coating on critically exposed surfaces was also assessed. Airframe developmental activities are in progress. Special attention was given to the nacelle for thermal flow field mapping as it houses hot components like the engine and its subsystems. This also facilitates design of thermal ventilation to keep the zone and bay temperature inside the nacelle within the applicable limits prescribed by the engine manufacturer.

In addition to mapping of the thermal flow field, another study carried out was to estimate an effect of exhaust stub angle and its orientation w.r.t engine axis on the jet thrust with symmetric and asymmetric inboard-outboard stub angles. This study was carried out for critical flight operating conditions such as maximum continuous and cruise rating covering Minimum Off-Route Altitude (MORA) on the overall aircraft performance.

To summarise, the aim of this research was to estimate the temperature levels caused due to the impingement of hot exhaust gases on the propeller and aircraft surfaces such as fuselage, wing, nacelle, and flaps using numerical analysis. In a few cases, the numerical study was validated by experimentation. The effect of stub geometry on the engine's performance was also studied. Detailed findings are discussed in the respective sections. This study is very much useful to powerplant and aircraft designers.

Keywords:- *Exhaust Stub, Engine, Aero-thermal, Nacelle, Turboprop, Aircraft, Jet flow, Propeller Blade*

TABLE OF CONTENTS

LIST OF FIGURES

Description **Page No**

LIST OF TABLES

Description **Page No**

NOMENCLATURE

a	speed of sound, [m/sec]
°C	Degree Celsius
Amb	Ambient
Cd	Coefficient of Drag
Cl	Coefficient of Lift
d_7	Exhaust stub diameter, [m]
dB	Decibel
D	Diameter of the domain [m]
2D	Two Dimensional
3D	Three Dimensional
ft.	Feet
F_{ty}	Tensile Yield Strength, [N/m^2]
°K	Kelvin
L	Axial distance from exhaust stub exit plane, [m]
M	Mach number
Ng1	Left Hand Engine Gas generator speed, [rpm]
Ng2	Right Hand Engine Gas generator speed, [rpm]
Np1	Left Hand Engine Propeller speed, [rpm]
Np2	Right Hand Engine Propeller speed, [rpm]
Pa	Pascal
rpm	revolutions per minute
Re	Reynolds Number
T	Local exhaust jet temperature, [K]
T_1	Free stream air temperature, [K]
T_7	Exhaust jet temperature (at stub exit), [K]
T_{amb}	Ambient Temperature [°C] [K]

Tq	Torque, [N-m]
V	Characteristic jet velocity, [m/sec]
V_1	Free stream air velocity, [m/sec]
V_7	Exhaust jet velocity (at stub exit), [m/sec]
X	Length of the domain, [m]

Greek Symbols:

μ	dynamic viscosity [N s m^{-2}]
ρ	density, [kg m^{-3}]
η_{prop}	propeller efficiency
k	Turbulent Kinetic Energy, [$m^2 \cdot s^{-2}$]
ω	Specific Dissipation Rate of Kinetic Energy, [m^2/s^3]

Abbreviations:

AMSL	Above Mean Sea Level
CAD	Computer-Aided Drawing
CATIA	Computer-Aided Three-Dimensional Interactive Application
CW	Clock Wise
CCW	Counter Clock Wise
CFD	Computational Fluid Dynamics
CROP	Contra Rotating Open Rotor
CRP	Contra Rotating Propellers
EGR	Engine Ground Run
ESHP	Equivalent Shaft Horse Power
FAR	Federal Aviation Regulations
FI	Flight Idle
GI	Ground Idle
HPC	High Performance Computing
IR	Infrared
ISA	International Standard Atmosphere

LHE	Left Hand Engine
LH-Throttle	Left Hand Engine Throttle Lever
LSTT	Low Speed Taxy Trials
LEOIT_RTD	Left Hand Engine Main Oil Temperature
LTA	Light Transport Airport
LTorq	Left-Hand Engine Torque
MCOR	Max Continuous Operation
MORA	Minimum Off-Route Altitude
MRF	Multiple Reference Frame
NACA	National Advisory Committee for Aeronautics
NURBS	Non-Uniform Rotational B-Spline
OAT	Outside Air Temperature
OEI	One Engine Inoperative
OEM	Original Equipment Manufacturer
PDE	Partial Differential Equation
RANS	Reynolds Averaged Navier Stokes Equation
RCS	Regional Connectivity Service
RHE	Right Hand Engine
SHP	Shaft Horse Power
SST	Shear Stress Transport
TBC	Thermal Barrier Coating
TAS	True Air Speed
Thermal-IR	Thermal Infrared Temperature
VBM	Virtual Blade Model

CHAPTER 1

INTRODUCTION

1.1 Background

India is a vast country with varied landforms/terrain in which air connectivity to smaller towns as well as to remote and difficult-to-access regions will play an increasingly significant role in the development/economic growth of the nation in the years to come. The growth of air transport in India is driven by the strong economic growth that the country has witnessed in the last decade as a result of increasing revenues of the Indian corporate sector and business needs to reduce travel time to improve productivity. In recent times, this has got a high impetus due to policy changes and initiatives taken by the state and the union governments. Though regional connectivity is increasingly being established in the last few years, very little parallel work has been done on the indigenous design, development and manufacture of civil aircraft in the country. Establishing a viable civil aircraft industry will play an important role in the Regional Connectivity Service (RCS) and national economy will throw up opportunities/possibilities to meet the commuter aircraft requirements of both civil and military transportation through indigenous design and development. This is to facilitate/stimulate regional air connectivity by making it affordable with a focus on providing air connectivity where it does not exist.

Currently around 123 (35 international) out of 489 airstrips/airports have scheduled operations. This is expected to increase to 200 airports in the coming years to meet the growing air traffic. In addition, a significant number of existing aging aircraft need to be retired, resulting in market demand for new aircraft. However, since existing short haul aircraft are unpressurised, an additional market exists for commuter aircraft capable of catering to tier-2 and tier-3 locations in high altitudes such as Himalayan regions, north east, hill stations, etc. The poor connectivity between the metros and smaller cities in India has further resulted in companies and individuals realizing the benefits of using private aircraft. A window of opportunity exists for a new-generation commuter aircraft. It is envisaged to initially certify the aircraft and deliver the basic version for troop transfer, medivac, case-vac, and executive roles. Subsequently, variants of this aircraft could be used for additional roles such as for security

applications using external hard points, cargo transport, supply role, aerial survey, navigator training etc. With civil certification, the aircraft could be used for other target beneficiaries, viz., low cost airline operators, business houses, tourism, coast guard services, postal services and other regional connectivity service providers. CSIR-NAL has a vast experience in the design, development and flight testing of several propeller-driven commuter aircraft and has built and test-flown prototypes. The perceived advantages of the pusher configuration were (shown in Figure 1.1); a clean wing undisturbed by wing-mounted nacelles on which near laminar flow could be sustained resulting in lower drag. Also, the aft mounted pusher propellers result in lower cabin noise and vibration when compared to a conventional wing mounted tractor configuration. There is definite advantage of using composite propellers against metallic propellers in terms of weight benefit of 30 to 35% lower. Composite props will not have reactionless mode vibration and hence ground operation restrictions of metallic propellers are not applicable.

During the development of this type of prototype aircraft, it was found that the service life of the composite propeller blades and rear fuselage structures would be adversely affected by the heat from the turboprop engine twin exhaust ducts. Prediction of seriously heated area locations and analysis of the thermo-structural effects become interesting topics. Engine exhaust plume impingement management while maintaining maximum jet thrust and prediction of temperature on the propeller blades and rear fuselage surfaces is one of the important requirements. Exhaust plume management, a technique for prediction of high temperature high velocity exhaust gas impinging on the rotating propeller, and validating the same in aircraft environment become interesting topics while few research works have devoted to them earlier.

1.2 Light Transport Aircraft (LTA)-Pusher Configuration

The Light Transport Aircraft (LTA) is an aircraft that has a maximum gross take-off weight of 7100 kg. Light Transport Aircraft are used as utility aircraft commercially for passenger and freight transport, tourism, photography, and other roles, as well as private use. LTA will be useful for military operations also. It would be equipped with a glass cockpit, autopilot, conventional flight control system, pressurized cabin with significant drag and weight reduction complying with FAR-23 (Federal Aviation and Regulation) part requirements. The landing gear is of retractable tricycle configuration. Most

primary aircraft structures are metallic, with primary and secondary control surfaces, empennage fabricated from composite material. The important parts of the LTA are the fuselage, wings, stub-wing, nacelle, vertical stabilizer, horizontal stabilizer, aileron, elevator, rudder, nose and main landing gears, and flaps.

It is crucial in pusher applications to minimize the propeller's exposure to the hot exhaust/flue gas. That exhaust gas do not attach itself to the aft nacelle and cause overheating of the spinner/hub area of the propeller. Due to overheating, the strength of propeller blades will be drastically reduced, as the propeller is the prime source of thrust generators in turboprop engines. The current aircraft noise regulations affected the design of propellers where tip speeds were reduced to meet the regulations. Reduced tip speeds were accomplished by reducing propeller rpm or propeller diameter. The propeller diameter or the number of blades increased to retain propeller performance. These changes affected the propeller weight drastically. Hence, a composite propeller blade has been developed that is significantly lighter than a blade fabricated from Aluminum alloy. Additional advantages of the composite blade are strength to weight ratio and maintenance characteristics.

The composite propeller has benefits compared to a metallic propeller in terms of corrosion, vibrations, and limitation of propeller operation on ground operations (certain speed range). However, the composite propeller blade surface temperature is limited to 80°C against 90°C for a metallic propeller. Despite the increased attention given to aircraft engine gas emissions, it is also essential to decrease the exhaust gas impingement on the propeller aircraft surface. The exhaust plume should deviate outwards radially towards the tip of the propeller. It is essential to design the engine exhaust stub, which meets the primary requirements of maximizing the jet thrust and to ensure that the exposure of the propeller/aircraft structure to the hot exhaust gas is minimized and to avoid overheating, and sooting.

When the design goal needs to be met and implemented on the aircraft, it must be validated through analysis and experiments. Preliminary investigations are conducted through computational simulations. Here, CFD estimations play an important role as direct testing without numerical estimations can be catastrophic as it is expensive to lose the propeller for exceeding allowable temperature limits. With the constraints and uncertainties of experimental analysis, it was decided to conduct the computational

simulations, which give designers confidence before installing and testing on aircraft. However, the propeller, in its installation in pusher configuration, is subject to several installation effects due to interactions with the airframe.

Figure 1.1 shows the major assemblies of typical LTA (Light Transport Aircraft) for pusher configuration.

Multi-roles of the LTA:

- Air taxi and commuter
- Community services like air ambulance, disaster relief
- Executive transport
- Light cargo carrier
- Aerial research service
- Remote sensing
- Coast guard
- Border patrol
- Special features
- Low cabin noise
- Operable from semi-prepared runways
- Operable from hot and high airfields
- Designed to meet FAR-23 requirements

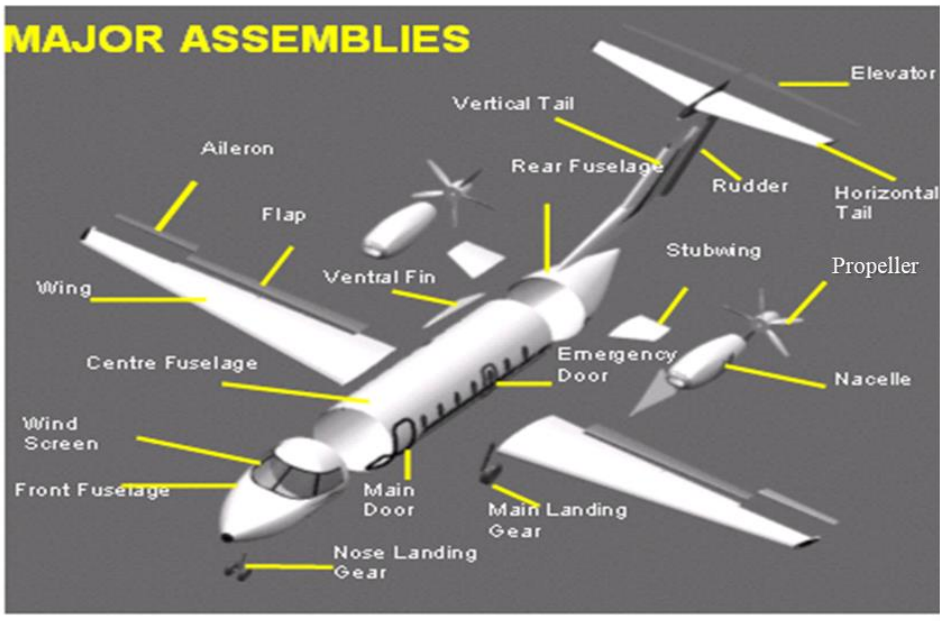

Figure 1.1 Major assemblies of LTA for pusher configuration

1.3 Commuter Category Aircraft-Tractor Configuration

A Commuter Aircraft in a tractor configuration will be useful for both civil and military versions because of the unique features like a full glass cockpit, pressurized cabin (operation at high altitudes), low cabin noise (<80 dB), autopilot, weather radar system and operable from semi-prepared runways. In the tractor configuration type, the propellers are placed before the nacelle that is in turn placed ahead of wing. Tractor propeller-configured aircraft is considered a conventional installation, and most turboprop-powered aircraft follow this configuration. This configuration helps many of the new aircraft development programmes where the prime system, i.e., powerplant (engine and propeller), is readily available with type certification of such engine-propeller combination and will facilitate good number of engine and propeller selection options based on the specific mission profile. Figure 1.2 shows the major assemblies of typical LTA (Light Transport Aircraft) for tractor configuration.

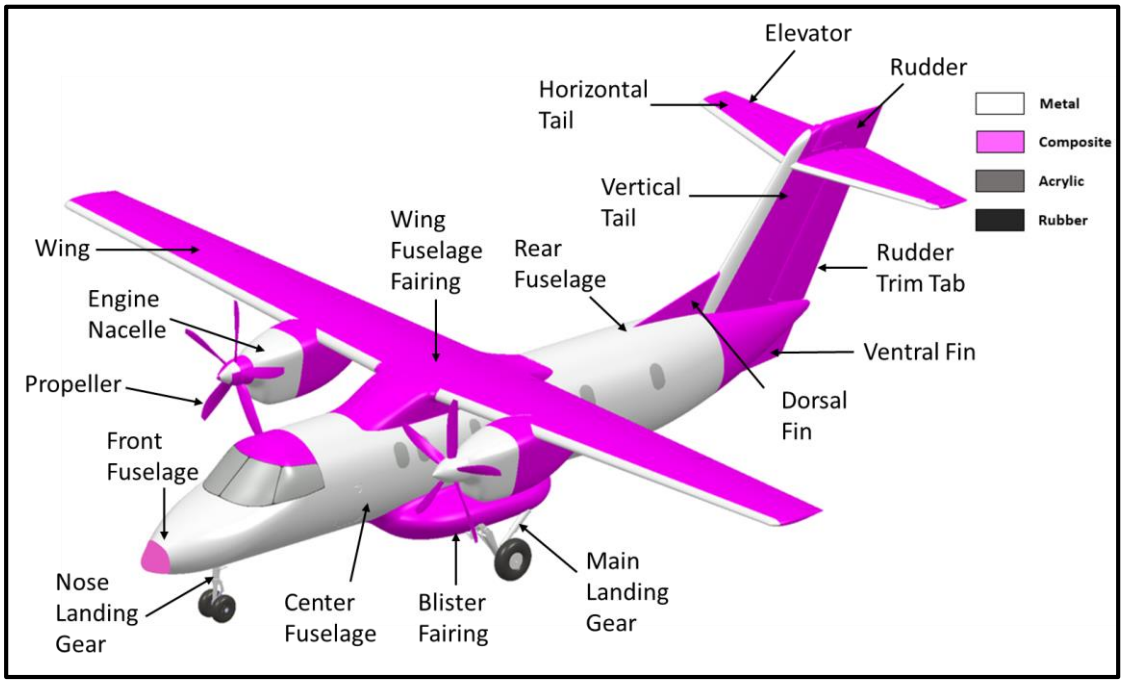

Figure 1.2 Major assemblies of tractor-configuration aircraft

1.4 Powerplant System

Two turboprop engines power the aircraft in the pusher configuration. The engines are installed on the stub wings on either side of the rear fuselage, and Figure 1.3 gives the principal features of the engine. Each engine is fitted with a 5-bladed composite propeller incorporating a constant speed unit and a propeller over-speed governor. The

nacelle structure consists of two moving vanes, which are electrically operated by actuators in the main air intake and bypass duct. It is a twin-shaft light-weight turbine engine driving a propeller via a two-stage reduction gearbox. Two major rotating assemblies compose the heart of the engine. The first is the compressor and the compressor turbine (compressor section), and the second, is the two-stage power turbines and the power turbine shaft (power section). The two rotors are not connected and rotate at different speeds and in opposite directions. This design is referred to as a "Free Power Turbine Engine." This configuration allows the pilot to vary the propeller speed independently of the compressor speed. The compressor draws air into the engine via an annular plenum chamber (inlet case), air pressure increases across 4 axial stages, one centrifugal stage and is then directed to a reverse flow annular combustion chamber. Air enters the combustion chamber via small holes. Fuel is introduced into the combustion chamber at the correct compressor speed via 14 fuel nozzles. Two spark igniters located in the combustion chamber ignite the fuel-air mixture. The hot gases generated by the combustion are then directed to the turbine inlet.

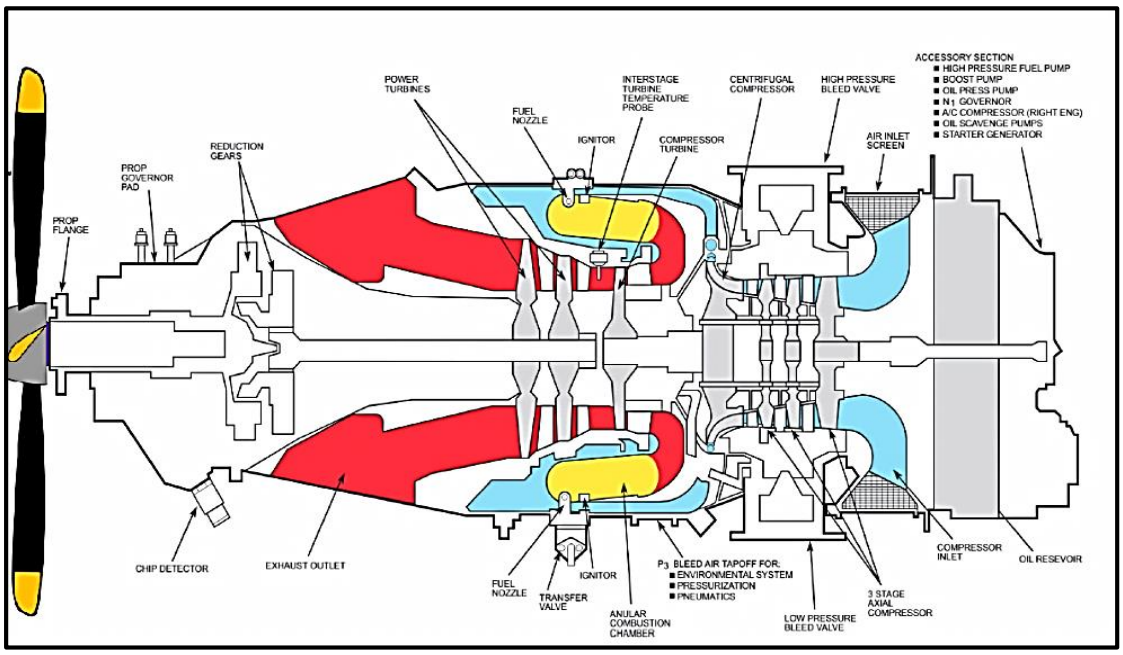

Figure 1.3 Engine principal features

The hot expanding gases accelerate through the compressor turbine vane ring and cause the compressor turbine to rotate (which rotates the compressor). The expanding gases travel further across the 1st and 2nd stage power turbines, which provide rotational

energy to drive the propeller shaft. The reduction gearbox reduces the power turbine speed (~30,000 rpm.) to a value suitable for propeller operation (1700 rpm). Gases leaving the power turbines are expelled into the atmosphere through a twin-port exhaust ducts. An integral oil tank between the inlet case and the accessory gearbox provides oil to the bearings and other systems, such as propeller and torque systems. A hydro-mechanical fuel control unit mounted on the accessory gearbox regulates fuel flow to the fuel nozzles in response to power requirements and flight conditions. The propeller governor mounted on the reduction gearbox controls the speed of the propeller by varying blade angle, depending on power requirements, pilot speed selection, and fight conditions, such that it always runs at a constant speed.

The engine is provided with firewall supports made of stainless steel, which the aircraft manufacturer could use to isolate the engine inlet from the fire zones. This provision ensures that the engine-provided firewall supports are not a design limitation for the OEM plenum integration in powerplant fire protection. The front fire wall is termed as 'L' frame, and the rear fire wall is termed as 'M' frame, as shown in Figure 1.4.

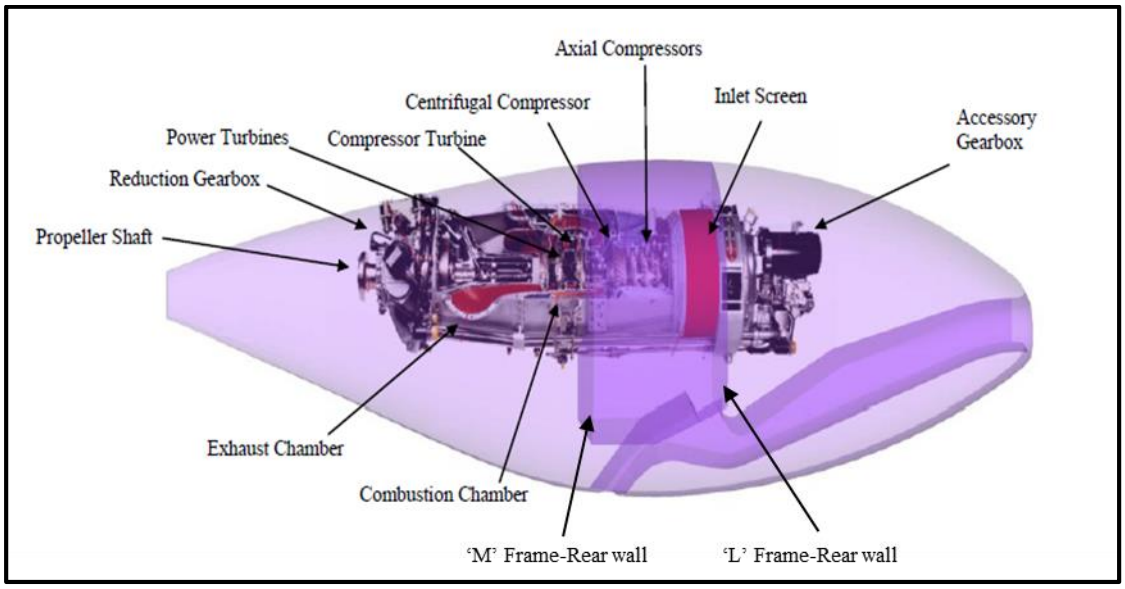

Figure 1.4 Engine components housed in the nacelle

Turboprop engine installation requires an exhaust nozzle/stub to duct the engine exhaust gas outboard of the aircraft. The different types of stub arrangements can be seen in Figure 1.5.

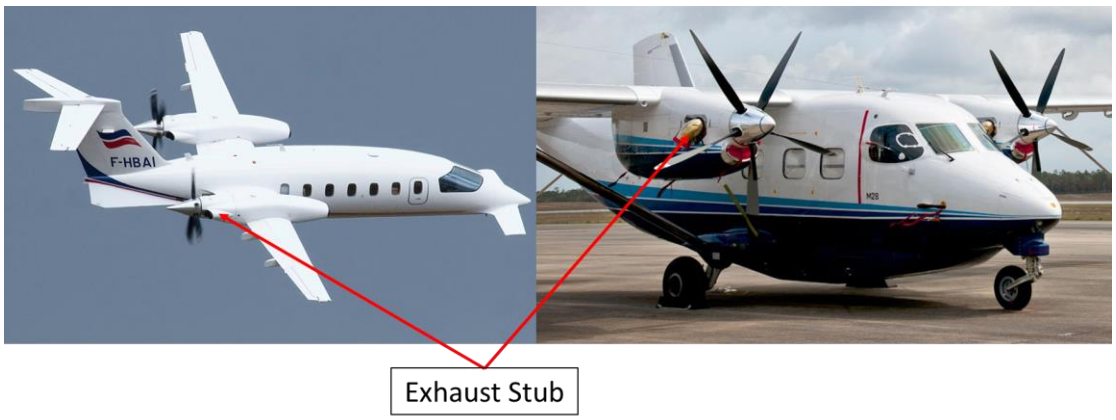

Figure 1.5 Different types of stub arrangements for tractor & pusher aircraft

1.5 Engine Propeller Integration and Propeller Operation

In pusher configuration, the propeller is installed behind the engine and wing and the thrust produced by the propeller pushes the aircraft forward. The propeller is installed aft of the engine (see Figure 1.6). In turboprop engines, thrust is accomplished by propeller thrust and exhaust thrust. One of the major difficulties in designing a pusher propeller installation for modern aircraft, is to prevent mutual interference between the pusher propellers and the engine exhaust flow without seriously reducing either the propeller efficiency or jet thrust. In numerous pusher-prop installations, a rotatable spinner assembly is located aft of the nacelle and includes a rearward convergent, generally conical surface, which provides environmental protection to the propeller mechanism. Preferably, the cross-sectional area of the spinner surface is reduced somewhat between the propeller blades to provide area ruling of the exhaust flow path.

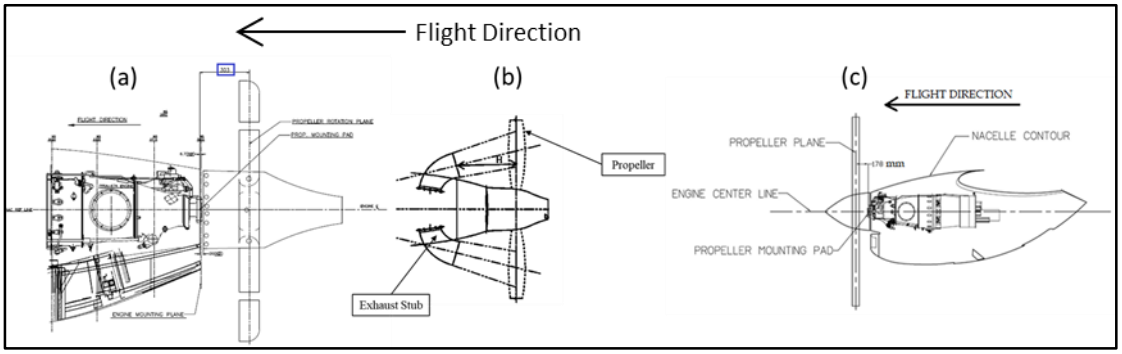

Figure 1.6 Engine Exhaust-Propeller Integration (a, b) Pusher (c) Tractor

1.5.1 Propeller Operation

The propeller mechanism is well-known and generally includes a hub containing the pitch control machinery and three to six radially extending propeller blades. Each blade is attached to the hub at its root and passes radially through an opening in the spinner surface. The propeller hub holds the blades in place and is connected to the engine through a propeller drive shaft and a gearbox. Modern propellers on large turboprop airplanes typically have 4 to 6 blades. For the present aircraft configurations co-rotating (LH and RH propellers rotate in the same direction, Pilot view) propellers due to the engine construction are selected. Major propeller components are shown in Figure 1.7, and other components typically include:

- The spinner creates aerodynamic streamlining over the propeller hub.
- The bulkhead allows the spinner to be attached to the rest of the propeller. The bulkhead typically has a slip ring arrangement that allows electrical power to be transmitted to the blade de-icing boots.
- The pitch change actuator transmits hydraulic energy to rotate the blades in the hub.
- A source of high-pressure oil to supply that hydraulic energy to the propeller actuator.
- The primary control, called the governor, controls propeller speed and blade pitch.
- The Over-speed governor, serves as a backup if the primary control malfunctions.

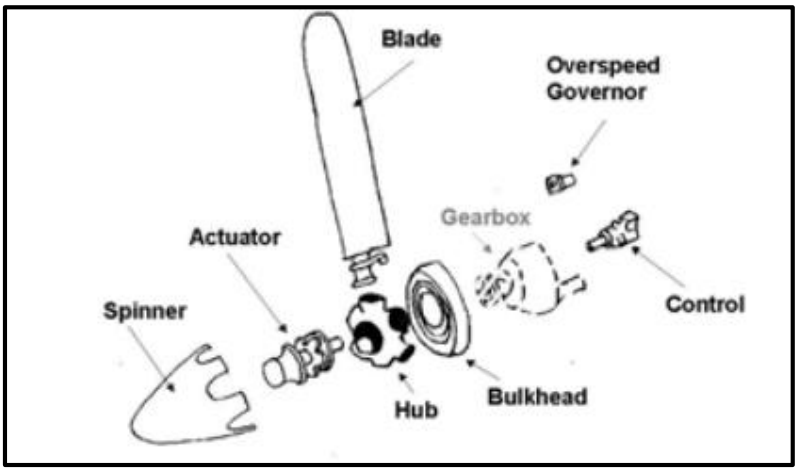

Figure 1.7 Major propeller components

The propeller system generally converts the engine's power into thrust to propel the aircraft through the air. The pitch change mechanism is used to maintain the constant propeller speed through various ambient conditions and power settings. In most conventional aircraft, oil from the propeller governor feeds into the propeller shaft and the servo piston via the oil transfer sleeve mounted on the propeller shaft. As oil pressure increases, the servo piston is pushed forward, and the feather spring is compressed. Servo piston movement is transmitted to the propeller blade via a system of levers. When the oil pressure is decreased, the return spring and counter-weights force the oil out of the servo piston and change the blade pitch to a coarser position. An increase in oil pressure drives the blades towards a finer pitch. The propeller blade pitch, also called the propeller pitch, is the angle that the blade presents to the plane of rotation of the propeller. The blade pitch, known as "feather" describes the pitch that results in no or slow rotation of the propeller at a specific flight condition with the engine shut down. A constant-speed propeller has a control system that maintains a constant propeller rotational speed (RPM) setting at any flight condition. To maintain constant propeller RPM, the pitch of the propeller blade keeps changing as airspeed and engine power are varied.

The blades, which act like rotating wings, have a leading edge, trailing edge, tip, shank, face, and back shown in Figure 1.8 and 1.9. The blade pitch may be fixed, manually variable to a few set positions, or of the automatically-variable "constant-speed" type. The propeller directly attaches to the power source's driveshaft or through reduction gearing, especially on larger designs. Most early aircraft propellers were carved by hand from solid or laminated wood, while metal construction later became popular. More recently, composite materials are often used in aircraft components.

- **Terms and Definitions**
  - Blade angle: Blade angle is the angle between the propeller plane of rotation and the chord line of a propeller airfoil section.
  - Blade station: Blade station is a reference position on a blade that is a specified radial distance from the center of the hub.
  - Propeller pitch: Propeller pitch is similar to any type of thread, defined as the axial distance that a propeller will move forward in one revolution. This is

typically based on the propeller blade angle at 75% of the blade radius. Propeller pitch is a general term that can be further specified, such as geometric pitch, which is theoretical in that it does not consider any losses due to inefficiency.

- Effective pitch is the distance an aircraft moves forward in one propeller revolution. Effective pitch may vary from zero, when the aircraft is stationary on the ground, to about 80% of the geometric pitch during the most efficient flight conditions. The difference between geometric pitch and effective pitch is called slip. Pitch distribution is the gradual twist in the propeller blade from shank to tip.

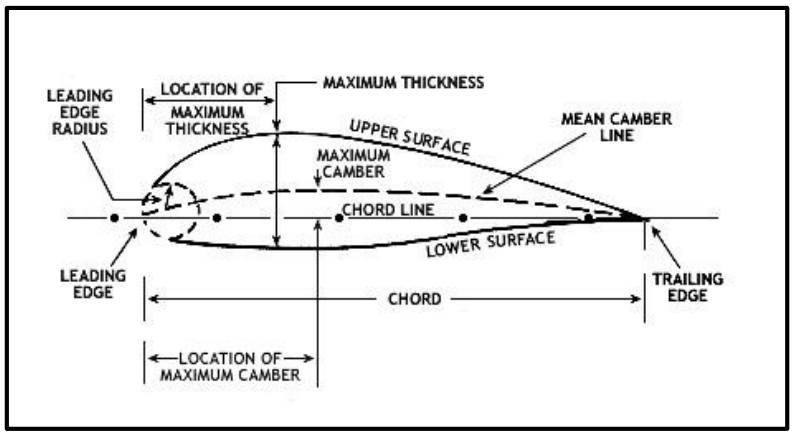

Figure 1.8 Cross section of a propeller blade

Figure 1.9 Propeller of a turbo-prop engine

The aircraft propeller is of mainly two configurations: pusher and tractor, as shown in Figure 1.10. In pusher configuration, the propeller is placed behind the engine and usually behind the fuselage. In this, the thrust produced by the propeller pushes the airplane forward. The most important advantage is the weight reduction achieved

through a shorter fuselage. This means the skin friction drag on the fuselage is considerably lower than in a normal tractor configuration. Also, the oscillatory wake of the propeller doesn't interfere with the wings and fuselage. Due to its position, the propeller blades interact with hot exhaust gas. Therefore, there is no need for a de-icing system.

In the tractor configuration, the propeller is mounted ahead of the engine where the thrust draws or pulls the airplane. Most modern aircraft use this propeller because of the unrestricted flow of air into the propellers. The tractor configuration is much more aerodynamically stable and makes the aircraft much easier to control. In this configuration, there is a need to put an anti-icing or de-icing system.

Figure 1.10 Aircraft with a) Pusher configuration b) Tractor configuration

1.6 Exhaust System

Typically, turboprop engine installations require an exhaust nozzle or stub to duct the engine exhaust gas outboard of the aircraft. The engine is fitted with a twin port exhaust case with flanges to which exhaust stubs should be directly attached and provided with a feature that permits rotation of the complete exhaust case in one 30º increment from the standard horizontal position. The design considerations are location, orientation, flange dimensions, and minimum load-carrying capacity. Exhaust stub (or nozzle) design must follow established practices for the design of internal flow ducts to ensure full flow at bends and in diffusing sections. Poor design can result in flow separation from the walls causing unnecessary pressure loss and reduced effective flow area.

Typically, prime parameters which controls the exhaust temperature to attain the exhaust jet temperature at the stub are: stub geometrical parameters such as exit area, exit angle, bend radius along with aircraft power setting (power demanded, fuel flow, bleed off take, power off take from gearbox) and flight operating conditions (altitude and speed).

The principal design requirements of an exhaust stub are as follows:

a. In the turboprop engine, power is available both as shaft power and as exhaust thrust. The power distribution between the shaft and the exhaust is governed directly by the exhaust nozzle exit area. The choice of an effective exit area is a trade-off between take-off and cruise requirements. At take-off conditions, exhaust stub thrust contributes less to the total propulsive thrust. Therefore, it is advantageous to have a large exit area. However, exhaust stub thrust can be effectively recovered at cruise, and optimization of the Equivalent Shaft Horsepower (ESHP) and reduction in exhaust stub drag is the objective.
b. The exhaust stubs should turn the exhaust gases to maximize the thrust recovery and minimize the effect of external aerodynamic drag.
c. When it is necessary to have geometrically different exhaust nozzles, the nozzles must be designed to equal the pressures at the engine exhaust flanges. Exhaust flange load limits must be within limits.
d. The trajectory of the exhaust plume must be managed to reduce potential problems due to overheating aircraft surfaces and sooting. The exhaust stubs may be slanted up or down a maximum of 30° relative to the engine center line to cater to the particular installation requirement.

1.7 Importance of Engine Exhaust Jet Thrust on Aircraft Performance

In turboprop engines, the thrust/power is available both as shaft power and exhaust jet thrust. In the case of pusher-configured turboprop engines, it is important to minimize the interaction/impingement of hot exhaust gases on the propeller and aft nacelle surfaces. This impingement might lead to overheating the propeller, spinner, and on aft-nacelle/aircraft surfaces, directly affecting the propeller's performance. The exhaust of the hot jet through the propeller blades may introduce vibrational and thermal problems in the blades and simultaneously interfere with the exhaust jet. Modern non-metallic, or even Aluminum, propeller blade life is affected by the hot jet. Even when the exhaust is mixed with cold ambient air to reduce its temperature to only a few hundred degrees, thermal fatigue could still shorten the life of the blades.

Further, it reduces the amount of jet thrust available for propulsion which assumes significance in one engine inoperative aircraft climb. Several approaches have been

proposed to avoid or solve some of these problems. Deflection of the jet gasses laterally to a point beyond the propeller radius has been tried but results in an excessive sacrifice of space to accommodate a gas duct of sufficient length and volume to carry the exhaust to a safe distance outboard of the propellers. In addition, the introduction of pronounced bends in the exhaust path, or the placement of the exhaust vent at an angle to the line of flight, leads to losses in jet thrust and to other detrimental effects, such as increased back pressure on the turbine, which reduces the power available for propeller thrust, and decreased aerodynamic efficiency due to higher drag losses.

1.7.1 Jet Flow

Jet flow is a type of fluid flow in which a liquid or gas passes through another fluid with properties, such as velocity, temperature, or density, different from the jets. Thus, in a jet flow, a stream of one fluid mixes with a surrounding medium, at rest or in motion. In various situations, the geometries, sizes, and flow conditions vary over a large range. Jet flow is a widespread phenomenon that exists in many forms, from the stream ejected through the exhaust nozzle of a rocket engine to the jet stream in the earth's atmosphere. The changes in the velocity, density, temperature, and concentration of the component fluids are studied both in the jet and in the ambient fluid.

Jet flows vary greatly, depending on the value of two dimensionless numbers. The first one is the Reynolds number, defined as $Re = \frac{\rho V L}{\mu}$, where ρ is the density, V is the characteristic jet velocity, L is the characteristic length (for example, the jet diameter), and μ is the viscosity of the jet fluid. The second one is the Mach number, defined as $M = \frac{V}{a}$, where a is the speed of sound.

As a turbulent jet fluid moves further away from its origin, it slows down due to the mixing with stagnant ambient fluid entrained and induced into the jet field. This is due to the boundary layer at the nozzle exit, which develops roll-up structures, or ring vortices, that grow up in size when they move down stream due to entrainment of the ambient fluid in to the jet stream. Thus, mass flow at any jet cross-section increases along the downstream direction. Hence, the centreline velocity decreases with the downstream distance to conserve the momentum. The resulting centreline decay is

proportional to the gradient across the shear layer and is a strong function of distance downstream of the jet exit.

The differential shear at the jet boundary forms vortices, and they bring fluid mass from the surrounding environment into the jet field. This mass transport from the surroundings in to the jet is called entrainment. There are vortices all over the jet boundary; thus, many eddies induct mass into the jet. This entrainment process reveals that the mass of jet flow increases as it flows downstream. The entrained mass is at a lower momentum compared to the momentum of fluid elements in the jet issuing from the nozzle or orifice. Therefore, the fluid masses of higher and lower momentum will try to come to equilibrium, leading to a decrease in the momentum of the jet mass issuing from the nozzle. Thus, the mass and momentum transport become active soon after the jet comes out of the nozzle. This process will try to carry the entrained mass toward the jet axis. This action causes the large-size mass entraining vortices formed at the jet boundary to fragment into small eddies and move towards the jet axis. Smaller vortices, efficient mixing promoters, assist the low momentum mass entrained at the jet boundary to gain momentum from the jet mass at the higher momentum and travels towards the jet's axis.

The viscous action ultimately reaches the jet axis at an axial distance downstream of the nozzle exit. Up to this location, the jet velocity (the velocity at the nozzle exit) remains unaffected along the jet axis. The jet flow that has a uniform velocity all over the exit plane of the orifice or nozzle is said to exhibit a top hat (i.e., resembling its shape) at the nozzle exit and thus can be assumed to be inviscid. But soon after exiting the nozzle the flow experiences vortex formation at the boundaries, because of the differential shear. The relatively large vortices formed at the jet boundary entrain the surrounding mass in-to the jet and get fragmented to mixing, promoting small vortices. Thus, the top hat velocity profile at the nozzle exit shrinks in size as the jet propagates downstream from the nozzle exit. In other words, the mixing initiated at the jet periphery spreads towards the jet axis, as the jet propagates downstream. The interactions of vertical structures produce strong flow fluctuations and entrain ambient fluid into the jet flow, enhancing the mixing. The shear layer and the jet spread along the direction perpendicular to the main jet flow. The jet centreline velocity is the direct

measurement of the proper mixing of the jet with the entrained fluid. Thus, the momentum of the jet gets reduced and jet mass increases.

1.7.2 Structure of The Jet Flow

Jet flows to take on a simple character for conditions where Re < 2300 and M <<1. An example is the water jet formed by a household tap when the valve is partially opened to produce a low flow. If the flow or the diameter is increased or the viscosity is decreased such that Re > 2300, the jet will change dramatically (Pandey and Virendra Kumar, 2010). For example, a water jet exiting into the water at rest with Re equal to 2300 is initially in the simple laminar state, but at this Reynolds number, that state is unstable, and the flow undergoes a transition to the more chaotic turbulent state. Turbulent structures called eddies are formed with an extensive range of sizes. The large-scale structures capture fluid from the surroundings and entrain it into the jet. However, the jet and external fluids are not thoroughly mixed until the small-scale structures complete this diffusion process.

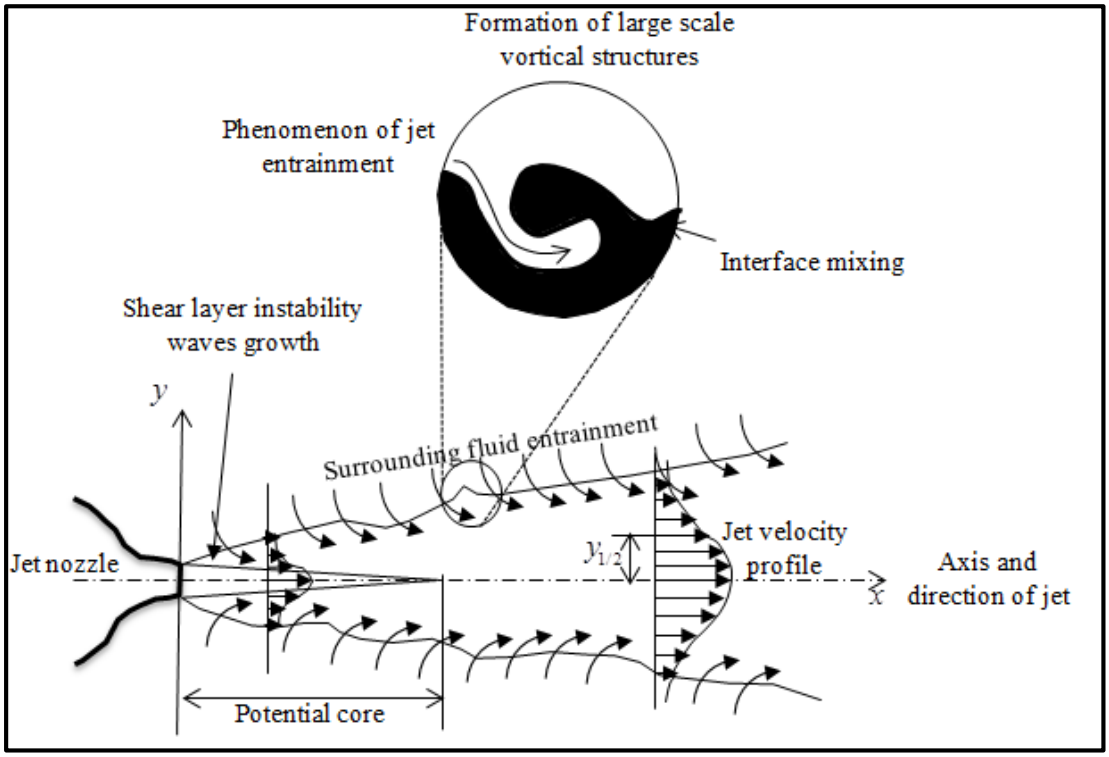

Figure 1.11 Schematic representation of jet flow issuing from a nozzle

Figure 1.11 shows some essential features of the jet. The velocity at the exit of the nozzle has a smooth profile and low turbulence. A thin shear layer is created due to the

difference in velocity between the jet and the ambient fluid. This shear layer is volatile and is subjected to flow instabilities. This will lead to the formation of large-scale vortical structures, as shown in Figure 1.11. The interactions of these structures produce a strong flow fluctuation that entrains ambient fluid into the jet flow and enhances the mixing. The shear layer formation results in the jet spreading along the direction perpendicular to the main jet flow. In the fully developed flow region, the velocity profile is self-similar.

The velocity steadily gets reduced up to the velocity of the surrounding medium. The potential core is said to be a jet's central region with almost uniform mean velocity. In other words, the axial distance from the nozzle exit at which the jet velocity (that is, the nozzle exit velocity) begins to decrease is the jet core. A pusher turboprop engine has an interior exhaust duct structure that directs the hot turbine gases through and out of the engine nacelle and around the rear spinner surrounding the propeller hub. The jet flow temperature at the stub exit varies with speed and altitude at different in-flight operating conditions. The exhaust jet temperature profile is a function of the exhaust jet velocity ratio. The jet temperature at a given axial distance from the exhaust stub can be estimated using various methods.

1.7.3 Aerothermal studies

Aerothermal involves aerothermodynamics coupling with spacecraft (or aircraft) surface chemistry. They are related to the heating of surfaces due to their contact with the flow of air or other gases. Key areas within this field are plume heating, aerodynamic heating, on-orbit contamination, and free molecular heat transfer. The convection causes an additional heat load through system heat dissipation and environmental radiation. At supersonic speeds, the temperature impact is such that material performance limits can be impacted. Studies to quantify and control aerodynamic heating include wind tunnel testing, numerical simulations, or flight testing. Aerodynamic heating is of interest in all aspects of flight and spacecraft.

1.7.4 Nacelle

A nacelle is the structural housing for an aircraft engine. In civil aircraft, nacelles are invariably externally pod-mounted, either slung or under mounted over the wing, or attached to the fuselage shown in Figure 1.12. The front part of the nacelle is the intake, and the aft end is the nozzle. Military aircraft engines are invariably located in the

fuselage; the front is called the intake in the absence of a nacelle. In addition to housing the engine, the main purpose of the nacelle is to facilitate the internal air flow reaching the engine face (or the fan inlet of gas turbines) with minimum distortion over a wide range of aircraft speeds and attitudes. The intake acts as a diffuser with an acoustic lining to abate noise generation for subsonic turbofans. The inhaled air-mass flow demanded by an engine varies considerably. At idle, just enough air flow is required to sustain combustion, whereas, at maximum thrust, the demand for air is many times higher (Ajoy Kumar Kundu, 2010). Figure 1.13 shows the pusher aircraft's nacelle, engine, and exhaust stub.

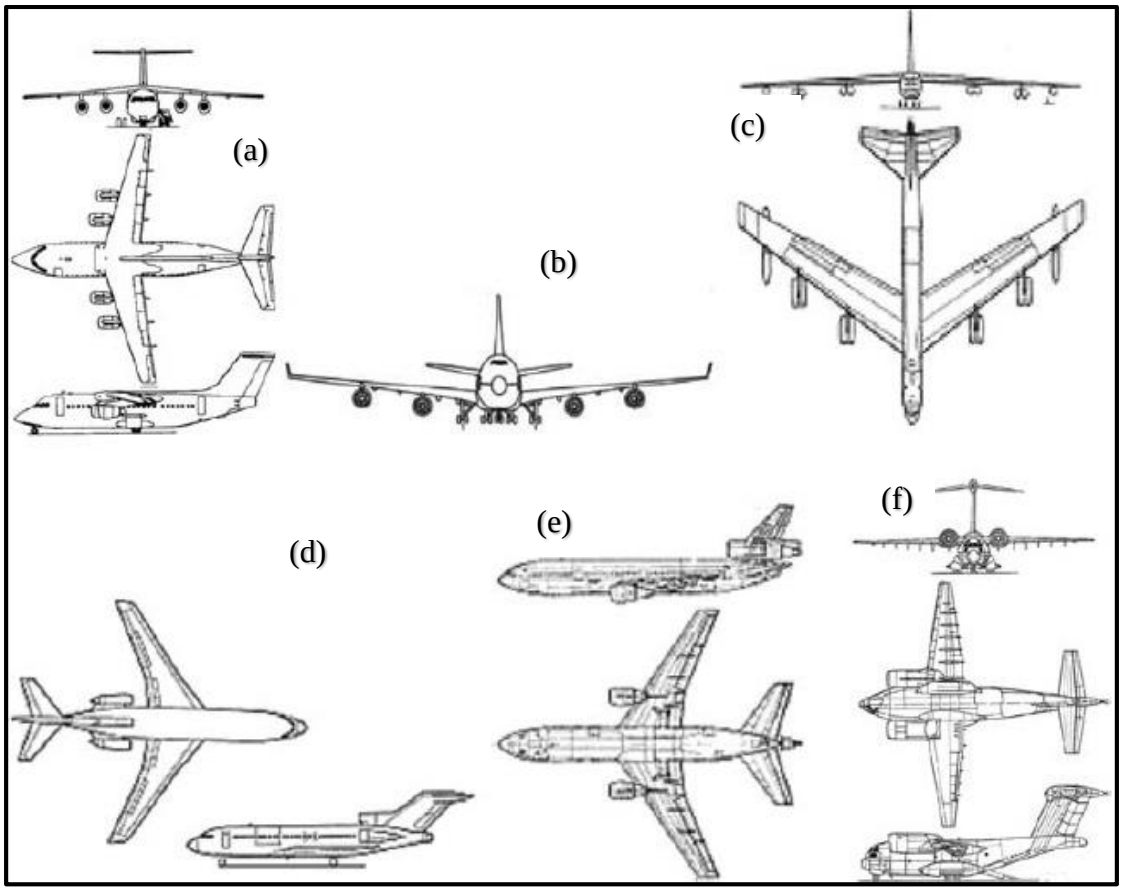

Figure 1.12 Options for conventional civil aircraft nacelle positions: (a) Four Engines on High Wing (b) Four Engines on the Low Wing (c) Six Engines on the high Wing (d) Centre S-Duct (e) Over Wing Three Engines (f) Centre Straight Duct

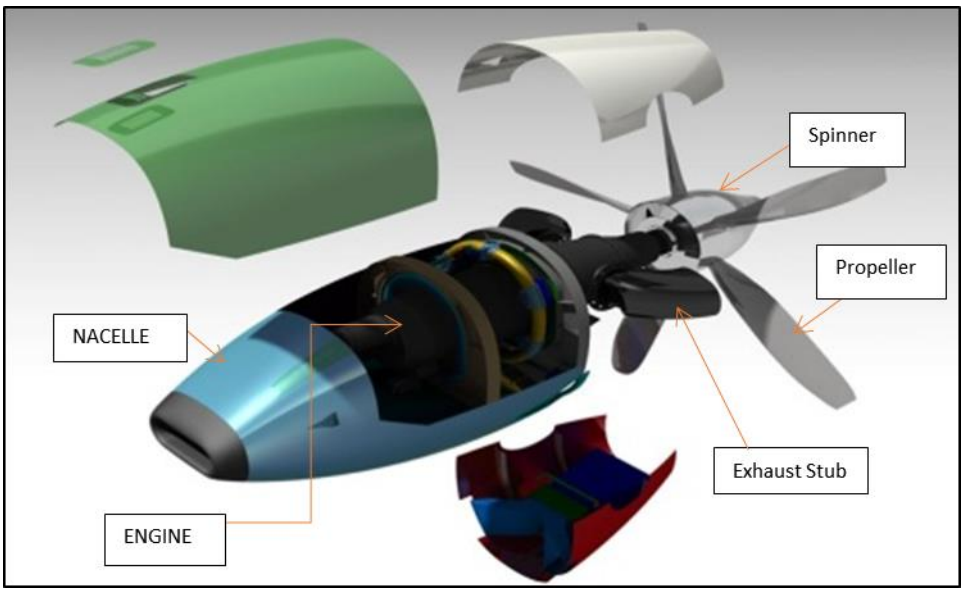

Figure 1.13 Nacelle and exhaust stub

1.7.5 Nacelle Zone Temperature

Fast growth is seen in aircraft manufacturing, and there is a rising demand for light weight, high-strength materials. Figure 1.14 (a) shows the light transport turbo-prop commuter aircraft with pusher propeller configuration considered in the present study. It consists of a nacelle and ducts made of Aluminum alloy sheets and composite material. This Aluminum alloy's tensile Yield Strength (Fty) is sensitive to temperature. With the temperature rise from 204°C to 276°C, the Tensile Yield Strength of the material drops from 60% to 40% of Fty (100% Fty considered at room temperature). The nacelle is expected to have a higher heat resistive capacity, as it houses the engine and its auxiliary components which dissipate heat energy at different temp ranges in a conjugated manner and reach elevated temperatures. The nacelle is made of an Al alloy sheet, so it cannot withstand high temperature dissipating from the engine. Hence, the bay region between the engine and the nacelle needs to be ventilated to circulate the air, enhancing the heat transfer and reducing the amount of heat reaching the nacelle.

Through numerical simulations, the rate of heat transfers and hence the nacelle surface temperatures can be predicted for any air flow value, inside the bay region, based on sizing the NACA flush inlet and louvers outlet. The inlet and outlet for the air circulation inside the bay area must be placed on the nacelle surface shown.

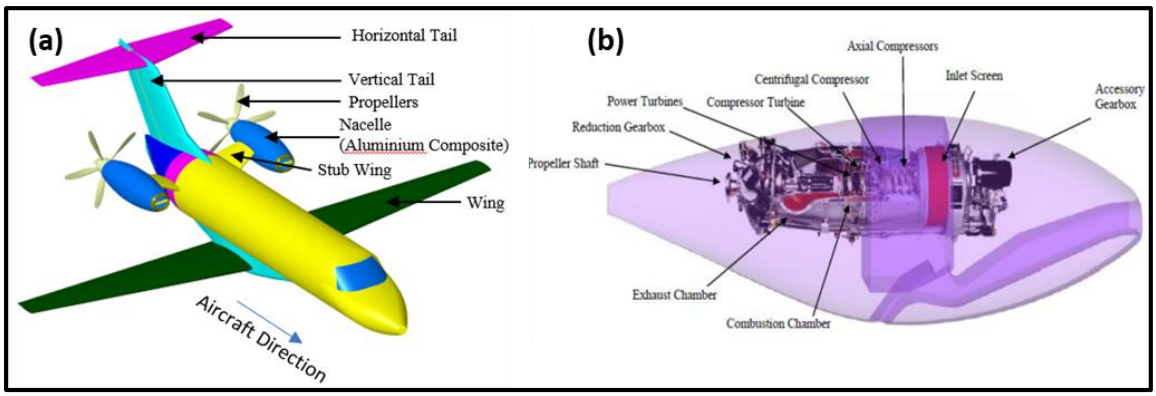

Figure 1.14 (a) Pusher-propeller aircraft overview (b) Engine components

1.8 Typical flight phases and engine ratings

The phases of an aircraft flight are the taxi stages before take-off, take-off, climb, cruise, descent, final approach, landing, and taxiing as depicted in Figure 1.15.

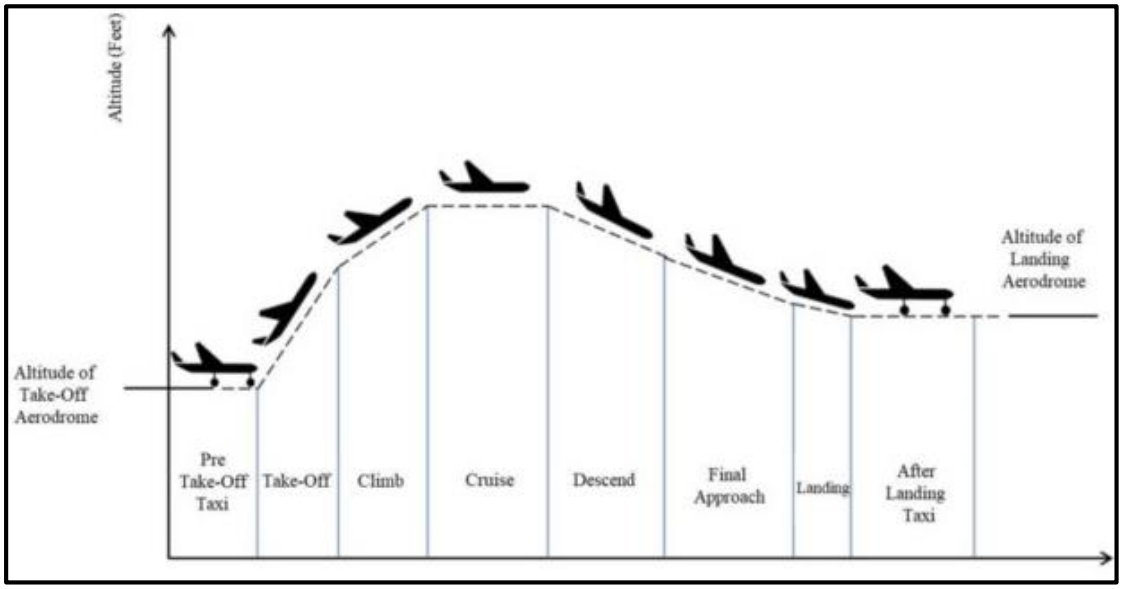

Figure 1.15 Typical flight phases of an aircraft

- Pre-Take-Off Taxi During the pre-take-off phase, the pilot initializes the flight management system and sets up various systems in the aircraft. Flight planning and performance planning happen during this phase.
- The TAKEOFF phase starts when applying take-off thrust and extends until reaching the acceleration altitude. At thrust reduction altitude, the thrust levers are normally set in the climb thrust detent (CL detent).

- The CLIMB phase extends from the acceleration altitude to the top of climb (ToC) cruise flight level.
- The CRUISE phase extends from the top of climb (ToC) point to the top of descent (ToD) point. It may also include intermediate climbs as well as en-route descents. At any time, the pilot can define a step climb to determine the cost and time savings of flying at a different flight level.
- The DESCENT phase starts at the top-of-descent point by pushing the altitude knob for a managed descent or pulling the altitude knob for an open or selected descent from the cruise altitude.
- The APPROACH phase starts when the pilot activates and confirms the approach or when the approach deceleration pseudo waypoint is passed, and the aircraft is below 9500 ft above ground level in managed flight.
- The GO-AROUND phase is activated when the thrust levers are moved to the TOGA (Take-Off and Go Around) position while in the APPROACH phase. The FMS then guides the aircraft through the missed approach procedure.
- The landing phase is the phase of flight from the point of transition from nose-low to nose-up attitude, immediately before landing (flare), through touchdown, and until the aircraft exits the landing runway, comes to a stop or when power is applied for take-off in the case of a touch-and-go landing, whichever occurs first.

1.8.1 Engine Ratings

The power of the turbo-propeller engine establishes ratings. These ratings, in the present case, are defined as they are either continuous or limited to specific time durations.

- Take-off - This rating is the maximum power permissible and corresponds to 1200 SHP at 1700 rpm at sea level up to 50ºC ambient temperature. The maximum allowable output torque must not be exceeded.
- Maximum Continuous - This rating corresponds to 1200 SHP at 1700 rpm up to 45ºC ambient temperature, sea level, and static conditions. It is intended for emergency use at the discretion of the pilot.

- Maximum Climb/Maximum Cruise - This is the maximum approved power for climb and cruising.
- Normal Climb/Normal Cruise - This power setting corresponds to 1000 SHP at 1700 rpm, sea level, up to 47ºC ambient temperature and is the maximum power approved for normal climb and cruise.
- Hi-idle/Flight Idle: Power is obtained by placing the power control lever in the Idle position with the fuel condition lever in Hi-idle position.
- Lo-idle/Ground Idle: power is obtained by placing the power control lever in the Idle position with the fuel condition lever in the Lo-idle position.
- Reverse - Either full or partial reverse thrust is obtained by moving the power control lever to any position below Idle.

1.9 Computational Fluid Dynamics

Computational Fluid Dynamics (CFD) is concerned with obtaining a numerical solution to fluid flow problems using computational techniques through proper mathematical modelling. The advent of high-speed and large-memory computers has enabled CFD to obtain solutions to many flow problems, whether compressible or incompressible, laminar or turbulent, and chemically reacting or non-reacting. The equations governing the fluid flow problem are the continuity (conservation of mass), the Navier-Stokes (conservation of momentum), and the energy equations. These equations form coupled non-linear partial differential equations (PDEs). Because of the non-linear terms in these PDEs, analytical methods can yield very few solutions. In general, closed-form analytical solutions are possible only if these PDEs can be made linear, either because non-linear terms naturally drop out (e.g., fully developed flows in ducts and flows that are inviscid and irrotational everywhere) or because nonlinear terms are small compared to other terms so that they can be neglected (e.g., creeping flows, small amplitude sloshing of liquid etc.). If the non-linearities in the governing PDEs cannot be neglected, which is the situation for most engineering flows, then numerical methods are needed to obtain solutions. CFD is the art of replacing the differential equations governing the fluid flow, with a set of algebraic equations (the process is called discretization), which in turn can be solved with the aid of a digital computer to get a final solution. The well-known discretization methods used in CFD are the finite

difference method, finite volume method, finite element method, and boundary element method. (ZEUS Numerix, 2009).

1.9.1 The working method of CFD

CFD applies numerical methods to develop approximations of the governing equations of fluid mechanics in the fluid region of interest. The domain is discretized into a finite set of control volumes; partial differential equations are discretized into a system of algebraic equations. All these algebraic equations are then solved numerically (on a computer) to render the solution field. The solution is post-processed to extract quantities of interest (e.g. lift, drag, torque, heat transfer, separation, pressure loss, etc.). The results of CFD analyses are quite useful in conceptual studies of new designs, detailed product development, troubleshooting, and redesign. (Ganesan S 2011).

1.9.2 Advantages and limitations of CFD

Advantages:

1. Relatively low cost.
    a) Using physical experiments and tests to get essential engineering data for design can be expensive.
    b) CFD simulations are inexpensive, and costs will likely decrease as computers become more powerful.
2. Speed
    c) CFD simulations can be executed in a short period.
    d) Quick turnaround means engineering data or changes if any, can be introduced early in the design process.
3. Ability to simulate real conditions
    e) Many flows and heat transfer processes cannot be (easily) tested, e.g., hypersonic flow.
    f) CFD provides the ability to simulate any physical condition theoretically.
    g) CFD provides an ability to study the flow in greater detail.
4. Hasten the process of realizing the product.

Limitations:

1. Physical models.
   a) CFD solutions rely upon physical models of real-world processes (e.g., turbulence, compressibility, chemistry, multiphase flow, etc.) which are complex to simulate numerically.
   b) The CFD solutions can only be as accurate as the physical models on which they are based.
   c) High Reynolds Number simulations require more powerful and high-speed computers.
2. Numerical errors.
   a) Solving equations on a computer invariably introduces numerical errors.
   b) Round-off error: due to finite word size available on the computer.
   c) Truncation error: due to approximations in the numerical models. Truncation errors will go to a minimum as the grid is refined.

1.9.3 Elements of CFD

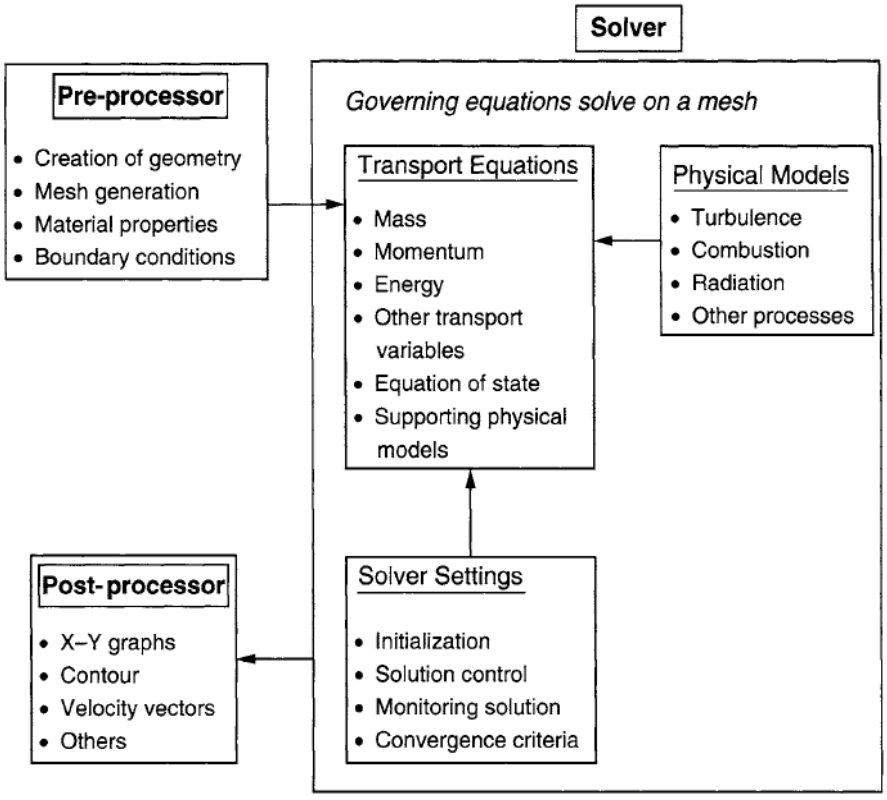

Figure 1.16 Elements of CFD

1.10 Thesis structure

This thesis reports an analytical methodology adopted for the engine exhaust stub design. Discusses the numerical studies for the estimation of the surface temperature on exhaust gas impingement on the propeller and aircraft surfaces and its validation by experimentation.

Chapter 1 of the thesis deals with Introduction, which gives insight on the growth in air transport in India and increasing demand for regional connectivity, and economic growth in the Indian corporate sector. In addition, it also provides an overview of the turboprop-powered aircraft powerplant and propeller integration and operational aspects with typical illustrations. The importance of turboprop engine exhaust systems and jet thrust on aircraft performance is discussed.

Chapter 2 covers an extensive Review of the Literature. In this chapter, work done by various researchers in the field of jet flow and its characterization and entrainment effects are reported. In addition, various research carried out on engine exhaust gas impingement on aircraft structures, and nacelle bay ventilation studies emphasize the technological progress that occurred throughout this period are discussed. The review examines several techniques for finding the thermal effect of the exhaust gases expelled over the aircraft's skin and propeller, which is an important analysis in arriving at several design recommendations and modifications, such as the use of thermal and corrosion preventive coating to operate within the safe limits of the material.

Chapter 3 provides the exhaust stub sizing approach and analytical calculation of the temperature of the exhaust plume at the exit plane, numerical analysis, and experimental setup preparation.

Chapter 4 deals with the detailed numerical and experimental results. It contains the results acquired from the numerical analysis for the pusher and tractor configuration. Also touches upon the experimental validation for a few cases.

Chapter 5 concludes the purpose of the research work with findings and justifiable explanations. Finally, it highlights the scope of future study and the prospect of collaborative multidisciplinary research.

Chapter 6 provides the backbone of the research by listing the various references cited throughout the thesis.

CHAPTER 2

LITERATURE SURVEY

The understanding and decision-making ability are motivated by the experience's inspiration. Obeying the concept of "standing on the shoulders of the giant," a scholastic review of some similar or near similar work is done to contrive objectives for the research. The research work and findings of these papers are categorized into three ways, one on the jet flow, the other on the engine exhaust effects on aircraft and zone and bay temperature studies, they are briefly summarized here.

2.1 Jet Flow

B. J. Goldstein, K. A. Sobolik and W. S. Seol (1990) have studied the behaviour of convective heat transfer of a heated circular air jet impinging on a flat surface. Also, the radial distributions of a recovery factor, the effectiveness and the local heat transfer coefficient are presented. In this study, the entrainment effect for a single circular impinging air jet has been investigated. The ratio of the jet-to-plate spacing to the jet diameter is varied between 2 and 12. The relationship between the effectiveness distribution and the mass flow rate is determined. The jet Reynolds number is varied between 61,000 and 124,000 to determine the effect of the mass flow rate. The recovery factor shows no dependence upon the mass flow rate of the jet. There exist significant local minima in the recovery factor near the impingement point ($R/D \approx 1.5$) for small jet-to-plate spacing ($L/D \leq 4$), apparently due to energy separation. The impingement region recovery factor is larger than unity for large jet-to-plate spacings ($L/D > 6$) due to the heating of jet flow by the entrainment of "warmer" ambient air. The concept of film cooling effectiveness has been adopted to express the adiabatic wall temperature in a dimensionless form. The impingement cooling/heating effectiveness is independent not only of the temperature difference between the jet and the ambient but also of the mass flow rate of the jet.

M. Behnia, S. Parneix, and P. Durbin (1997) aimed at accessing the ability of computational fluid dynamics to accurately and economically predict the heat transfer rate in an impinging jet. Due to difficulties in performing and comparing experiments, a numerical simulation of the problem would be ideal for quantifying the effect of

parameters of interest. However, turbulent impinging jets have complex features due to entrainment stagnation, and high streamline curvature. The behaviour of Nusselt number variation with the jet-to-pedestal distance needs to be known for designing and optimizing impingement cooling or heating systems. The k-ϵ computations yield over estimated values, whereas V2F simulations are very close to the experiment. The only disagreement is for H/D=4 where the experimental maximum Nusselt number is higher than for H/D=1 and 2. At the outset, the confinement present in most industrial applications does not significantly impact the wall heat transfer coefficient unless the jet-to-target spacing is considerably reduced (H/D < 0.25).

2.2 Engine Exhaust Gas Impingement on Aircraft Structures

Zong-Hong Xie and Shi Wu (2016) have studied the thermal effects of the engine exhaust jet flow impingement on E-2C aircraft structures. Prediction of heated areas on the aircraft structures and the structural thermal strain is analyzed and addressed using unidirectional fluid-thermal-structure coupling (Monolithic coupling approach), using CFD solver-based FLUENT software and the CSD solver-based MpCCI method. The steady thermal flow analysis was carried out on aircraft with the outer-wing folded and unfolded. Multi-reference frame (MRF) model in steady state condition and a sliding mesh technique in the transient state was adopted to solve the structure-thermal strain. ABAQUS was adopted to analyse the heat transfer inside the aircraft structure and the structure's thermal strain. However, the CFD result showed a seriously heated area located at the lower vertical tail, especially at the composite leading edge when wings were folded and the maximum temperature were about 70°C. In comparison, the vertical tail remained at a normal temperature at 30°C with wings unfolded. Besides, the thermal flows showed little effect in other places of the aircraft, where the temperature was observed 30°C. A steady coupled temperature-displacement analysis was presented using the temperature data in the steady CFD results. The CFD results showed that the maximum principal strain in the vertical tails appears at the boundary of the composite leading edge and the value is about 1700 micro-strains, while in the other metal structures the maximum principal strain was only 784 micro-strains. However, the periodic thermal strain on the leading edge which was made by composite materials would result in thermal fatigue and adversely affect the mechanical

performance. Besides, structures became apt to undergo chemical corrosion in the wet sea environments. A structure enhancement or special thermal protection, such as Thermal barrier coatings (TBCs), was suggested.

Jianping Yin and Arne Stuermer (2012) have studied the aeroacoustics phenomena characteristic of a pusher-propeller configuration, and their aerodynamic causes are discussed in this paper. The configuration under study is an industrially relevant design with a wing-mounted pusher propeller, which features a close coupling of the turboshaft engine exhaust nozzles and a five bladed propeller. The numerical analysis approach is applied in this study, which couples a high-fidelity unsteady aerodynamic simulation using the DLR TAU-Code with the DLR APSIM code for a subsequent aeroacoustics evaluation. The flow field exhibits strong unsteady phenomena, which are periodic in nature, linked to the rotational speed and the number of blades of the propeller. Therefore, it is convenient to refer to an azimuthal position during propellers' rotation instead of using time itself. The initial position, the angle of $\Psi = 0°$, is defined as corresponding to the reference blade pointing upwards along the z-axis. The blade reference angle increases in the direction of rotation, i.e., counter- clockwise when looking at the propeller from behind. Vorticity contours are plotted for one instant in time taken from the unsteady simulation of the simplified test rig with the engine jet simulation to show the important vertical structures such as the engine jets and the blade wakes and tip vortices. The interaction with the engine jet has a significant effect on the propeller forces. During one rotation, each blade passes through the engine jet twice, once on the downward sweep on the inboard side and once on the upward sweep on the outboard side of the nacelle. The final important interaction effect is the influence of the wing wake. For both of the STR configurations, this effect can be seen in the local increase in blade thrust production at blade azimuthal positions of around $\Psi = 108°$and $\Psi = 142°$. Due to the reduced axial flow velocity in the wake deficit, an increase in the blade section angle of attack results, which dominates the slight reduction in effective velocity.

Wienczyslaw Stalewski (2016) has developed and optimized the exhaust system for light turboprop aircraft. The optimization process aims to design the exhaust system, which removes the exhaust gases possibly far from the airframe, especially during a

descent flight. Apart from removing the exhaust from the turboprop engine, the engine supports the cooling of the engine bay. Three-dimensional analysis of flow around the airplane (including the effect of the propeller) and inside the exhaust system is conducted by the application of URANS solver-based ANSYS FLUENT software. The design and optimization of the exhaust system were conducted using the parametric-design methodology. The parametric model was built using the in-house software PARADES in the present methodology. The software uses the NURBS (Non-Uniform Rational B-Splines) representation of parameterized objects. The design criteria in the presented design problem were formulated mainly based on airflow properties both externally, around the aircraft, and internally inside the exhaust ducts. Aerodynamic analyses were conducted using the CFD-software package. The Navier-Stokes equations were used to solve the problem, and the Virtual Blade Model (VBM) was used to simulate the rotating propeller. Time-averaged aerodynamic effects of rotating blades are modelled using momentum source terms placed inside the fluid-disk zone. The source terms are computed based on the Blade Element Theory. The research consisted in determining the influence of changes of design parameters, such as the direction, length or diameter of the exhaust channels, on the effectiveness of alleviating unfavourable effects associated with the propagation of the exhaust gases.

Arne Stuermer (2008) carried out the unsteady simulations on Contra Rotating Open Rotor (CROR) or Contra Rotating Propellers (CRP) and also known as Propfan configurations. A generic 8×8 pusher CROR powerplant configuration was designed, and simulations were carried out using URANS at cruise conditions of M = 0.75 and an altitude of 35,000 ft. for an angle of attack of $\alpha = 0°$ and $\alpha = 2°$ respectively. The generic baseline pusher CROR configuration and blades were modelled using CATIA V5. The rotor was designed with a diameter of D = 4.2672m, and the hub-to-tip ratio was d/D = 0.355. The blade features NACA65-series aerofoils near the root to the radial position of r/R = 0.4 and then transitions to NACA16-series aerofoils, which are used from r/R = 0.55 outward. The mean line tip sweep is $\varphi = 35\circ$. The performance of this blade design was verified through RANS computations of an 8-bladed SRP with the DLR TAU-Code. An infinite cylindrical hub of a diameter equal to the spinner diameter of d/D = 0.355 is used, for which a structured Euler mesh was created using the ICEM

HEXA mesh generation software. Computations were run both for the design cruise case (M = 0.75 h = 35,000ft) and the take-off case (M = 0.2 at sea level conditions). The report's outcome describes the propeller surface flow topology at low and high speeds. The blade suction side shows a significant flow separation at low-speed flight conditions. The leading-edge separation region also shows up as regions of high vorticity levels. The vorticity contours show the complex interaction of the forward rotors blade wakes and tip vortices with the aft rotor.

B. Han and R. J. Goldstein (2006) studied the heat transfer impingement on a circular or slot jet examined in this paper. Flow characteristics of each region are reviewed. Local and averaged heat transfer characteristics for both single jet and array of jets are considered, including the effect of Reynolds number and nozzle-to-plate spacing. Characteristics of the major flow region – free jet, stagnation flow, and all jet regions are briefly described. With certain airplane configurations, be placed sufficiently far forward so that the gases are cool enough when passing through the propeller to avoid overheating the propellers. However, the presence of a hot, one-sided exhaust gas column, through which the major thrust-producing portions of the propeller blades must intermittently rotate, introduces undesirable vibrations and high stresses into the propellers, and in high-power installations, such conditions cannot be tolerated. It has been seen that the local Nusselt number near the stagnation region is nearly independent of the impact angle becoming less than 30°. Some parameters that affect the heat and mass transfer of hot impinging gas are listed below

- Nusselt Number
- Reynolds Number
- Nozzle to rotating plane spacing
- Curvature of surface
- Angle of impact
- Nozzle geometry
- Rotation

J. M. Mergin (1953) invented a method to minimize the propeller blade temperature caused due to the exposure of exhaust gases, and the invention aims to overcome the general disadvantage of the pusher turboprop installations. The main objective of his

invention was to provide a means of inhibiting undue temperature rise in a propeller system which is disposed of in an enveloping flow of hot gas, and a further objective is to provide a cooling means for the propeller when heated due to impingement of hot gases in pusher configuration. To accomplish this, the single embodiment of the invention is applied to a pusher-type power plant and propeller installation in an aircraft body associated with an aircraft wing. This arrangement allows the continuous flow of cool air over the engine exhaust manifolds but also permits selective operation of propeller de-icing while maintaining a substantially uniform flow of air, regardless of its temperature, through the propeller.

Greco et al. (1990) invented the apparent method to improve the design of pusher turboprop engines. The primary object of the invention is to provide an improved method, structure for ducting turbine exhaust directly out the rear of the engine nacelle without passing through the nacelle sidewalls. It is also an object to provide a turboprop engine in which standard pusher propellers can be separated from the detrimental effects of the hot turbine exhaust gases. The nacelle includes an outer sheet metal skin or wall which surrounds the engine and gearbox with an aerodynamically favourable outward configuration. A nacelle cavity is thereby formed between the outer wall and the engine housing. The lower portion of the nacelle also includes a cooling air inlet which directs air through the engine oil cooler and hence rearward through the cooling air exhaust duct towards and out the aft end of the nacelle. Each of the blades is attached to the hub at its root and passes radially through an opening in the spinner inner wall, through the hollow cuff member and finally through an opening in the outer wall.

Mahesh S. Mali, Vinay C A, and Sanjay V. Kadam (2018) have conducted a numerical study on the optimized exhaust system to estimate the exhaust jet impingement on the propeller and on the aft nacelle surfaces using RANS-based k-epsilon model in commercially available ANSYS FLUENT software. The contours of velocity magnitude along the cut plane (for both actual & optimized stub) indicate that the exhaust gas coming from the stub and mixing with the outer air because of propeller rotation. A high-velocity region was observed at the downstream side of the propeller; it indicates that the propeller developed a greater amount of thrust. From this study, it is observed that the temperature increases from the root to tip of the blade for the

optimized stub. It occurred because the exhaust gas flow was diverted to the tip side of the propeller blade. However, the optimized duct was found satisfactory at given flight operating conditions, and the same duct will be further used for flight testing.

Kong (2000) came up with a study on integrating turboprop engines with engine cooling systems and exhaust-duct and engine-fuselage systems to maximize ram recovery and minimize drag. At cruise, the exhaust duct throat area was decreased from 74 Sq.in to 56 Sq.in to get the discharge coefficient (Cd) of 0.85. The sooting of fuselage was prevented by maintaining a discharge angle of 12° and 4-inch clearance.

Lapka et al., (2019) presented research on the thermal effect of exhaust gas expelled over the aircraft's skin. Aircrafts considered for the study were I-23 with a single engine and EV-55 with two engines. For I-23, the exhaust gas did not hit the airplane skin; hence the temperature dropped from 910K to 400K at a distance of 1-1.5m. For EV-55, at a 20° flap angle, the exhaust gas interaction was observed to be slight, but at 40° and at reverse torque/thrust, the temperature was observed to reach 575K, which was not safe. The researchers tackled the issue by rotating the exhaust stub down slightly to obtain exhaust gas interaction with the airplane skin 370K, which was found to be safe.

2.3 Zone and Bay Temperature

Segal et at., (1997) presented a new engine bay design for a military aircraft which ensured its good ventilation and cooling on the ground and in flight. In addition, a one-dimensional (1D) flow model of the analysed system was proposed.

Balland et al., (2005), A joint Airbus & Snecma study on the aero-thermal methodology that is applied to the nacelle compartment is presented. From that study, radiative and convective heat transfer in the nacelle core compartment of an aircraft engine and compared the results obtained with real engine data.

Olejnik et al., (2021) In this paper, the methodology used in this research is based on computational fluid dynamics tools to adequately model the internal and external flow, find the state of the cooling system and research the results of baffles modification inside the engine cover. Additionally, two types of covers with different sizes of inlets and outlets are tested.

Buonomo et at., (2013) This paper reports on a thermo-fluid-dynamic analysis of the flow field around the aircraft nacelle equipped with a small pusher turbine engine, with the purpose of determining the thermal field on the nacelle surface.

Lapka et al., (2014) Numerical simulations of fluid flow and heat transfer in the engine bay of a small airplane in a tractor configuration were performed in this paper for different conditions at the air inlets and different configurations of the air inlets and outlets. Results of these simulations indicated that the inlet round the spinner mount is beneficial and ensures good cooling of the exhaust system. Moreover, they suggest the additional inlets in the rear part of the hot compartment above the engine and in the cold part of the nacelle instead of the outlet located in the landing gear bay.

Many researchers have come up with various bay ventilation design and analysis to manage the nacelle temperature in the aircraft. These papers show a limited experimental and numerical analysis work carried out on pusher type commuter category aircraft with combination of Al. alloy and composite nacelle material. In the present study, conjugate heat transfer analysis is carried out with fluid mass flow into the engine bay region through inlets placed on the nacelle surface and the temperature values thus obtained is validated with the experimental results obtained from the sensors placed in the aircraft. The nacelle volume is divided in three zones by the adiabatic walls (L frame and M frame) to differentiate the interference of heat from different regions of engine and to avoid heat transfer between zones. This helps in the division of engine bay volume thereby reducing bay ventilation air inlet area. Temperature distribution obtained from the numerical analysis is validated with the experimental data.

2.4 Summary of the literature survey

The literature review involved three different types of research work related to the measurement of exhaust gases from the exhaust duct and their impingement on propeller and on aircraft surfaces. From these papers, some of the important and motivational facts have been gathered to set the objectives for the research work. These summarized facts are pointed below;

- Exhaust gases from the exhaust duct effectively impact the propeller blade surface, especially in pusher-configured aircraft. The high diffusivity of exhaust jets is responsible for the rapid increase in temperature on propeller blades and on aircraft surfaces.
- The studies have shown an improved method, and structure for ducting turbine exhaust directly out to the rear of the engine nacelle without passing through the nacelle sidewalls. Also, a methodology to provide a turboprop engine in which standard pusher propellers can be separated from the detrimental effects of the hot turbine exhaust gases.
- The heat transfer impingement on a circular or slot jet is examined, and the flow characteristics of each region is reviewed. Local and averaged heat transfer characteristics for both single jet and array of jets are considered, including the effect of Reynolds number and nozzle-to-plate spacing.
- The heat transfer coefficients for impinging jets with $T_J=T_\infty$, which have been extensively studied.
- The ability of computational fluid dynamics to accurately and economically predict the heat transfer rate in an impinging jet situation is studied, and due to difficulties in performing and comparing experiments, a numerical simulation of the problem for quantifying the effect of parameters of interest, is brought up.
- It was observed a method was invented to minimize the propeller blade temperature caused due to the exposure of exhaust flue gases, and the invention aims to overcome the general disadvantage of the pusher turboprop installations. Further, a cooling means for the propeller when heated due to impingement of hot gases in pusher configuration was proposed.
- A numerical study on the exhaust system was carried out to estimate the exhaust jet impingement on the propeller and on the aft nacelle surfaces using commercially available ANSYS FLUENT software.
- The thermal effect of the exhaust gases expelled over the skin of the aircraft and propeller is an important analysis in arriving at several design recommendations

and modifications, such as the use of thermal and corrosion preventive coating to operate within the safe limits of the material.

The outcomes of the literature survey are summarized here, as follows:

- The thermal effect of the exhaust gases expelled over the skin of the aircraft and propeller is an important analysis in arriving at several design recommendation and modifications, such as the use of thermal and corrosion preventive coating to operate within the safe limits of the material.
- The thermal analysis of the interaction of the hot exhaust gases with the engine nacelle, wing and flaps of the twin-engine airplane, revealed safe temperature distribution on the skin for the standard operating mode.

2.5 Research gap

The research work reviewed so far shows limited experimental work carried out on estimating the exhaust jet temperature on the propeller blade and aft-fuselage surface in pusher-configured turboprop engines. The research works related to numerical simulation with a rotating propeller disk are also limited. In most of the papers, it has been observed that the exhaust duct is locally optimized to control or divert the jet impingement on the propeller and aircraft surfaces. The study of thermal effects from the engine exhaust jet flow impingement on aircraft structures is also limited. The heat transfer methodology whenever possible was adopted, but the effectiveness of measuring jet temperature was limited. Experimental validation of the numerical model and adaptation of the validated numerical method to aircraft configuration design change is sparse in the available literature. Hence, these limitations in the research work are helping to set objectives for further research to assess the research gap. CSIR-NAL being an aircraft design and development organisation, the issue of thermal flow field mapping management and its exposure to the various parts of the aircraft become critical and mandatory to resume flight tests due to a change in the propeller material from metallic to composite. This called for substantial design change in exhaust stub for plume trajectory management with negligible loss in the jet thrust. The design change mandate and application-orientated problem supported by the gap in the research motivated me to take up this work.

2.6 Objectives of research

The research study is completely focused on analytical, numerical, and experimental studies to find the effect of engine exhaust jet flow on propeller and airframe surfaces for various stub parametric conditions with maximum jet thrust recovery.

The specific objectives of the research work are;

- **Design of exhaust stub to meet optimum jet thrust and satisfy engine and airframe operating conditions.**
- **Using numerical analysis, estimate the temperature of hot exhaust gases impinging on the propeller and aircraft surfaces.**
- **To measure the temperature of hot exhaust gases impinging on the propeller and aircraft surfaces experimentally.**
- **To assess the effect of exhaust jet thrust on overall (Propeller & Jet thrust) engine performance.**

CHAPTER 3

CFD ANALYSIS AND EXPERIMENTATION

3.1 Exhaust stub design and sizing: Analytical Method

It is important to design the engine exhaust stub, which meets the primary requirements of maximizing the jet thrust. Equivalent shaft horse power is sum of shaft horse power and equivalent jet thrust horse power. The designer has to ensure that the exposure of the propeller/aircraft structure/nacelle/wing surfaces to the hot exhaust gas is minimized and overheating is avoided. The design of these exhaust stubs is dictated primarily by the aircraft's configuration. The main geometrical parameters of the stub that influence its performance are as explained below:

a) **Exit area and distance:** Selection of an effective exit area of the stub is governed by the exit distance. It is the minimum distance, measured at the exit plane of the stub, between the aircraft cowling and the exhaust stub. Optimum distance help to limit the exhaust boundary layer attached to the cowling which will help to reduce sooting. Keeping this distance short also reduces the load on the engine exhaust flange. A long exit distance and the resulting overall distance will potentially increase drag, thus reducing aircraft performance. It will also increase the exhaust flange load.

b) **Exit angle:** The turning of the stubs maximizes thrust recovery and minimize the effect of external aerodynamic drag. The exit angle refers to the angle between cowl line and exhaust stub exit direction. A negative angle increases sooting, while a positive angle increases the drag slightly, thus reducing aircraft performance shown in Figure 3.1.

c) **Cutback length:** This length refers to the stub length parallel to the cowling. A longer cutback length will favour flow turning at the inner radius which increases performance.

d) **Stub slant:** The exhaust stub slant refers to the stub's angle with respect to the aircraft side view. Because of propeller wash, the exhaust stub plume can result in turbulence and/or heat build-up on the stub wing (if pusher configuration), wing (if tractor configuration) and tail surfaces. Orienting the exhaust stub in the

opposite direction of the propeller wash can redirect the exhaust plume to avoid these effects.

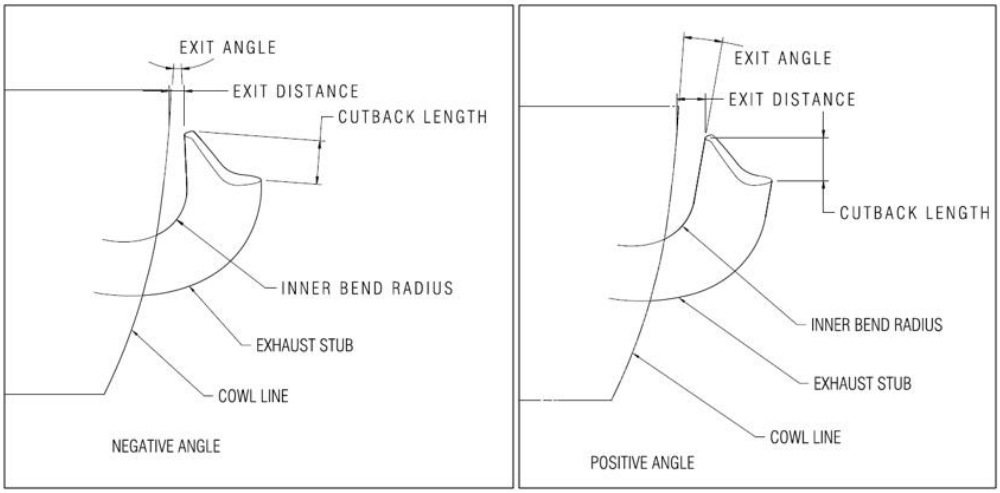

Figure 3.1 Negative and Positive stub angle/exit angle

e) Section shape: The section shape of the exhaust stub must be carefully selected. Basic profiles such as reverse aerofoil, elliptical and aerofoil have their own advantages and the following table shows the main characteristics of each profile.

f) Bend radius: Larger inner bend radius will increase the engine performance by allowing a better exhaust flow, but it also needs a larger cut-out in the cowling.

All the above parameters are very critical from the effective design and operational point of view to control the plume trajectory. Proper exit flow guiding and impingement to reduce potential problems due to overheating aircraft surfaces and sooting. The geometrical parameters of the stub are shown in Figure 3.2.

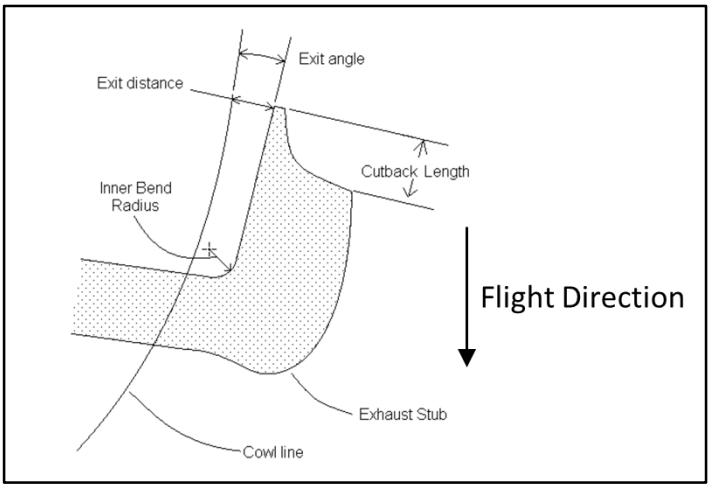

Figure 3.2 Exhaust stub design parameters

3.2 Design considerations

In addition to geometrical parameters, the other main design considerations are a) The exhaust port location, b) Orientation, and c) Engine flange dimensions shown in Figure 3.3. From the geometrical, installation requirements, design consideration, and engine installed performance estimation, the optimum effective stubs exit area chosen is 93 Sq.in (for two stubs as engine having twin ports). For all the conditions and analysis, this exit area is used. The effect of exit area on the engine performance is discussed in subsequent section and details are presented in Figure 3.4 to Figure 3.7.

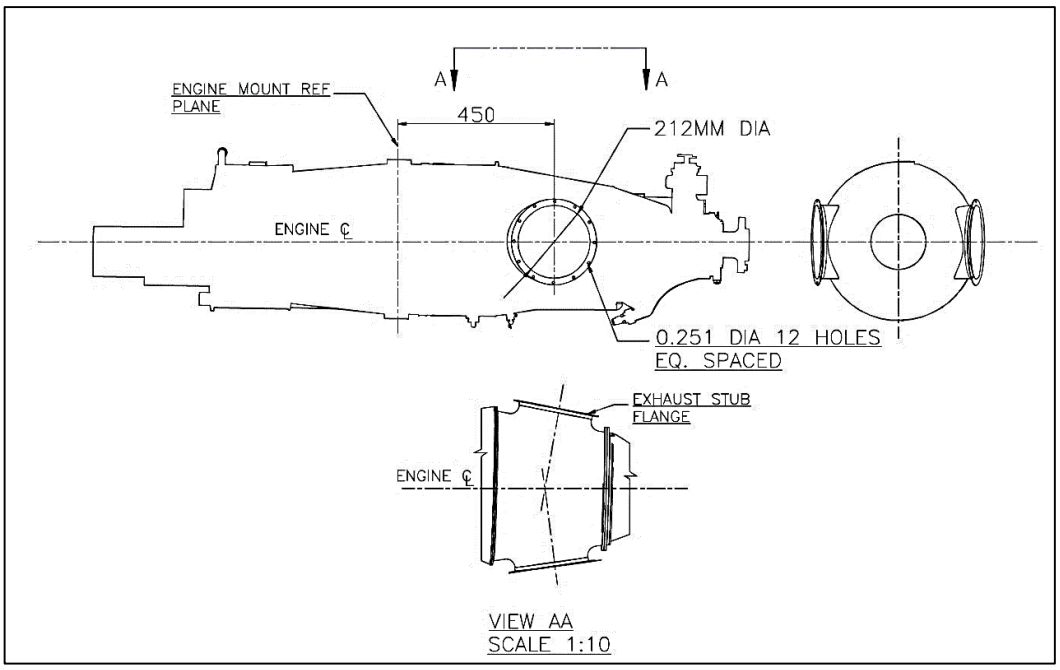

Figure 3.3 Engine Exhaust Twin Port Location

Figure 3.4 shows the carpet plot of ESHP as a function of free-stream Mach number and effective stub exit area, which was generated using the Estimated Engine Performance Program, in the engine installed condition at 30,000 ft, ISA+15°C, and at maximum cruise rating. It is seen from Figure 3.4 that the effect of the stub exit area at a higher Mach number is not significant in terms of ESHP. Also, there is no significant change in ESHP beyond 90 Sq.in total stub exit effective area at all Mach numbers.

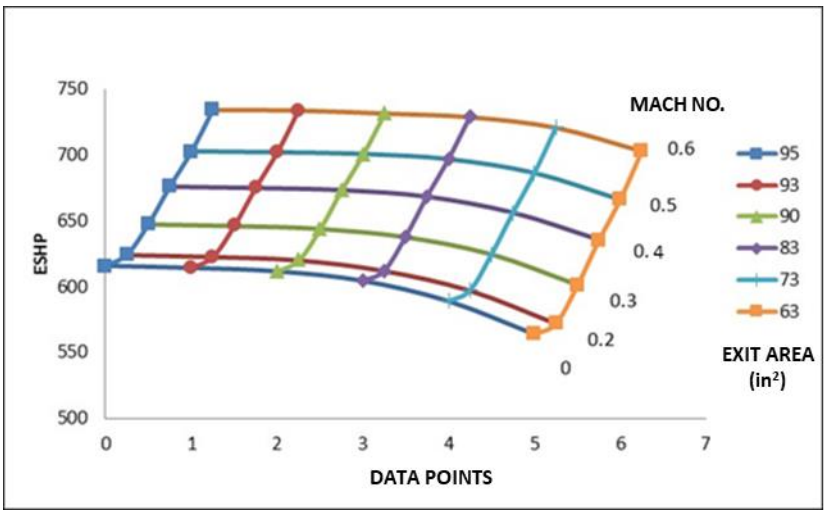

Figure 3.4 Stub Area Studies. Installed case, Altitude: 30,000 ft, ISA+15

The SHP variation with temperature from ISA to ISA+50°C and with various stub exit areas at sea level and for 2 km altitude is shown in Figure 3.5 and Figure 3.7, respectively. It is seen from both the figures that with an effective stub area of 93Sq.in, it is possible to get the full power of 1200 SHP up to ISA+40°C at sea level. It can be seen from Figure 3.7 that as the exit area reduces, the drop in SHP increases. Thus, for the 93 Sq.in stub area at ISA+45°C, there is a drop of about 20(6) SHP, and at ISA+50°C there is a drop of about 75(5) SHP at 2 km altitude.

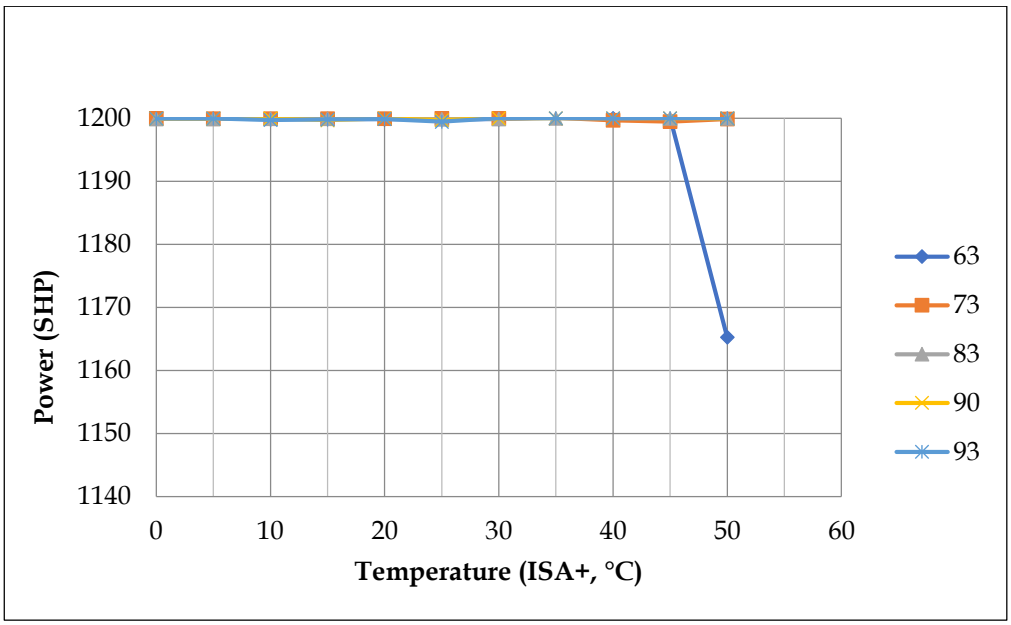

Figure 3.5 Stub Area Studies. Installed case, Altitude: Sea Level

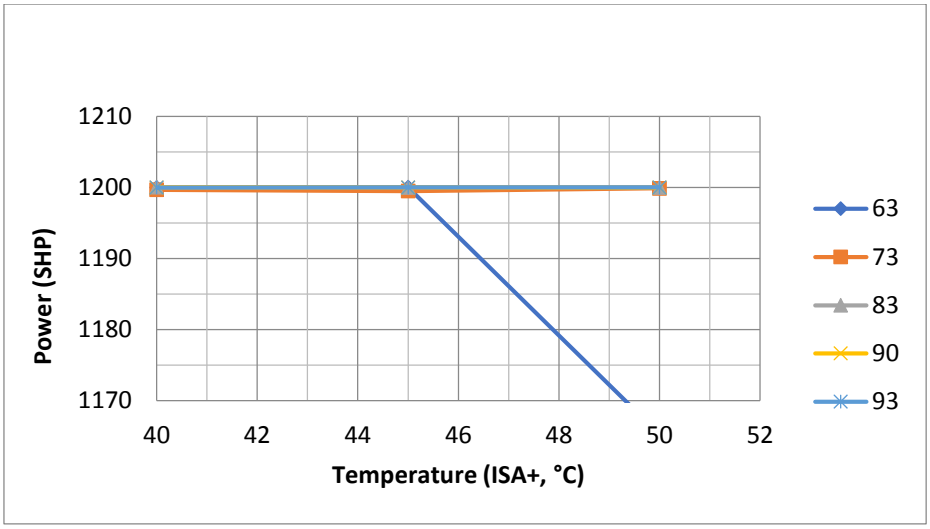

Figure 3.6 Stub Area Studies. Installed case, Altitude: Sea Level zoomed at 45 °C

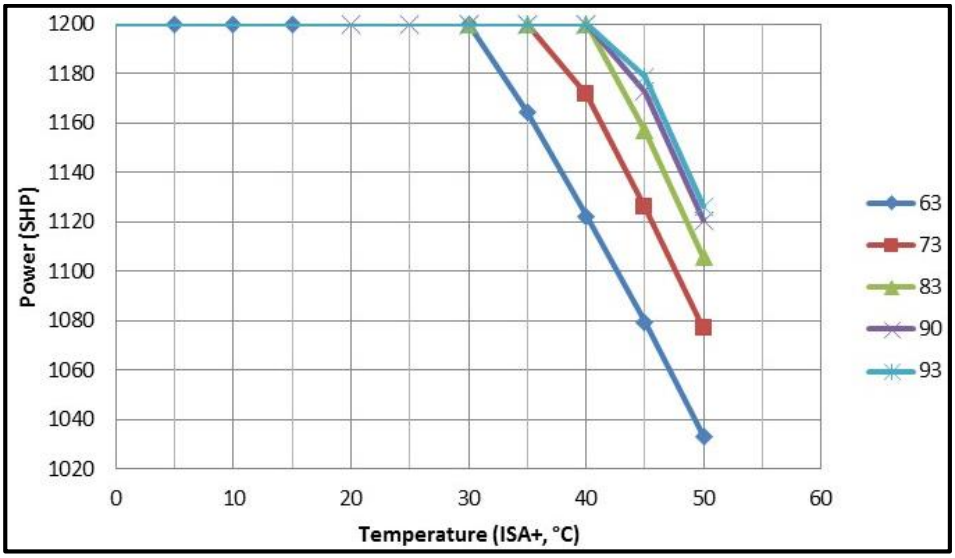

Figure 3.7 Stub Area Studies. Installed case, Altitude: 2 km

In twin-engine aircraft, in an emergency case of single-engine failure (One Engine Inoperative), the other engine must produce full power as per FAR 23 regulations. As per FAR23, the desired climb gradient must be met with a single engine in such conditions. In such a scenario, even a marginal drop in power becomes critical. From Figure 3.6, it can be seen that an effective area of 93 in^2 (0.06 m^2) produces a minimum drop in power. Hence, the selection of 93 Sq.in is justifiable for the present case.

This area gives the coefficient of discharge of 0.85, and the resultant geometric area is 109.4 in^2. (Discharge co-efficient= effective area/geometric area). The stub exit cross-

section selected is elliptical with a cutback angle to minimize the aerodynamic drag. The stub design shown in Figure 3.8 (a) & (b) is adapted for pusher and tractor configurations aero-thermal analysis. Since the geometric area at the exhaust duct ports is 109.4 in^2 (0.07m^2) (54.70 in^2 (0.035m^2) per exhaust port) is slightly larger than the engine flange area (54.62 in^2), the resulting stub will be relatively simple to design aerodynamically. The supplementary studies involving various parameters which affect the aircraft and engine performance are evaluated and tabulated in Annexure 1.

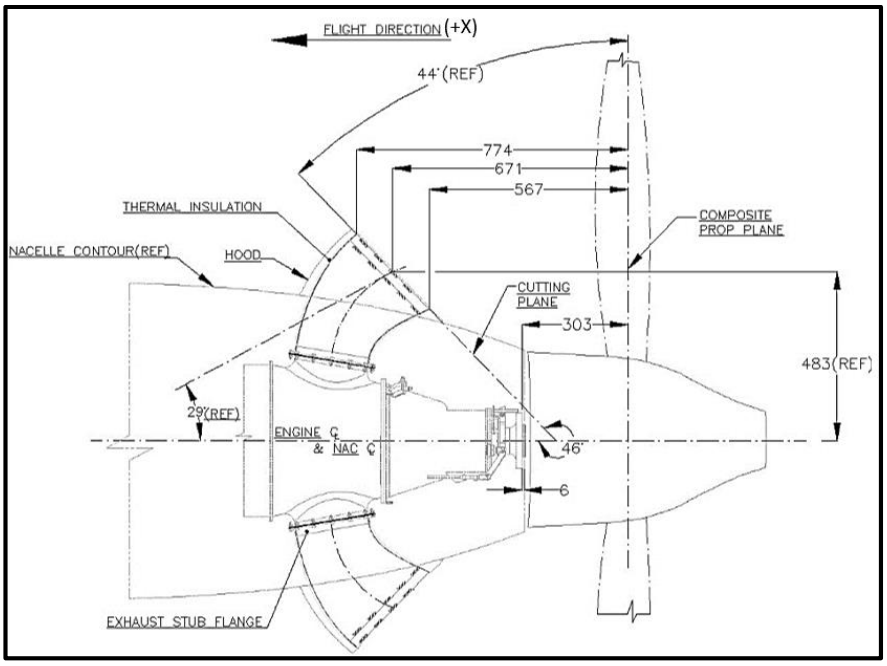

(a)

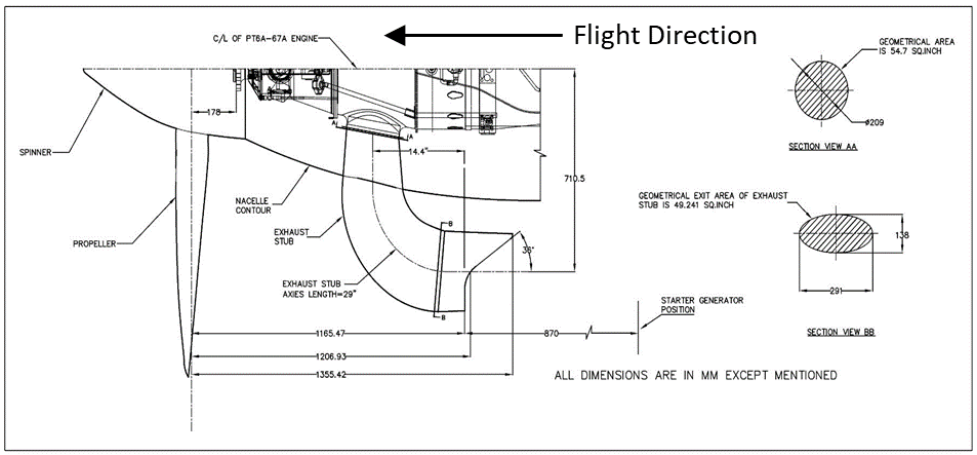

(b)

Figure 3.8 Exhaust Stub –(a) Pusher configuration (b) Full turning contoured stub Tractor configuration

3.3 Estimation of the plume temperature at engine exhaust exit plane-pusher and tractor configurations

Figure 3.9 shows the variation of the exhaust jet temperature (at stub exit) with speed and altitude at maximum cruise power rating. The jet temperature at a given axial distance from the exhaust stub exit plane is calculated as follows:

a) At static condition ($V_1/V_7 = 0$): The distance of the propeller plane from the stub exit plane (L) is 671 mm (for the composite propeller, Figure 3.8 a), and the stub diameter (d_7) is 212 mm. Referring to Figure 3.10, $L/d_7 = 671/212=3.1$.

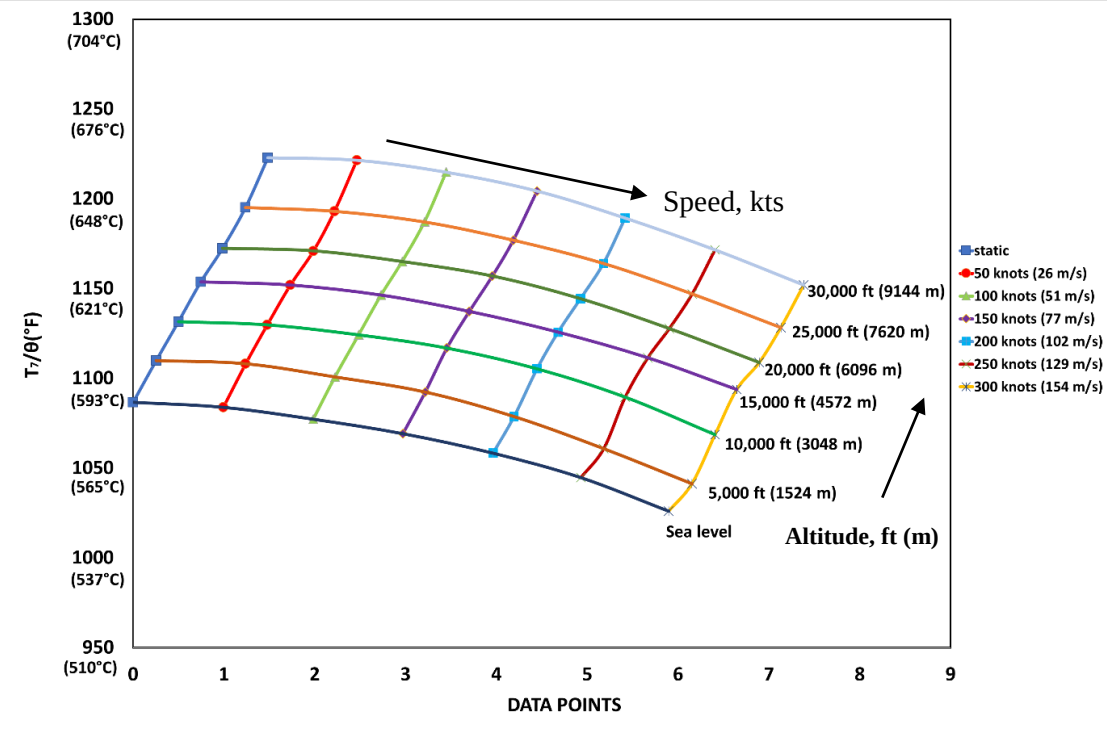

Figure 3.9 Variation of the exhaust jet temperature (at stub exit) with speed and altitude at ISA+25

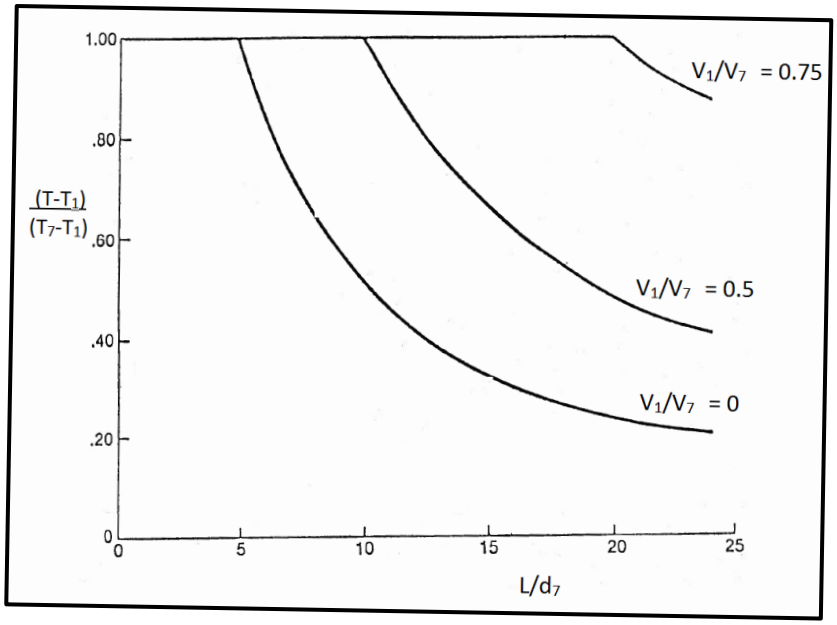

Figure 3.10 Exhaust Jet Temperature Profile (Courtesy engine OEM)

Where,

L/d_7 = Ratio of axial distance from exhaust stub exit plane to exhaust stub diameter

T = Local exhaust jet temperature

T_7 = Exhaust jet temperature (at stub exit)

V_1 = Free stream air velocity

V_7 = Exhaust jet velocity (at stub exit)

Figure 3.10 illustrates the exhaust jet temperature profile as a function of the exhaust velocity ratio (relative to free stream). It should be noted that the temperature profile is based on a one-dimensional analysis that excludes free-stream inflow effects due to aircraft pitch, yaw, and propeller swirl.

From Figure 3.10,

$$(T-T_1)/(T_7-T_1) = 1 \qquad (3.1)$$

Where T - local exhaust jet temperature

T_1 - Free stream air temperature

T_7 - Exhaust jet temperature (at stub exit)

From Figure 3.9, at static, Sea level, ISA + 25°Ccondition

T_7/θ = 1085.4 °F (858.3 K)

Free stream air temperature, T_1 = 40 °C = 104 °F (313.15 K)

Hence, $\theta = \frac{(T_1+460)}{518.7} = \frac{(104+460)}{518.7} = 1.09$

Therefore, T_7 = 1183°F and T = 1183°F (912.5 K) from equation 3.1

Cruise condition (V1/V7= 1.2):

For cruise condition, V1/V7= 1.2 and for the same L/d7 (= 3.1), (T-T1)/(T7-T1) = 1 as before.

T7/θ at M = 0.5 (295 TAS) (151.8 m/s) at 30,000 ft (9144 m) from Figure 3.7 is 1149.3 °F (893.8 K).

Now θ = 0.92 and T7 = θ* 1149.3= 569 °C = 1057.4 °F (842.8 K)

Thus, the local exhaust jet temperatures for static and cruise conditions are 1183 °F (912.5 K) (639°C) and 1057.4 °F (842.8 K) (569°C), respectively, for the proposed stubs. This data is used as inputs to the CFD analysis to evaluate the effect of exhaust temperature on the nacelle & aircraft surfaces. Similar calculations are done for tractor configuration aircraft exhaust stubs as shown in Figure 3.8 (b), for the temperature of the plume at the engine exhaust exit plane & mid-section of the nacelle and tabulated in Table 3.1.

The optimized stub has been fitted on the pusher configuration aircraft. Numerical studies and experimentation carried out are discussed in a subsequent section.

Table 3.1 Temperature at various locations of the exhaust stub-Tractor configuration

Sl. No	Flight Condition	Location		
		Engine stub exit temperature (T_7) °F [K] (°C)	**Exhaust Stub exit plane °F [K] (°C)**	**Local plane exhaust jet temperature (Nacelle midsection) °F [K] (°C)**
1.	Static	1184 [913.15] (640)	1184 [913.15] (640)	1076 [853.15] (580)
	Cruise	1080 [855.3] (582)	1080 [855.3] (582)	982 [800.9] (527)

3.4 Numerical studies with the stub: Pusher Configuration

The Reynolds Averaged Navier Stokes (RANS) Equations are numerically solved to compute the airflow field. Based on the literature and past experience, for this kind of problem, SST k-ω is the most popular turbulent model used in the aero industries. This model is considered appropriate for predicting the flow behaviour in regions away from the wall (Lapka P, 2019). The SST k-*ω* turbulence model is a two-equation eddy-viscosity model which combines the Wilcox k-omega and the k-epsilon models that are used for many aerodynamic applications. It uses a blending function to activate the Wilcox model near the wall and the k-epsilon model in the free stream. It contains a modified turbulent viscosity formulation to account for the transport effects of the principle turbulent shear stress. Generally, the SST k-ω model accurately predicts the onset and the separation size under adverse pressure gradient, and Menter improves the k-ω turbulence models for aerodynamics applications. The three-dimensional flow over the airframe and propeller was solved using commercially available finite volume-based ANSYS-FLUENT software. Spatial discretization of the governing equations was done using a second-order upwind scheme. The SIMPLE scheme achieved the pressure-velocity coupling, and all the computations were performed using a double-precision arithmetic scheme (K. V. S. Phani, 2021).

The governing equations evolved in the SST k-ω turbulence model are formulated by Wilcox (Wilcox, 1993 and 1998). The averaged equations for the conservation of mass, momentum, and energy are as follows:

SST k-ω and Energy Governing Equations (Equation 3.2-3.7):

$$\frac{\partial \rho}{\partial t} + \frac{\partial}{\partial x_i}(\rho u_i) = 0 \tag{3.2}$$

$$\frac{\partial}{\partial t}(\rho u_i) + \frac{\partial}{\partial x_j}(\rho u_j u_i) = -\frac{\partial p}{\partial x_i} + \frac{\partial}{\partial x_j}(t_{ji} + \rho\tau_{ji}) \tag{3.3}$$

$$\frac{\partial}{\partial t}\left[\rho\left(e + \frac{1}{2}u_i u_i + k\right)\right] + \frac{\partial}{\partial x_j}\left[\rho u_j\left(h + \frac{1}{2}u_i u_i + k\right)\right] = \frac{\partial}{\partial t}\left[\rho\left(e + \frac{1}{2}u_i u_i + k\right)\right]$$

$$= \frac{\partial}{\partial x_j}\left[u_i(t_{ij} + \rho\tau_{ij}) + \left(\frac{\mu}{Pr_L} + \frac{\mu}{Pr_T}\right)\frac{\partial h}{\partial x_j} + \left(\mu + \sigma^*\frac{\rho k}{\omega}\right)\frac{\partial k}{\partial x_j}\right] \tag{3.4}$$

Turbulent Kinetic Energy

$$\frac{\partial}{\partial t}(\rho k) + \frac{\partial}{\partial x_j}(\rho u_j k) = \rho\tau_{ij} - \beta^* k\omega + \frac{\partial}{\partial x_j}\left[\left(\mu + \sigma^*\frac{\rho k}{\rho\omega}\right)\frac{\partial k}{\partial x_j}\right] \tag{3.5}$$

Specific Dissipation Rate of Kinetic Energy

$$\frac{\partial}{\partial t}(\rho\omega) + \frac{\partial}{\partial x_j}(\rho u_j \omega) = \alpha\frac{\omega}{k}\rho\tau_{ij}\frac{\partial u_i}{\partial x_j} - \beta\rho\omega^2 + \sigma_d\frac{\rho}{\omega}\frac{\partial k}{\partial x_j}\frac{\partial \omega}{\partial x_j} + \frac{\partial}{\partial x_j}\left[\left(\mu + \sigma\frac{\rho k}{\omega}\right)\frac{\partial \omega}{\partial x_j}\right] \tag{3.6}$$

Energy Equation

$$\frac{\partial}{\partial t}\left[\rho\left(e + \frac{V^2}{2}\right)\right] + \nabla.\left[\rho\left(e + \frac{V^2}{2}\right)V\right] = \rho q + \frac{\partial}{\partial x}\left(k\frac{\partial T}{\partial x}\right) + \frac{\partial}{\partial y}\left(k\frac{\partial T}{\partial y}\right) + \frac{\partial}{\partial z}\left(k\frac{\partial T}{\partial z}\right) - \frac{\partial(up)}{\partial x} - \frac{\partial(vp)}{\partial y} - \frac{\partial(wp)}{\partial z} + \frac{\partial(u\tau_{xx})}{\partial x} + \frac{\partial(u\tau_{yx})}{\partial y} + \frac{\partial(u\tau_{zx})}{\partial z} + \frac{\partial(v\tau_{xy})}{\partial x} + \frac{\partial(v\tau_{yy})}{\partial y} + \frac{\partial(v\tau_{zy})}{\partial z} + \frac{\partial(w\tau_{xz})}{\partial x} + \frac{\partial(w\tau_{yz})}{\partial y} + \frac{\partial(w\tau_{zz})}{\partial z} + \rho f.V \tag{3.7}$$

3.4.1 Geometry and grid generation around the computational model

When dealing with such a complex problem, the geometry must be as realistic as possible, considering analysis time and cost. The computational domain considered for the analysis consists of the nacelle (which includes an inlet, and engine exhaust) and propeller in the aircraft aft-body (Prem Kumar et al., 2013) inferred the propeller domain modelling, where experimental and numerical studies are conducted to optimize the oil cooler duct position for a pusher-type light transport aircraft. In the present work, a turboprop engine with a constant speed five-bladed propeller running at 1700 rpm with ~2.6 m diameter was considered for the computations. A circular domain is enclosed to capture the propeller effects, modelled 1.5 times the propeller diameter as radius. Figure 3.11 presents the model, which comprises mainly the propeller spinner model, nacelle, stub wing, fuselage, and exhaust stub.

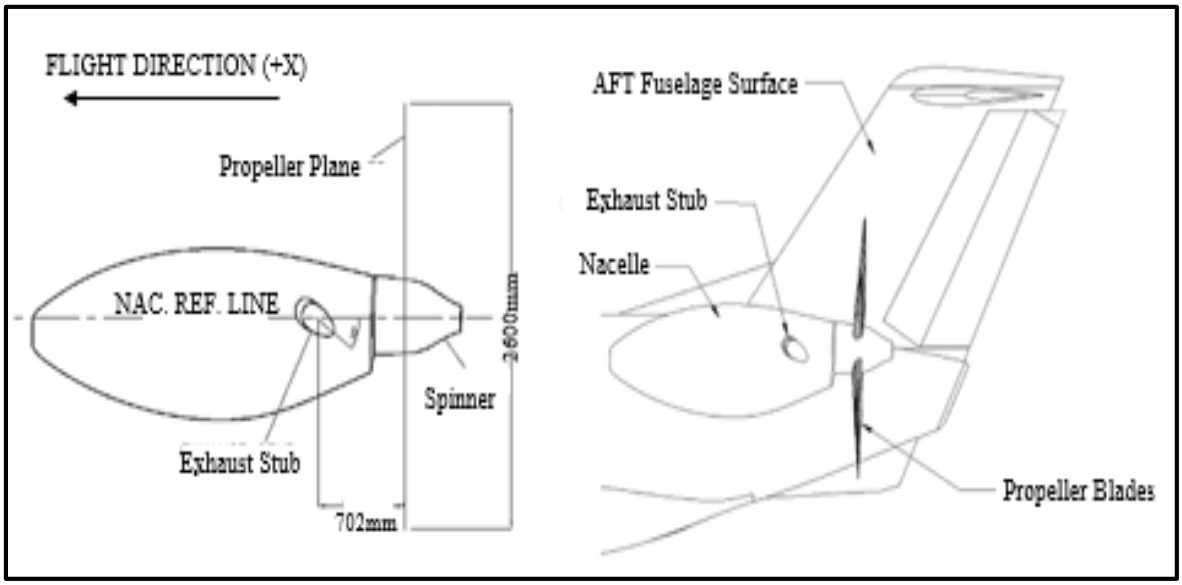

Figure 3.11 Geometry Model of Nacelle, propeller, and empennage considered in the current simulations (side view looking outboard)

The unstructured finite volume tetrahedral mesh was generated using commercially available ICEM-CFD software. The inlet and outlet domain boundaries were located at 4X and 7X upstream and downstream from the geometry reference. The entire domain enclosure is set to 11D, where X is the length and D is the diameter of the model considered for analysis. A circular disk was enclosed around the propeller blades, referred to as the rotating domain. The rotating domain is associated with the main outermost domain, which encloses the nacelle and propeller, referred to as the static

domain, as shown in Figure 3.12. The computation of propeller flows presents some unique requirements for the CFD method. The solver must be capable of handling multiple rigid bodies in relative motion because the propeller needs to rotate relative to the stationary nacelle, and it must be possible to compute a time-accurate solution.

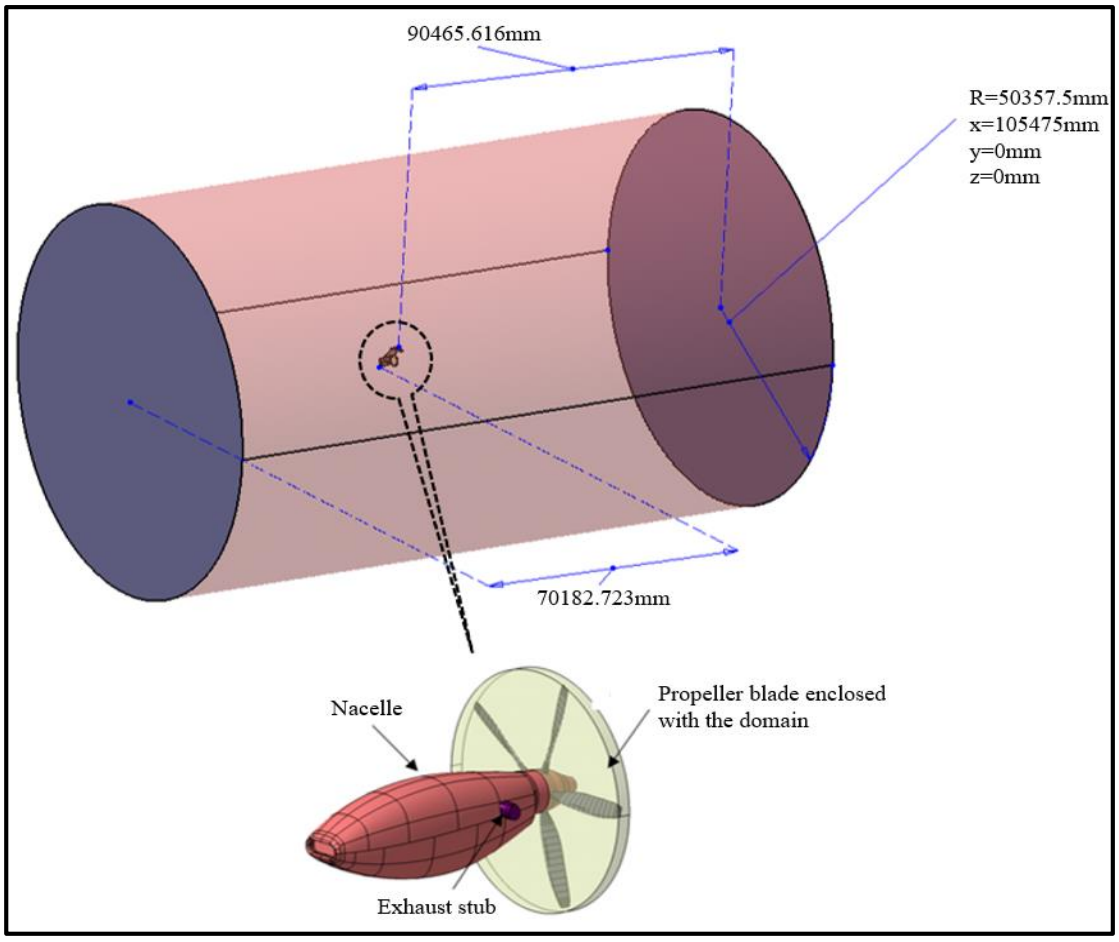

Figure 3.12 Domain enclosing fuselage and propeller

It was ensured that the cell size near the wall was small and gradually higher towards the outer boundary. The Grid Independence Study (GIS) was carried out to ensure that results are independent of mesh sizes. The study was carried out with three grids G1 with 19.96 million, G2 with 20.23 million, and G3 with 20.51 million grid points. The results obtained from the steady-state simulations, showed a negligible variation in the temperature for all the grids as shown in Table 3.2. Figure 3.13 shows the grid independence graph as there is not much variation in the results and considering the available computational resources Grid 2 was chosen for the further simulations.

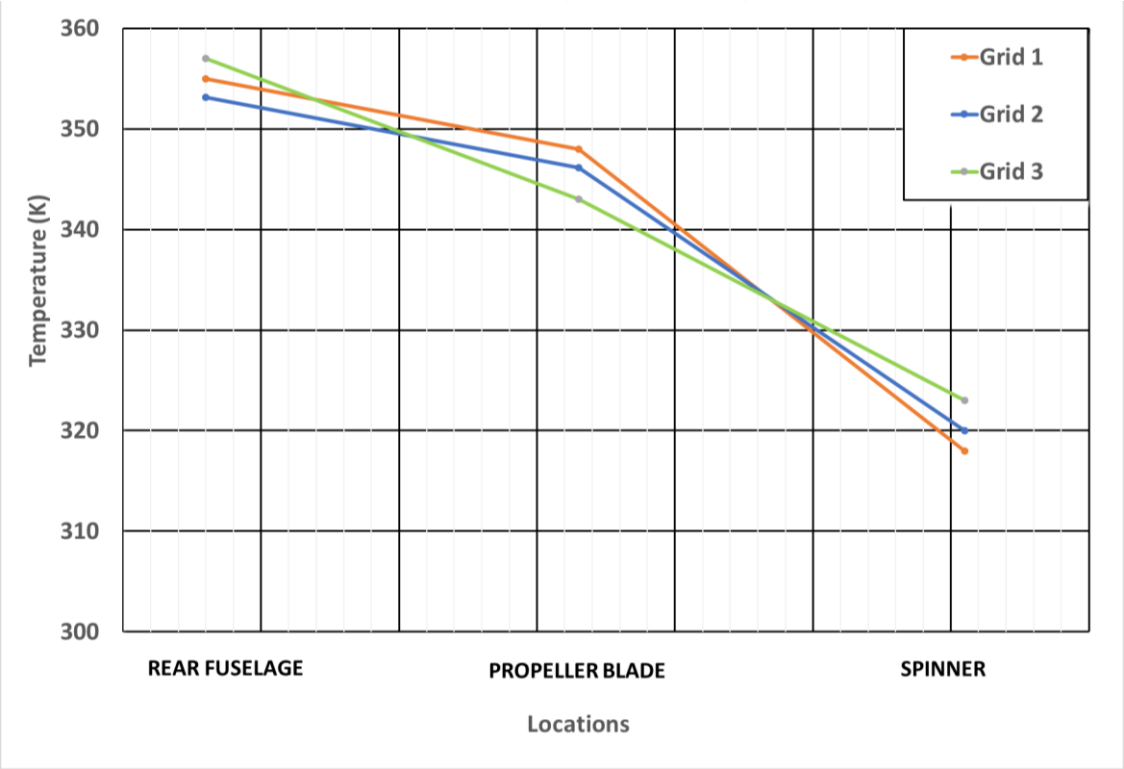

Figure 3.13 Grid Independence Graph

Table 3.2 Grid Independence Study

Part name	Grid 1	Grid 2	Grid 3
Total number of nodes, millions	332.93	348.08	371.46
Total elements, million	~19.96	~20.23	~20.51

Particular emphasis was laid during the mesh generation to obtain good quality mesh. The prism layers were generated on the wall surface to capture the near-wall effects of the nacelle and propeller. The mesh quality was found to be satisfactory and tabulated in Table 3.3. Figure 3.14 shows the volume mesh on the nacelle, propeller, and fuselage surface.

Table 3.3 Mesh Quality

Parameter	Achieved quality	Acceptable Range
Aspect Ratio	10-76	<100
Skewness	0.5-0.75	>0.5-1.0
Orthogonality	0.3-0.6	>0.166

3.4.2 Challenges faced in geometry and mesh generation

Meshing complex 3D geometry in ICEM CFD is challenging to achieve within the acceptable mesh quality. Although the complex geometry was generated in CATIA V5 and imported to ICEM CFD, in the process, it omits some of the vertices and edges during data conversion; also, other surfaces and edges will be duplicated. Subtracting the aircraft and nacelle from the flow domain is an important step if this is not correctly done, it later creates a wrong domain. These the -related issues will become a major drawback in the generation of good-quality mesh for much effort is required in cleaning the geometry, filling the gaps and deleting the multiple edges etc. The inclusion of a boundary layer on the aircraft makes meshing the surrounding areas and volumes more difficult, so interval counts must be given very carefully to ensure the smooth transition between fine and coarse elements.

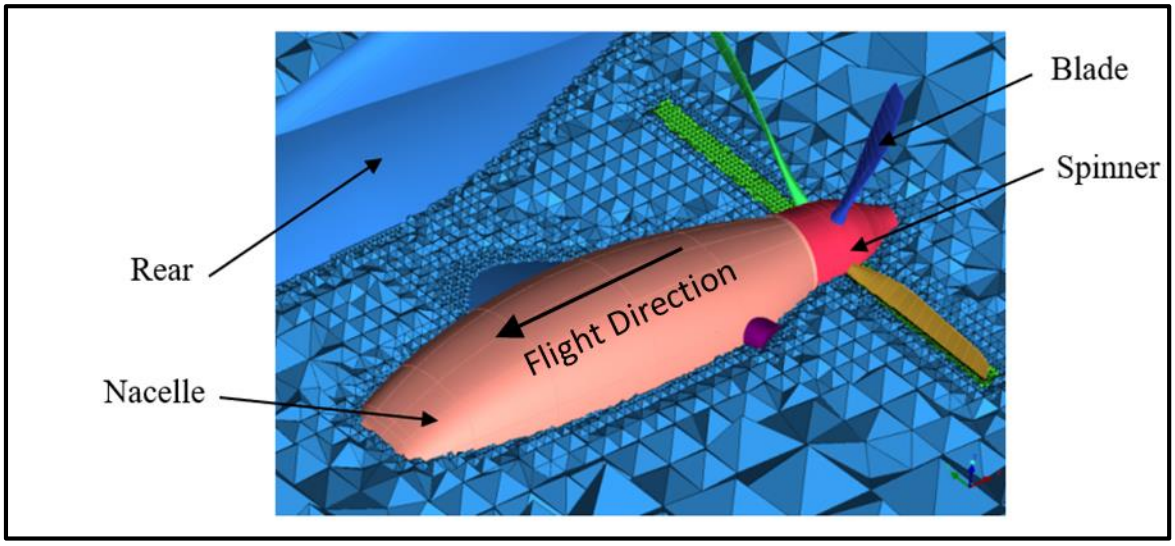

Figure 3.14 Volume mesh around the nacelle and propeller

3.4.3 Boundary conditions and flow parameters

Prescribing the boundary condition for the geometry chosen is the most crucial part of ANSYS ICEM CFD. Any inconsistency in defining boundary conditions leads to

FLUENT converting a few faces to walls and consequently to a wrong domain giving wrong results. So, boundary conditions should be applied with extreme care and a complete understanding of flow physics. The boundary conditions like velocity inlet and pressure outlet were applied at the domain inlet and outlet. The nacelle, propeller, spinner, and fuselage were set to no-slip wall boundary conditions. In contrast, the domain enclosing the propeller was set to interior boundary conditions. Concerning the exhaust stub, the stub inlet and outlet were set to mass flow inlet and interior boundary conditions, respectively, as shown in Table 3.4 and flight conditions where shown in Table 3.5.

Table 3.4 Boundary and Operating Conditions for Pusher Configuration

Sl. No.	Zone	Boundary Condition	Magnitude	Temperature K (°C)
1.	Domain Inlet	Velocity Inlet	10.2 m/s	313 (39.85)
2.	Stub 1 and 2 Inlet	Mass flow Inlet (per stub)	1 kg/s (Reverse condition)	713 (439.85)
3.	Domain Outlet	Pressure Outlet	Operating pressure (91700 pa)	313 (39.85)
4.	Stub 1 and 2 Outlet	Interior	-	-
5.	Domain Far Field	Wall	No-slip condition	-
6.	Nacelle & stub's wall	Wall	No-slip condition	-
7.	Aircraft body	Wall	No-slip condition	-
8.	Rotating Domain	Interior	-	-
9.	Spinner & Propellers	Wall	No-slip condition	-

Table 3.5 Flight conditions and Inputs for Analysis for pusher configuration

Case No.	Propeller Speed (rpm)	Inlet Velocity (m/s)	Mass flow rate at exhaust inlet (per engine) (kg/s)	Domain Inlet Temperature (K)	Exhaust Inlet temperature (K)	Remarks
1.	1700	X = 6.8	4	307	913	Ground Static forward/ Tq/ Thrust condition with the propeller at max speed and full power 100%Tq
2.	1020	X = 6.8	2	313	713	Ground Static Max reverse Tq/Thrust condition
3.	1020	X = 10.2	2	313	713	Maximum reverse Tq/Thrust condition with A/C speed 20kts

The operating conditions (ground static) used for the simulations are taken for the altitude of 914.4 m with a temperature of 307 k and a Mach number of 0.02. The working fluid was modelled as an incompressible or ideal gas, and the exhaust gas was assumed to be carbon-di-oxide. A turbulence intensity value of five percent behind the nacelle was assumed. The computations were set up for a steady-state solution. The simulations were carried out for the designed test matrix as per Table 3.6 to capture the temperature profile at the ground. The low-speed taxi trials (LSTT) were conducted with a max of up to 80 knots speed and reverse Tq as per standard procedure restricting Tq below 15% to capture the dynamic and crosswind effect. The above method had been used and the same adopted for aerothermal analysis of stub fitted to the tractor configuration.

Table 3.6 Test Matrix for blade surface temperature tests

SI. No.	Condition	Cycle
Test 1	5 minutes of ground idle	Engine start, unfeather propeller, establish an idle ground condition for at least 5 min, engine shut down
Test 2	10 minutes flight idle	Engine start, unfeather propeller, establish idle flight condition for at least 10 minutes, and engine shut down.
Test 3	5 minutes feathering	The engine starts remaining in a feather for at least 5 minutes, and the engine shuts down.
Test 4	1 minute 480 SHP, 40% Tq	Engine start, unfeather the propeller, and set the propeller to the maximum RPM, increase power to 40% Tq at least 1 Min, return to idle, engine shut down
Test 5	1 minute 720 SHP, 60% Tq	Engine start, unfeather the propeller, and set the propeller to the maximum RPM, increase power to 60% Tq for at least 1 Min, return to idle, and engine shut down
Test 6	1-minute 1000 SHP, 80% Tq	Engine start, unfeather the propeller, and set the propeller to the maximum RPM, increase power to 80% Tq for at least 1 Min, return to idle, engine shut down
Test 7	1 minute1200 SHP, 100% Tq	Engine start, unfeather the propeller, and set the propeller to the maximum RPM, increase power to max power, 100% Tq for at least 1 Min, return to idle, engine shut down
Test 8	3 min 5% Reverse Torque	Engine starts, unfeather propeller, and set the propeller to the maximum RPM, set the power to 5% reverse torque, return to idle, and turn the engine shut down.

Test 9	3 min 10% Reverse Torque	Engine starts, unfeather propeller, and set the propeller to the maximum RPM, set the power to 10% reverse torque, return to idle, and turn the engine shut down.
Test 10	3 min 15% Reverse torque	Engine starts, unfeather propeller, set the propeller to the maximum RPM, set the power to 15% reverse torque, return to idle, engine shut down.

3.4.4 Methodology

After creating the mesh with desired resolution in appropriate areas, along with the required resolution at the wall and with proper boundary conditions, it is read in fluent solver for the particular case setup. The pressure-based solver with the coupled implicit method is used for the analysis of the problem. The grid is scaled (scale factor: 0.001) to get the appropriate dimensions corresponding to the actual dimensions. The whole problem is then setup based on the boundary conditions and operating conditions prevailing in actual conditions for designing the simulation.

3.4.5 Solution

The solution was initialized by setting the flow quantities in the domain equal to the values at the free stream air inlet. The first-order upwind scheme was initially used along with the SIMPLE and coupled for a pressure-based solver. Further, the discretization scheme was changed to second order after a stable solution, and a substantial reduction in residuals with the first-order discretization approach was obtained. Table 3.7 shows the details of solution settings.

Table 3.7 Solver Settings

Details of Solver	
Solver	Segregated
Formulation	Implicit
Space	Axis-Symmetric
Time	Steady
Velocity Formulation	Absolute
Unsteady formulation	1st order implicit
Gradient Option	Node Based
Energy Equation	On
Details of Viscous Model	

Model	k-ω
k-ω model	SST
Material	
Air	Ideal gas
Carbon dioxide (Co_2)	Ideal gas
Cell Zone Conditions	
Exhaust Stub Inboard	Fluid
Exhaust Stub Outboard	Fluid
External Fluid	Fluid
Rotating Fluid	Fluid (Frame motion)
Boundary Conditions	
Inlet	
Domain Inlet	Velocity Inlet
Exhaust Stub Inboard	Mass Flow Inlet
Exhaust Stub Outboard	Mass Flow Inlet
Turbulence Specification Method	Intensity and Viscosity Ratio
Turbulent Intensity	5%
Turbulent Viscosity Ratio	5
Outlet	
Domain Outlet	Pressure Outlet
Solution Methods	
Pressure	SIMPLE
Density	Second Order Upwind
Momentum	Second Order Upwind
Turbulent Kinetic Energy	Second Order Upwind
Specific Dissipation rate	Second Order Upwind
Energy	Second Order Upwind
Residual Monitors	Convergence criterion
Continuity	1e-06
x-velocity	1e-06
y-velocity	1e-06
z-velocity	1e-06

energy	1e-06
k	1e-06
omega	1e-06
Solution Initialization	Standard Initialization

3.4.6 Iteration and convergence (graph)

It was observed that around 15,000 iterations were required for the convergence of the solution, which was determined by the drop in the continuity residuals below 1e-2 and all other residuals below 1e-6. The balance of mass at all inlets and outlets was checked and iterations continued till typically less than 0.3% mass imbalance was found. A typical solution run required around 120 hours of computing time in the computer using 8 processors and 20 hours in the CSIR-NAL HPC.

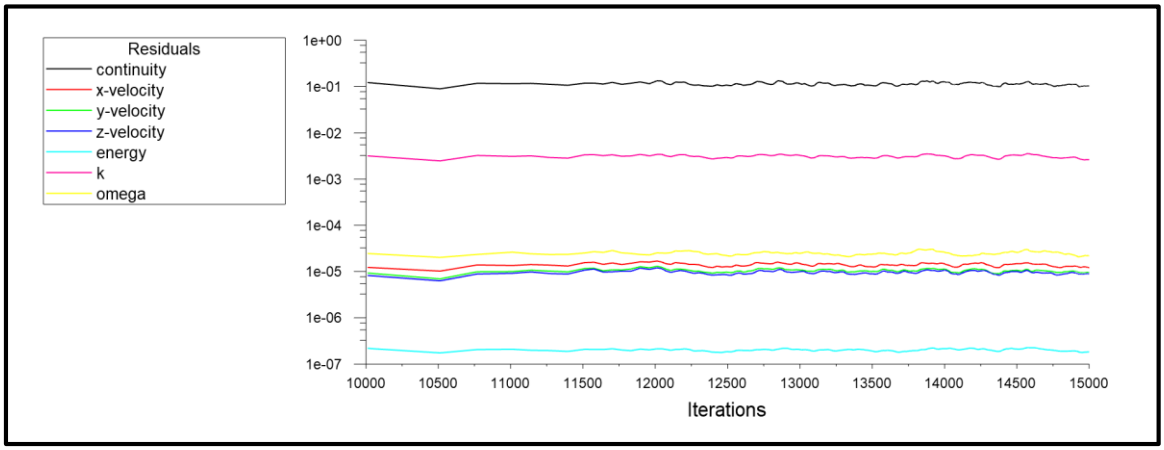

Figure 3.15 Convergence plot

3.5 Numerical studies with the stub: Tractor Configuration

Subsequently, the experimentally validated numerical model developed as discussed in the section 3.4 (pusher configuration) was used and adapted to perform a configuration change design to study of tractor-configured aircraft which is under development. This design is under testing at engine test facility for the tractor configuration. This study is aimed to check the airplane skin material, and its geometry, including the Plexiglas passenger window material degradation, due to hot exhaust gas plume impingement. The impact of changes in exhaust stub angle and asymmetric inboard-outboard stubs on the jet thrust at various flight operating conditions like Minimum Off-Route Altitude and Cruise performance is assessed. In the first stage, heat and fluid flow analysis was

performed over a twin-engine airplane's nacelle, wing, and centre fuselage with its powerplant mounted in the high wing configuration. Subsequently, numerical simulations of thermal interactions between the hot exhaust gases, which leave the exhaust system close to the nacelle, flaps, and the center fuselage, were estimated for various combinations of exhaust stub angles with asymmetry between inboard-outboard stubs at different airplane configurations and operating conditions. The results of the simulations are used to recommend modifications on the design of the considered airplane in terms of material selection and/or special coatings. The importance and impact of exhaust jet thrust on the overall aircraft performance are investigated.

3.5.1 Geometry and grid generation around the computational model

A similar approach to the geometry simplification and grid generation strategy is adopted, as discussed in section 0. Figure 3.16 shows the geometry and domain. The unstructured finite volume tetrahedral mesh was generated using ICEM-CFD software. The inlet and outlet domain boundaries were located at 8X and 11X upstream and downstream from the geometry reference. The entire domain enclosure is set to 5.6D, where X is the length and D is the model's diameter considered for analysis. A circular disk was enclosed around the propeller blades, referring to the rotating domain.

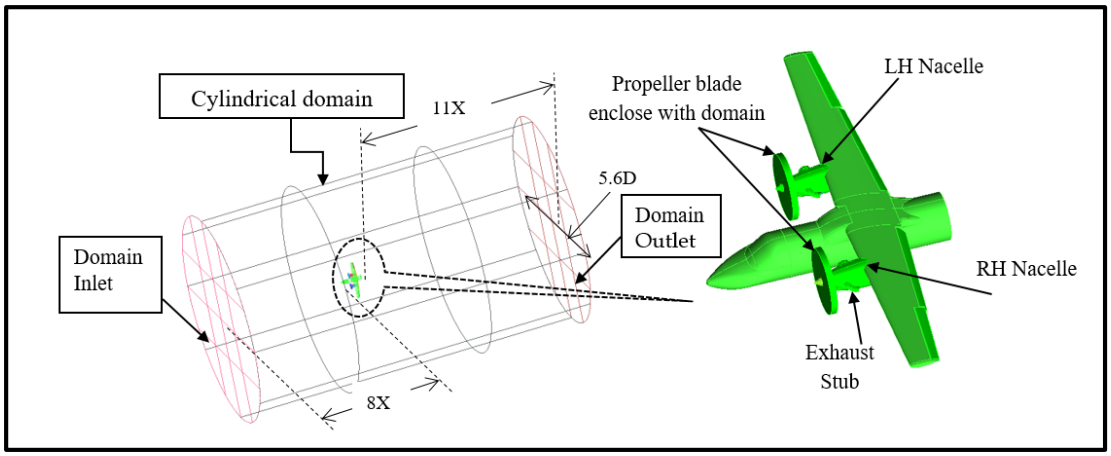

Figure 3.16 The geometry of the Complete Aircraft Model (side view looking outboard)

An unstructured volume mesh at the cut section (centre of the computational domain) of the complete aircraft model for 20° exhaust stub angle and 35° flap angle, as shown in Figure 3.17.

The grid independency study is performed for different mesh element numbers, and the peak temperature on the nacelle surface, blade, and fuselage is compared for the mesh model with three element numbers. Three different meshes with Grid 1 = 64.4 million element numbers, Grid 2 = 65.2 million, and Grid 3 = 67.3 million generated. The grid independency is plotted for all these considered mesh sizes, as shown in Figure 3.18. Among the considered mesh sizes, the mesh with 67.3 million elements and higher showed the same results. Hence 67.3 million elements are considered suitable for further CFD studies.

The mesh with ~ 67.3 million elements were generated and had ~11.4 million node count.

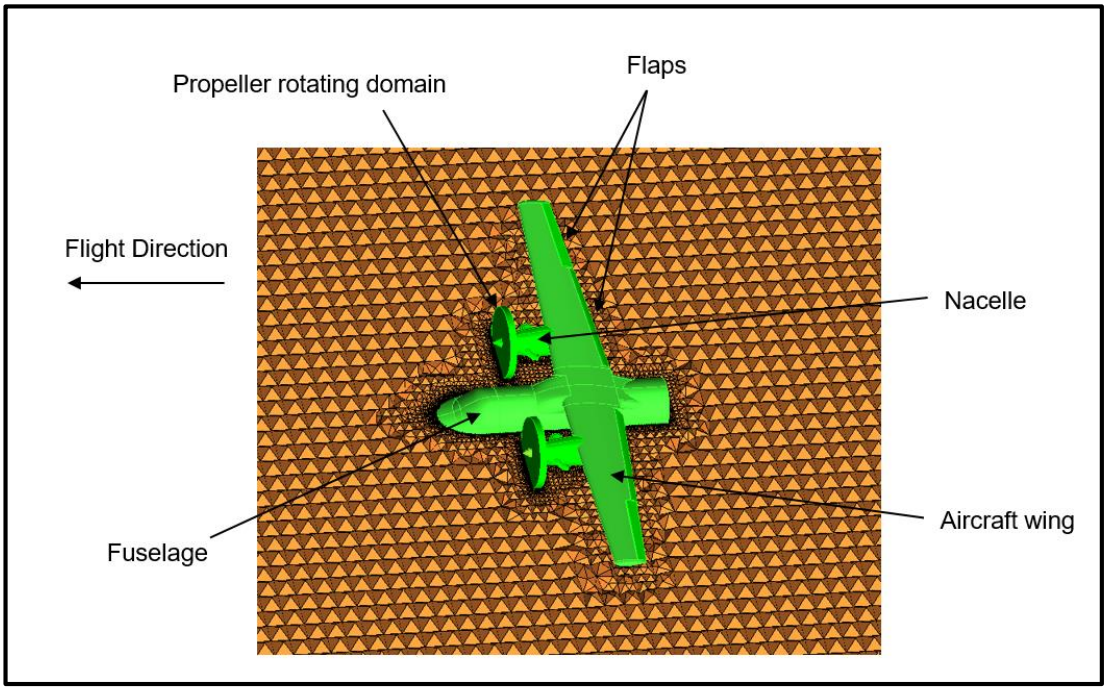

Figure 3.17 Volume Mesh around the Complete Aircraft Model

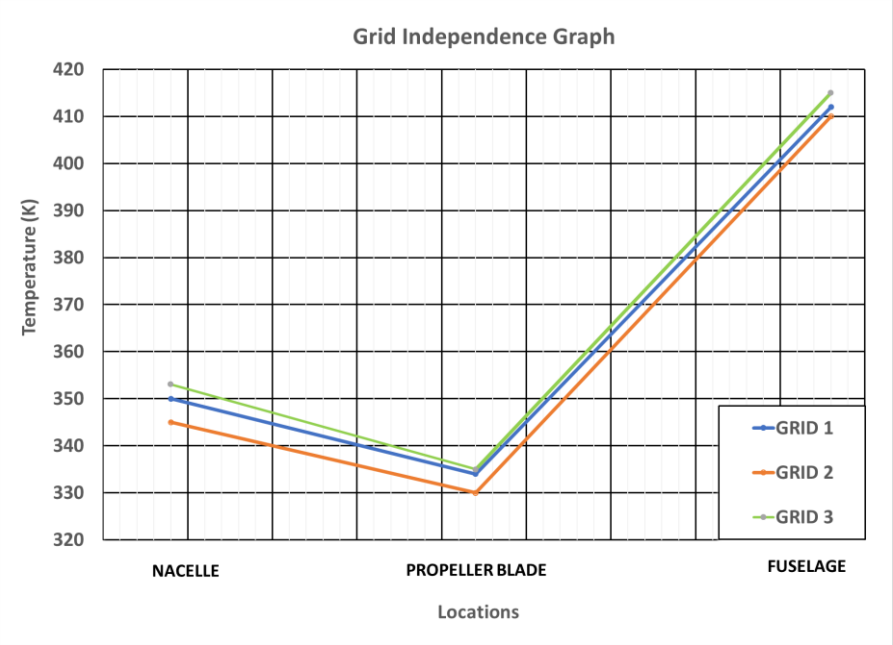

Figure 3.18 Grid independence graphs

3.5.2 Boundary conditions and flow parameters

For the boundary conditions, velocity inlet and pressure outlet were applied at the domain inlet and outlet, respectively. The nacelle, propeller, spinner, and fuselage were set to no-slip wall boundary conditions, and the domain enclosing the propeller was set to interior boundary conditions. For the exhaust stub, the inlet and outlet were set to mass flow inlet and interior boundary conditions, respectively. Ambient atmospheric conditions in both simulations were with pressure and temperature set to 91700 Pa (13.29 psi) and 323 K (50°C), respectively which is considered for 3000 ft (914.4 m) altitude. Domain walls were set to no-slip and adiabatic conditions since the outer boundary was placed away from the body, as in Figure 3.16.

The boundary and flight operating conditions used for the present simulations are shown in Table 3.8 and Table 3.9, respectively.

Table 3.8 Boundary and Operating Conditions for Tractor Configuration

Sl. No.	Zone	Boundary Condition	Magnitude	Temperature K (°C)
1.	Domain Inlet	Velocity Inlet	6.8 m/s	323 (50)
2.	Domain Outlet	Pressure Outlet	Operating pressure (91700 pa)	323.02
3.	Domain Far Field	Wall	No-slip condition	-
4.	Stub 1 and 2 Inlet	Mass flow Inlet (per stub)	2 kg/s (Forward condition) 1 kg/s (Reverse condition)	913 (640)
5.	Stub 1 and 2 Outlet	Interior	-	-
6.	Nacelle &stub wall	Wall	No-slip condition	-
7.	Flaps & Aileron	Wall	No-slip condition	-
8.	Aircraft body	Wall	No-slip condition	-
9.	Symmetry wall	Symmetry	-	-
10.	Rotating Domain	Interior	-	
11.	Spinner& Propellers	Wall	No-slip condition	

Table 3.9 Flight/Ground Conditions

Sl. No.	Conditions for CFD	Altitude m (ft)	OAT, K (°C)	Propeller rotational velocity (rpm)	Blade angle (degree)	Flap angle (degree)	Engine air mass flow rate kg/sec (lb/min)	Speed m/s (Mach no.)	Exhaust gas temperature K (°C)
1.	**Case 1:** Ground Static **(Start Cycle)**	914.4 (3000)	323 (50)	1700	20°	10°	0.5 (66)	6.8 (0.02)	913 (640)
2.	**Case 2:** Ground Static Forward Thrust Condition **(Idle Condition)**			1020	20°	35°	1 (132.2)		
3.	**Case 3:** Ground Static Forward Thrust Condition **(Take-off Condition)**			1700	20°	35°	4 (529.10)		
4.	**Case 4:** Ground Static Reverse Thrust Condition **(Reverse Condition)**			1020	-9°	35°	2 (264.5)		
5.	**Case 5:** Ground Static Forward Thrust Condition **(Take-off Condition)** Complete Aircraft			1700	20°	35°	4 (529.10)		

3.6 Numerical studies: Nacelle Zone and Bay temperature estimation

This section is carried out to estimate the nacelle structure surface temperature distribution due to the rise in engine surface temperature for various operating conditions. In the aerospace industry, developing composite materials for increased strength and reduced weight is always a priority. The external body of aircraft, i.e., fuselage, nacelle, wings etc., are made of Al alloy and composites. A Nacelle of a light turboprop pusher aircraft houses hot components like engines and their subsystems. The Nacelle is also made of thermally sensitive composite material (skin), requiring a specified thermal management study.

The Reynolds Averaged Navier Stokes Equation is numerically solved to compute the airflow field and the turbulence effect. While the turbulent fluctuations are not resolved, their impact on the mean flow is modelled using the Reynolds Averaged Navier Stokes (RANS) Equations. This approach introduces additional unknowns and the Reynolds stresses, heat flux, and mass flux terms that reprint the effect of turbulent fluctuations upon the mean flow. The SST k-ω models were considered appropriate for this study and ideal for predicting the flow behaviour in regions away from the wall, and it was thought that they would be the best suited for resolving these kinds of flows similar to the validated model as per section 3.4 of this report.

3.6.1 Mathematical models

The k-ω SST turbulence model is a two-equation eddy-viscosity model that combines the Wilcox k-omega and the k-epsilon models used as per section 3.4 of this report.

3.6.2 Simulation set-up

The model for numerical analysis is created using CATIA software. The geometry is simplified to retain the components actively involved in bay ventilation. Internal simulation is performed to capture the steady-state temperature values over the nacelle and other locations. The engine is over-simplified from a complicated external geometry shown in Figure 3.19 (a) (left) to a cylinder body shown in Figure 3.19 (b) (right). Exhaust stubs are considered in the model as they affect the airflow pattern. The numerical input and boundary conditions are provided such that they are similar to the experimental conditions.

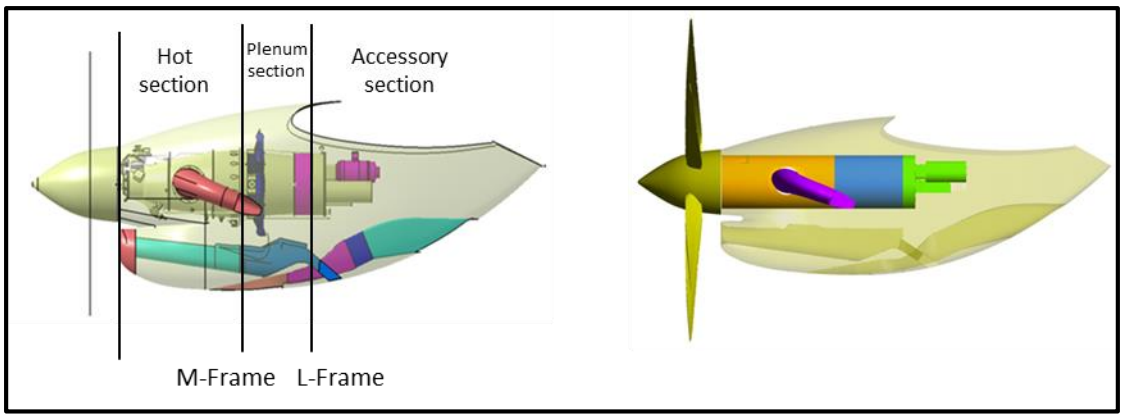

Figure 3.19 (a) Complicated external geometry (b) Simplified geometry

3.6.3 Geometry and Mesh generation (CFD domain)

The geometry simplification is carried out in CATIA CAD software. Complex systems like cooling oil ducts, fuel ducts, engine control cables etc., are not considered in the geometry as they do not significantly contribute as a heat source, and the additional effort involved in generating the engine geometry details along with clean up and meshing is quite complex.

The region inside the nacelle and the engine surface is divided into 3 zones/bay viz., Front, Centre, and Rear zone, separated by L frame and M adiabatic frames as shown in Figure 3.20. The rear zone Auxiliary Gear Box, Fuel Control Unit, and Oil Scavenging Pump are housed. In the Centre zone, a compressor zone, there is no external air circulation in this bay region. The front zone consists of exhaust stubs on each side of the nacelle, and also Reduction Gear Box, Propeller governor, and Magnetic Chip detector are present. The inlets and outlets for the air flow contribute to the bay ventilation present in the front and rear zone at the central combustion zone, there is no requirement for heat transfer through the airflow, and hence no inlets and outlets on the nacelle surface at that zone is considered. NACA inlets at the front and rear of the nacelle surface are designed according to standards and placed on the nacelle surface to trap rammed air. Louver cut-outs are designed over the front nacelle surface for the air to flow out of the front nacelle bay. In the rear bay, the annular space around the exhaust ducts is present to avoid direct contact of the nacelle surface with the hot exhaust ducts. Airflow can also be observed in this region, which helps in bay

ventilation. The airflow out of the front bay occurs through the nacelle entry, which is a space between the nacelle body and the spinner.

To obtain an undisturbed flow, a large cylindrical domain is considered around the engine-nacelle geometry of length 5000mm upstream and 40000mm downstream (larger domain distance downstream is to capture turbulence generated by the propellers downstream), and the domain diameter of 15000mm is considered shown in the Figure 3.20. The domain sizing is finalized by observing Turbulent Intensity regions in the preliminary study.

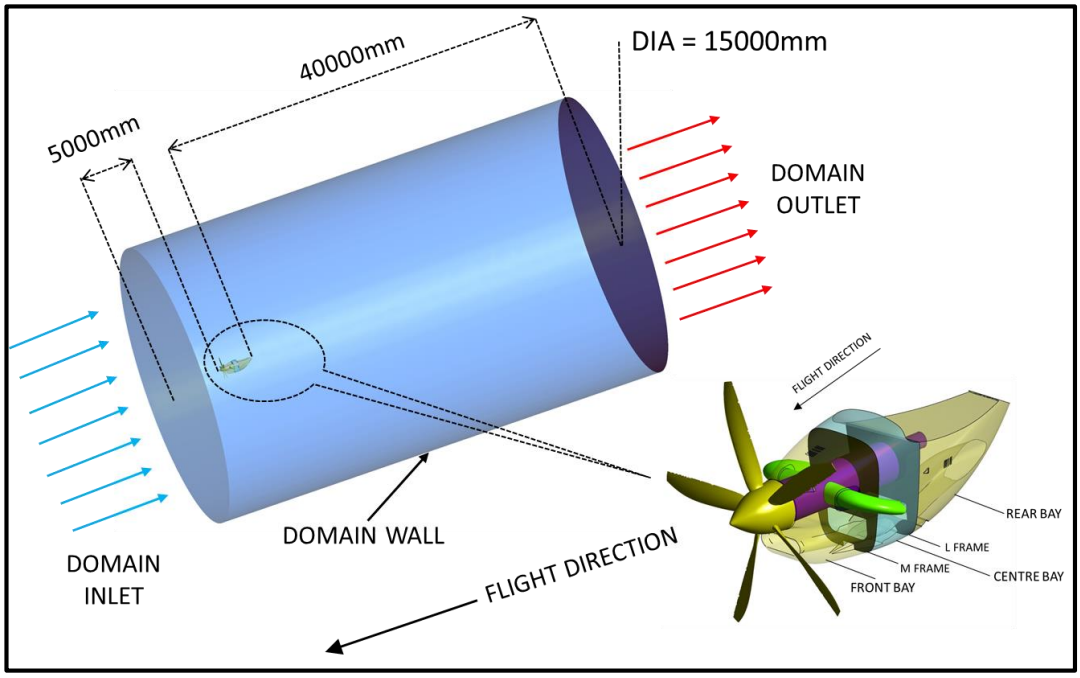

Figure 3.20 Domain sizing and simplified nacelle and engine model used for simulation

A geometrically simplified aircraft model is considered during CFD analysis to reduce the computational and meshing time. The air surrounding the nacelle is assigned as external fluid, which is present in the entire domain. The engine bay viz., front, center, and rear are provided with a separate working fluid, and to account for propeller suction, a rotating fluid is provided surrounding the propellers, and all the fluid is made as tetra volume mesh. The surfaces are provided with the quad-dominant, path-independent type of mesh. A tetrahedral mesh with inflation on boundaries of heat transfer is considered with y+=1.

The Aero thermal analysis is performed by considering the physical parameters of the actual Engine run so that the CFD results can be validated with that of experimental values. The values of ambient temperature, pressure, wind speed, and propeller speed are extracted from the experimental data.

3.6.4 CFD solver set-up

The simulation is carried out considering the aircraft's operational conditions similar to experimental conditions. The 3 zones of the engine are given a surface temperature as a heat source when producing 100% torque. The front engine surface temperature is 442.2K, the centre engine is 419.4 K, and the rear engine zone is 463.8K shown in Figure 3.21. The values are obtained by referring to the experimental data. These are the temperature that arrived after considering engine insulation, which gets dissipated to the nacelle. The boundary conditions are given in Table 3.10. The nacelle surface was taken as the wall with a thickness of 0.012m and the properties of the Al2219-T81 alloy sheet material. Thickness is considered for the nacelle wall to avoid the default setting in FLUENT for walls as thermal insulators. SST k-ω turbulence model is considered to capture temperature changes near the walls, the gravity is neglected, and the pressure-based solver type is considered. Table 3.11 shows the different cases and conditions.

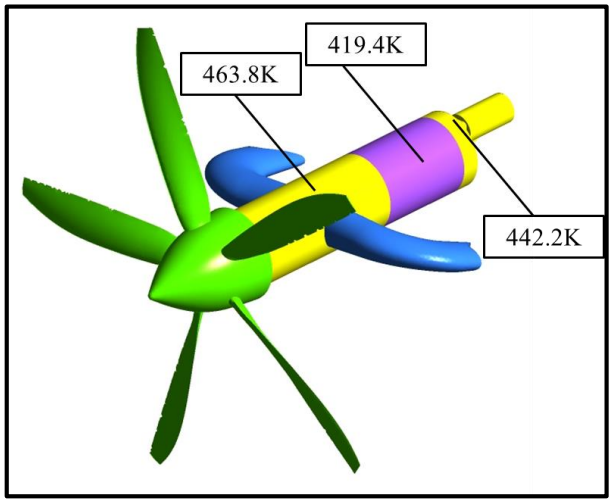

Figure 3.21 Temperature distribution on the engine surface

Table 3.10 Boundary Conditions for Zone and Bay Tractor Configuration

Sl. No.	Domain	Boundary Conditions
1	Domain Inlet	Velocity Inlet
2	Domain Outlet	Pressure Outlet
3	Domain	Wall
4	Engine	Constant Temperature Wall
5	Exhaust Annular Ring	Interior
6	Exhaust Stub	Wall (813 K)
7	L-frame	Wall
8	Louvers	Interior
9	M-frame	Wall
10	NACA Inlets	Interior
11	Nacelle	Wall (t=0.0012 m)
12	Nacelle Entry	Interior
13	Propeller Blades	Wall
14	Rotating Domain	Interior
15	Spinner	Wall
16	Wing & Flaps	Wall

Table 3.11 Different cases and conditions

Case No.	Flight Case	Altitude m (ft)	Free Stream Total Pressure, Pa	Free Stream Static Pressure, Pa	Outside Air Temperature, °C (K)	Speed, m/s (M)	Mass Flow Rate, Kg/s (lb/s)	Nacelle AOA, deg	Propeller Speed, rpm
1	Case 1 (Min. Climb)	1371 (4500)	88578	85908.6	6.1 (279.25)	71.46 (0.21)	4.036 (8.90)	6.60	1700
2	Case 2 (Best Rate of Climb)	3810 (12500)	66222	63190.5	9.75 (263.4)	88.47 (0.26)	3.43 (7.61)	5.45	1700
3	**Case 3 (Max. Cruise)**	**7620 (25000)**	**43743**	**37576.4**	**-34.5 (238.65)**	**159.94 (0.47)**	**2.56 (5.65)**	**0.90**	**1700**
4	**Case 4 (Economy Speed Cruise)**	**7620 (25000)**	**41983**	**37576.4**	**-34.5 (238.65)**	**136.2 (0.4)**	**2.5 (5.50)**	**2.67**	**1700**
5	Case 5 (Economy Speed Cruise)	4572 (15000)	61661	57157.5	-14.5 (258.45)	112.3 (0.33)	3.22 (7.08)	2.56	1700
6	**Case 6 Ground Run (Take off Condition)**	**914.1 (3000)**	**91709**	**91700**	**34 (307.15)**	**6.8 (0.02)**	**5.0 (11.0)**	**0**	**1700**
7	**Case 7 (Flight Idle Condition)**	**914.1 (3000)**	**91709**	**91700**	**34 (307.15)**	**6.8 (0.02)**	**0.5 (1.1)**	**0**	**1020**
8	**Case 8 (Ground Static Take off Condition)**	**914.1 (3000)**	**91709**	**91700**	**50 (323.15)**	**6.8 (0.02)**	**5.0 (11.0)**	**0**	**1700**

3.5 Experimental Set-up for Pusher Configuration

Two methods were adapted to experimentally measure the surface temperatures on the propeller and aircraft surface, i.e., through Thermal Imaging by infrared (IR) temperature scanner and Temperature Stickers. Before implementing on the aircraft, the bench setup was developed to validate the infrared camera results using a standard pre-calibrated thermocouple. The primary test setup used for the calibration of IR camera results is shown in Figure 3.22.

The general specification of the IR camera used to capture the temperature effects during ground testing is shown in Table 3.12.

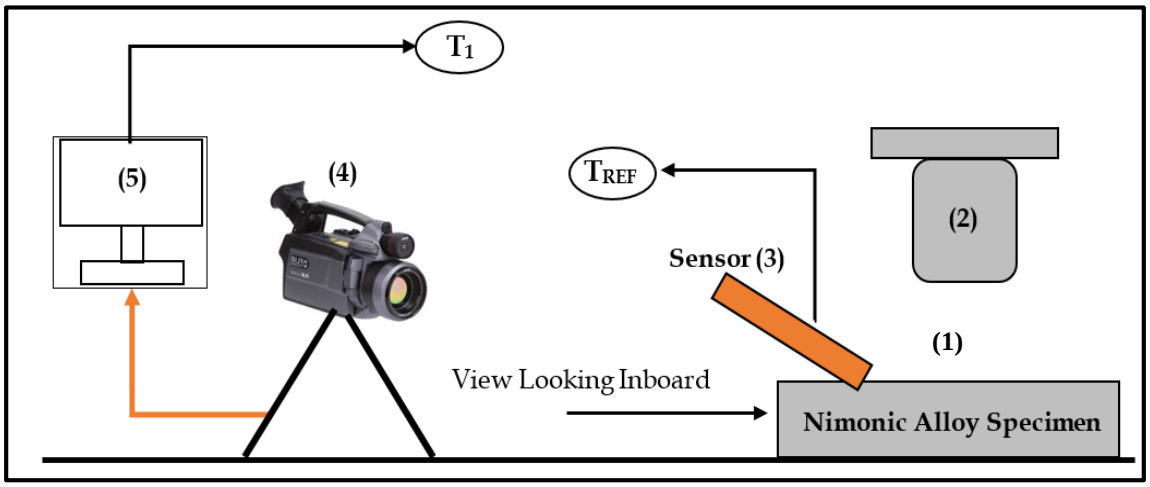

Figure 3.22 Experimental Bench Setup (IR Temperature Capturing)
1. Nimonic Alloy Specimen 2. Heat Gun
3. Pre-calibrated Sensor (Thermocouple) (Calibrated Std. Ref.)
4. Infrared Thermal Camera 5. Data Acquisition system

Nimonic Alloy (Ni-75) exhaust stubs are fabricated by heavy duty high precision forming process and assembled using TIG welding. All the manufacturing process were carried out under controlled environment as per the aerospace standards. This stubs were fitted on to the engine exhaust flange for the experimentation.

Table 3.12 Infrared Thermal Camera Specifications

Product	Infrared Thermal Camera
Detector Material	InSb (Indium Antimonide)
Spectral Response	2.5 µm to 5.1 µm
No. of pixels of Image	320 × 256
Video frame rate	5 Hz to 380 Hz (Full Frame)
Frame rate resolution	1 Hz step
Cooling type	Integral Sterling Cooler
Cooling time	<7min at 25° ambient
Power supply	12 VDC/5A
Operating temp range	-20°C to 55°C
Digital Video	GigE/Camera LINK

Test Procedure: Referring to the Figure 3.22, the Nimonic alloy specimen [1] (the same as exhaust stub material) is preheated using the heat gun [2]. The specimen temperature is measured using the pre-calibrated thermocouple [3] and Infrared Thermal Camera [4]. The temperature measured using the thermocouple is inferred as $T_{ref.}$, and through the camera, is referred to as T_{ref1}. The calculated results are compared and validated. It was found satisfactory with a minimal percentage error (<5%), and the same methodology was implemented during actual ground testing. The accuracy in measurement were established through repeatability for the given test condition and all the measurements were within OEM specified error band of 5%.

Finally, the flight/ground test was carried out on a full-scale composite propeller under maximum power/thrust conditions during the profile engine ground run (EGR). The temperature on the propellers and aft fuselage surfaces is measured using temperature stickers during flight testing. The OMEGALABEL permanent colour

change temperature stickers are small heat-sensitive indicators sealed under transparent, heat-resistant windows. These heat-sensitive, fusible materials consist of crystalline solids. When heated, a temperature will be reached in which the solids change sharply to liquid.

The primary test setup has been developed to measure the temperature on the actual aircraft propeller blade and aft-fuselage surfaces, as shown in Figure 3.23. The OMEGA temperature stickers were placed on the pressure and suction side of the propeller blade at a certain distance to measure the surface temperature. The temperature stickers used to measure the effects of exhaust gas impingement was ranging from (40°C-82°C and 80°C–123°C).

On the ground bench test setup, the temperature measurement accuracy with IR was within 5%, whereas in an actual case on the aircraft it was within 7-8%. The measurement inaccuracy in the actual case on aircraft was slightly higher due to variations in the operating conditions (Viz., exhaust soot effects, cross-winds etc.) compared to bench setup. The outcome of these tests will be discussed in detail in the results and discussions.

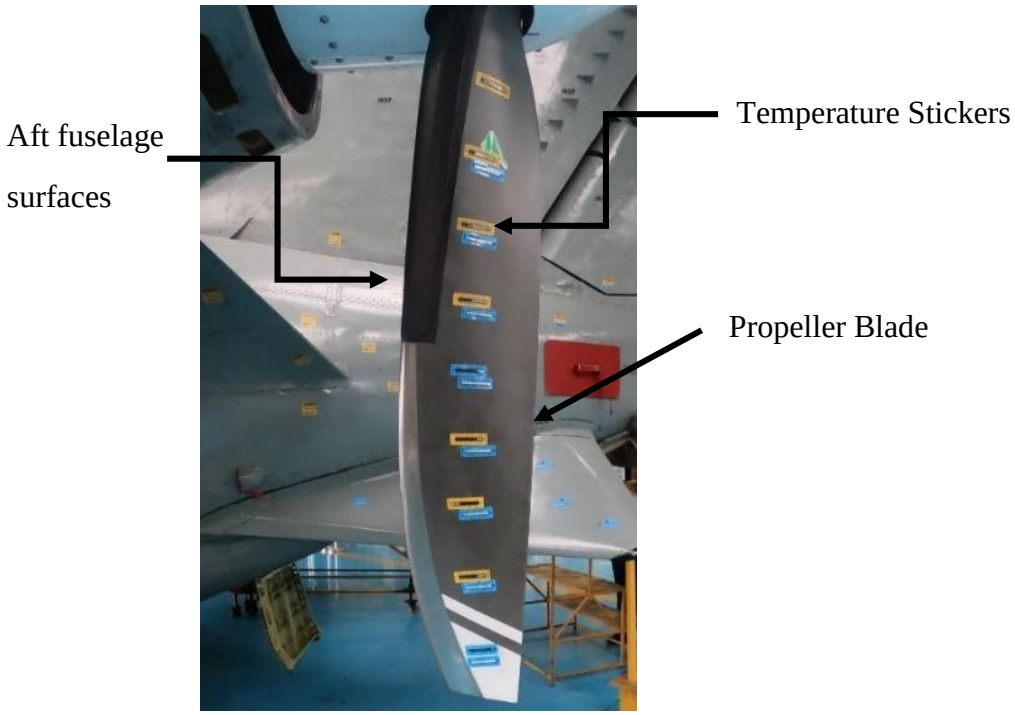

Figure 3.23 Temperature Stickers on Propeller Blade and aft fuselage surface

CHAPTER 4

RESULTS AND DISCUSSIONS

4.1 Numerical studies with the stub: Pusher Configuration

All the computations were performed using the same numerical schemes and operating conditions at various flight conditions, as mentioned in Table 3.5. The main aim was to estimate the propeller surface blade and aircraft surface temperature during different in-flight operating conditions. The main flow characteristics were monitored at the propeller blade and on aft-nacelle surfaces to determine the temperature effect caused by the exhaust gases.

4.1.1 Ground Static Forward Tq/Thrust Condition (Case 1)

Figure 4.1 shows that for forward thrust operation, the minimum propeller blade area gets exposed to the exhaust gas because of the narrowed and guided exhaust jet created due to the propeller suction. This condition is favourable condition for propeller as well as the airframe. Figure 4.2 shows the total temperature contours on the propeller blade surface and the aft-fuselage surface at ground static forward Tq/Thrust condition (case 1).

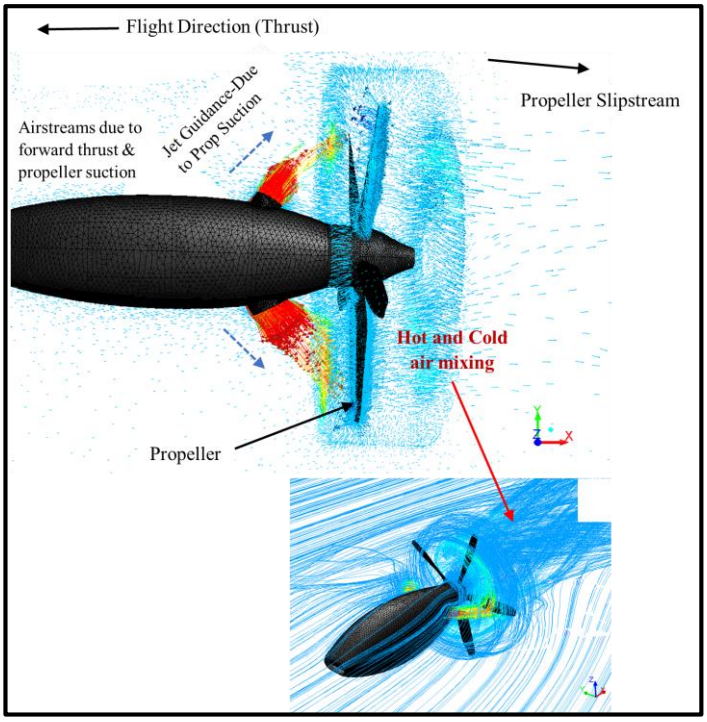

Figure 4.1 Vector plot for forward Tq/Thrust Condition Case 1 (Pusher)

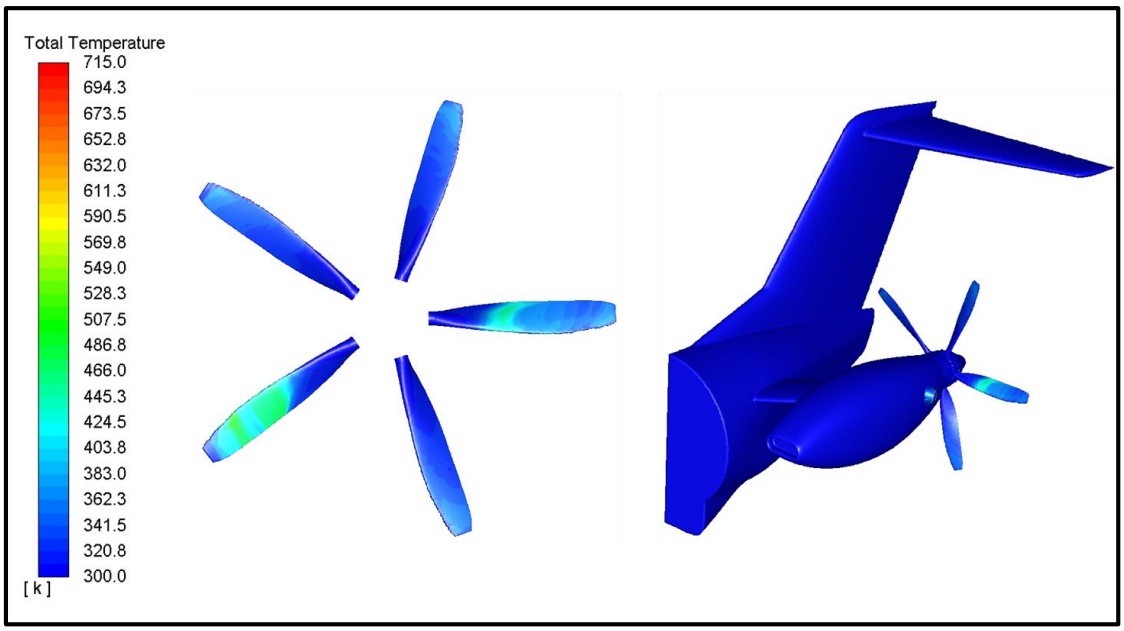

Figure 4.2 Total temperature contour on propeller blade surface (K) at ground static forward Tq/Thrust Condition-Case 1 (Pusher)

4.1.2 Ground Static Reverse Tq/Thrust Condition (Case 2 & 3)

Figure 4.3 shows the total temperature contours on the propeller blade surface and the aft-fuselage surface at ground static reverse Tq/Thrust condition (case 2). The maximum temperature on the propeller blade was 73°C and on the aft-fuselage it was 80°C. Further, the total temperature contours on the propeller blade surface and the aft-fuselage surface are shown in Figure 4.4 at maximum reverse Tq/thrust condition with 20Knots aircraft forward speed (case 3). The maximum temperature on the propeller blade was 69°C, and on the aft-fuselage, 105°C, respectively.

Figure 4.3 & Figure 4.4 show that for ground static reverse thrust operation, the maximum propeller blade area gets exposed to the exhaust gas due to the non-guided exhaust jet. This condition happens due to the propeller blade reversal and the flow phenomenon is exactly opposite to the forward thrust case. This condition is a must to decelerate the aircraft during landing & taxing. However, the localized flow phenomenon caused due to the reverse thrust is unfavourable to the propeller and to some extent on the airframe. This operation has to be time-limited to typically ~10 seconds. This situation slightly gets improved in the case of reverse thrust with forward velocity. For the 20 knots forward speed, even though the propeller operation is at reverse thrust condition, the jet effect gets diluted (due to colder air stream caused by forward velocity),

and exhaust spreads towards the propeller and fuselage, which can be seen in Figure 4.4. This further improves with higher forward velocity.

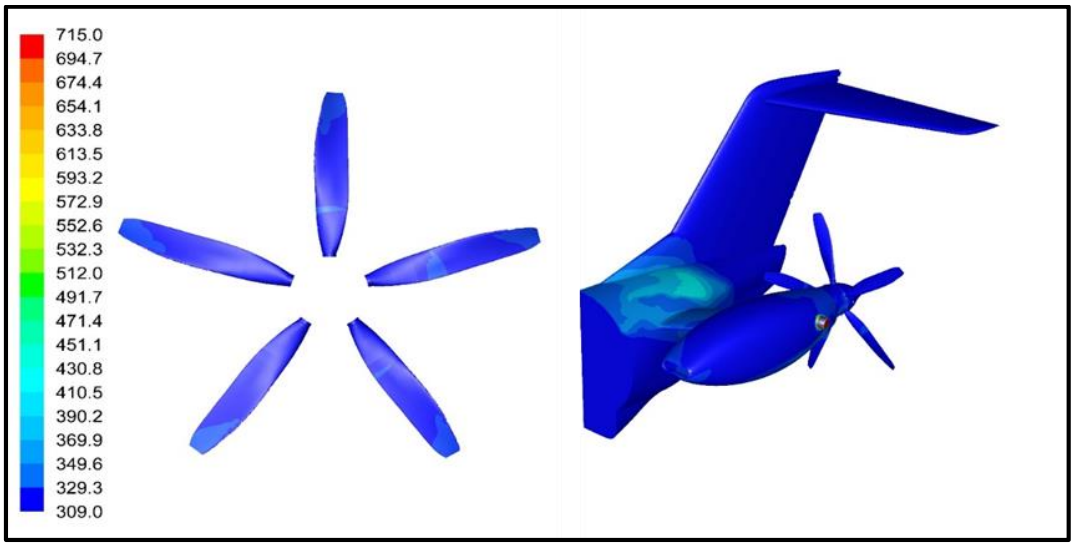

Figure 4.3 Total temperature contour on propeller blade surface (K) at ground static reverse Tq/Thrust Condition-Case 2 (Pusher)

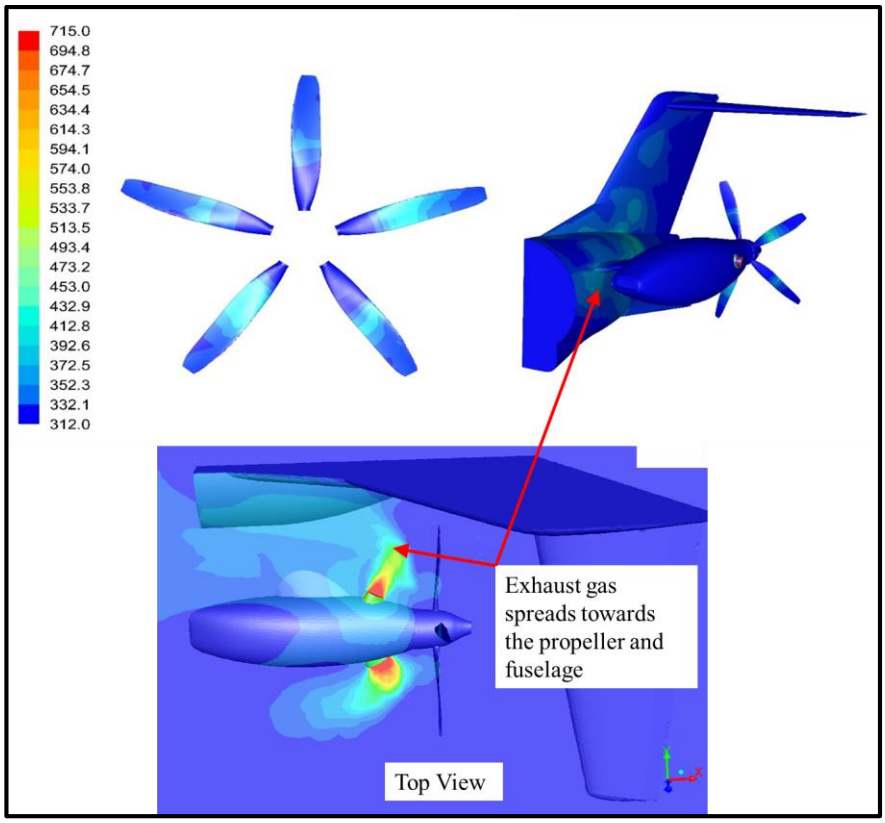

Figure 4.4 Total temperature contours on propeller blade surface (K) at maximum reverse Tq/Thrust condition with aircraft speed 20 Knots-Case 3 (Pusher)

Based on the results, it is observed that the estimated temperature on the propeller blade surfaces is within the applicable limits prescribed by the composite propeller OEM. Thus, the benefits such as weight reduction, improved noise characteristics and aero-performance associated with the composite propeller can be fully utilised.

4.2 Numerical studies with the stub: Tractor Configuration

All the computations were performed using the same numerical schemes and operating conditions at various flight conditions, as mentioned in Table 3.9. The flow characteristics were monitored at the propeller blade, nacelle, and aircraft surfaces to determine the temperature effect caused by the exhaust gases.

Unlike the flow phenomenon explained in section 4.1, in the tractor-configured propeller, it can be seen from Figure 4.5 exhaust jet effects on the propeller is not significant for any given flight condition because the propeller is upstream of the jet. The propeller slipstream and jet flow in the same direction downstream from the propeller.

However, it is seen from Figure 4.4, for the reverse thrust case, due to the flow reversal, the exhaust jet gets retarded and deflects towards the fuselage inboard of the RH engine side. This phenomenon occurs due to the propeller co-rotation for LH and RH engines. This can be avoided for contra-rotating propellers.

Similarly, computational results of temperature distribution at various flight conditions are performed for all the cases given in Table 3.9, and results are tabulated in Table 4.1. Critical case 4 & 5 are discussed in detail as follows.

4.2.1 Ground Static Reverse Thrust Condition (Reverse Condition-Case 4)

Figure 4.5 and Figure 4.6 represent the total & static temperature contours across the cut-sectional view and the propeller blade surface. The maximum expected throttle setting is around 15-20% during this condition. The nacelle surface temperatures at the inboard and outboard are 395K (121°C) and 380K (106°C), respectively. The overall nacelle surface temperature was found to be 350K (77°C) shown in Figure 4.7. The propeller blade temperature is 334K (61°C). During this reverse condition, the fuselage surface is exposed to exhaust gas, and the aft surface is exposed to higher temperatures.

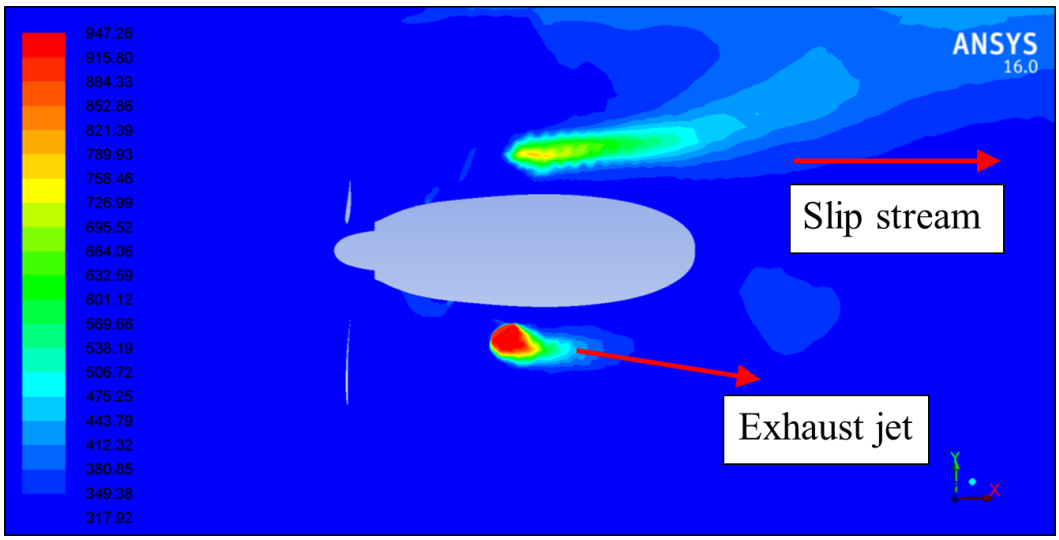

Figure 4.5 Total Temperature Contours along Z-axis – LHE (Reverse Condition) [Temperatures are in Kelvin]- Case 4

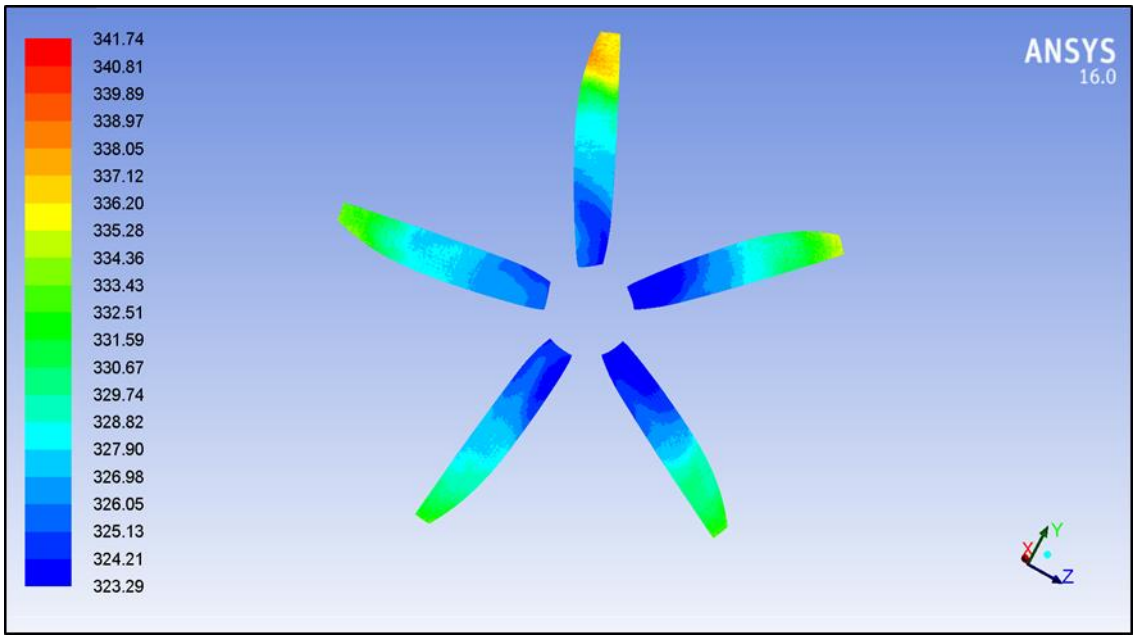

Figure 4.6 Static Temperature Contours on Propeller Blade – LHE (Reverse Condition) [Temperatures are in Kelvin]-Case 4

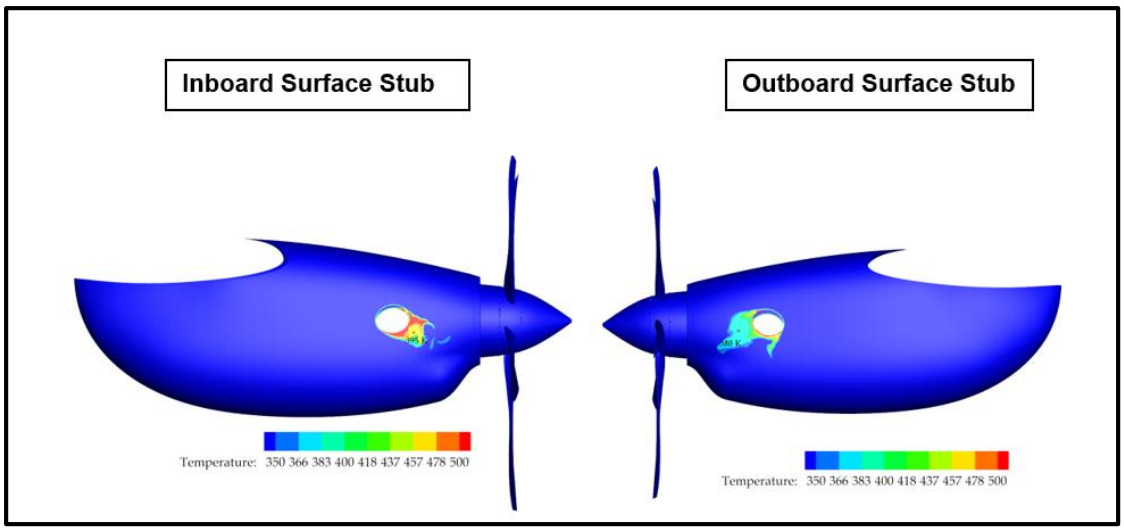

Figure 4.7 Total Temperature Contours on the Aircraft Structure Surfaces – LHE (Reverse Condition) [Temperatures are in Kelvin]- Case 4

The fuselage surface temperatures are found to be a minimum of 340K (66°C) – a maximum of 437K (163°C), as shown in Figure 4.8. However, the surface temperature across the inboard and outboard flaps is 400K (127°C) and 349K (76°C). It should be noted that reverse thrust application in ground static conditions will be time-limited for maintenance/engine rigging ground runs and landing. The reverse thrust application is typically between 90 - 40 knots. Thus, exhaust plume impingement effects on the adjacent aircraft surfaces are negligible.

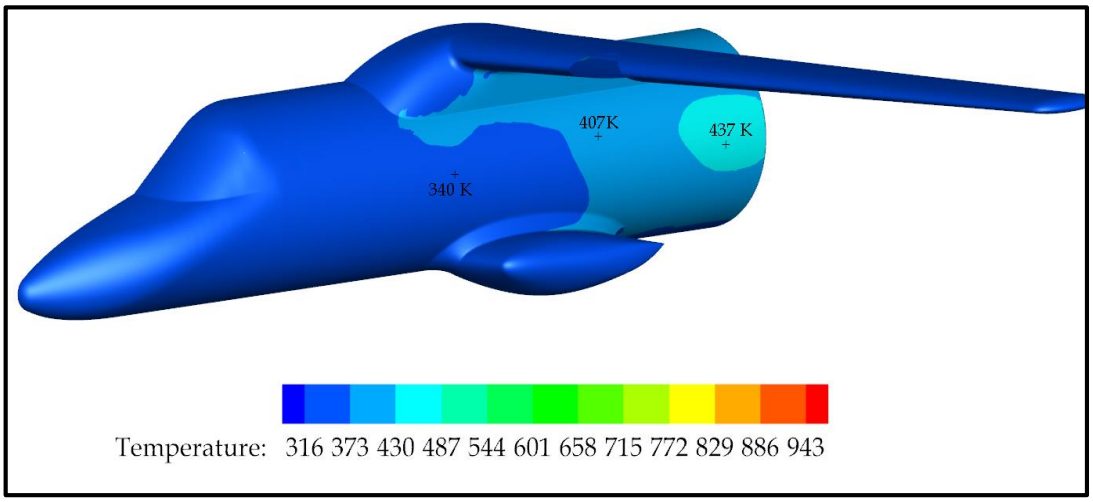

Figure 4.8 Total Temperature Contours on the Aircraft Structure Surfaces – LHE (Reverse Condition) [Temperatures are in Kelvin]-Case 4

4.2.2 Ground Static Forward Thrust Condition with Complete Aircraft Model (Take-off Condition-Case 5)

The propeller blade and aircraft structure surface temperatures are further estimated considering the complete aircraft model. The whole model includes both LH and RH nacelle and propellers. The propeller rotational speed is set to 1700 rpm (both propellers rotate counter-clockwise, viewing aft from the propeller spinner cone).

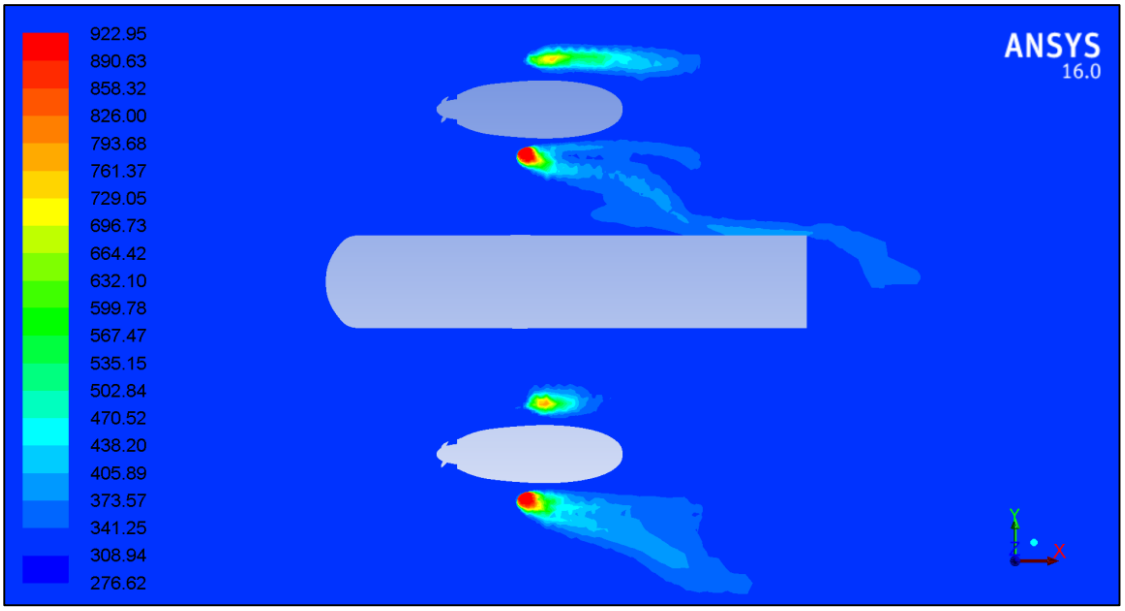

Figure 4.9 Total Temperature Contours along Z-axis (Take-off Condition) Complete Aircraft [Temperatures are in Kelvin]-Case 5

Figure 4.9 represents the total temperature contours across the cut-sectional view. Figure 4.10 illustrates the static temperature contours on the LHE and RHE side propeller blade surfaces. It is visualized from the total temperature contours that the aircraft structures on the inboard and outboard sides are not exposed to the exhaust flue gas, and the effects of exhaust hot gas impingement are very minimal.

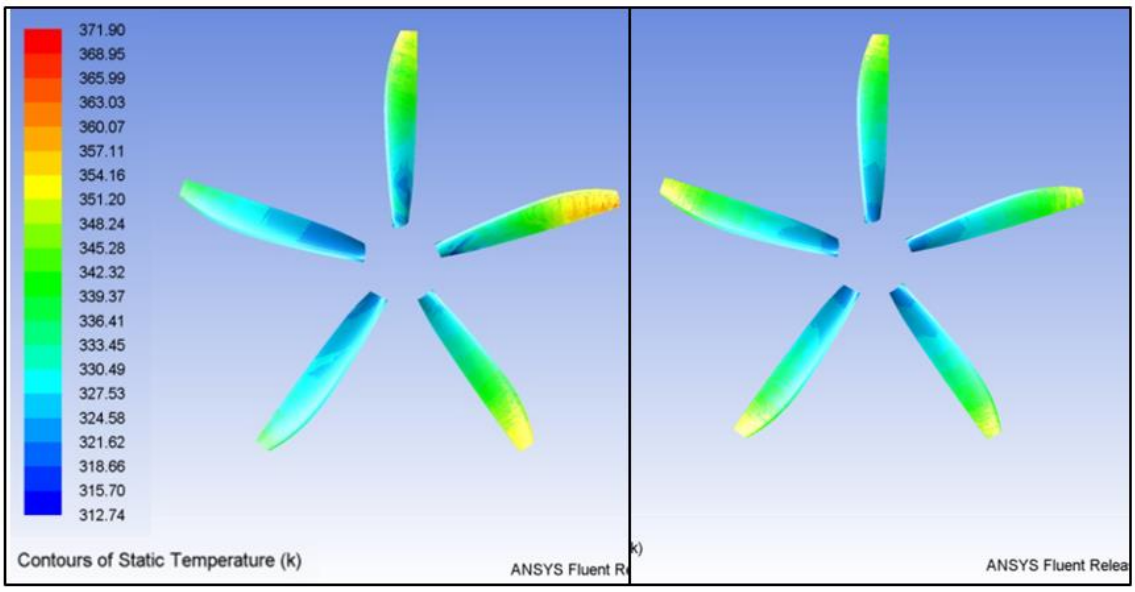

Figure 4.10 Static Temperature Contours on Propeller Blade – LHE and RHE (Take-off Condition) [Temperatures are in Kelvin]-Case 5

It is observed that computed temperatures on the nacelle and wing surfaces near RHE are 341K (68°C), and the fuselage is exposed to the higher temperature of the order 389K (116°C), as shown in Figure 4.11. The RH propeller blade surface temperature is 341K (68°C). The corresponding value for the nacelle and wing surfaces near LHE is in the order of 341K (68°C). The LHE propeller blade surface temperature is 345K (72°C). The estimated aircraft surface and blade temperatures obtained from the CFD simulations for different operating conditions are summarized in Table 4.1. The effect of crosswind on the propeller and aircraft surfaces is not considered for the present computations, and these studies will be carried out in further phases.

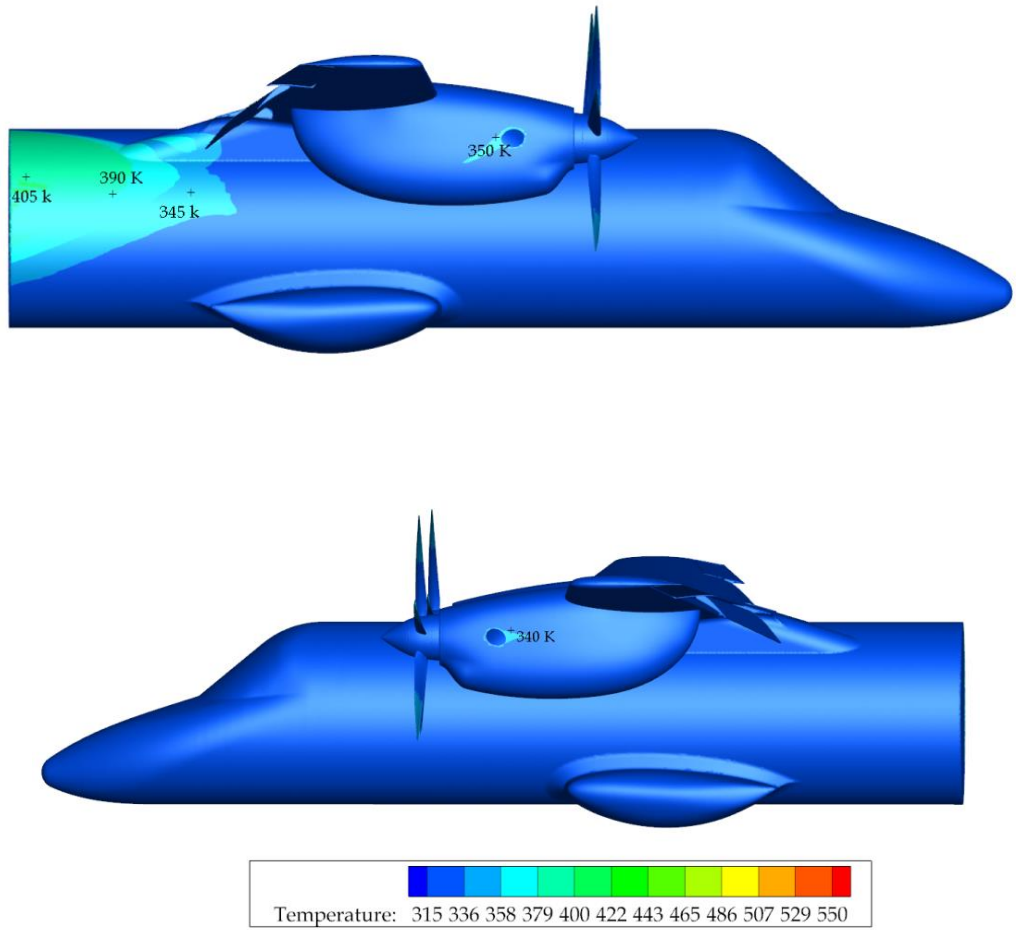

Figure 4.11 Total Temperature Contours on the Aircraft Surfaces – RHE (top) and LHE (bottom) (Take-off Condition) [Temperatures are in Kelvin]-Case 5

Table 4.1 Computational Results

Sl. No.	Case	Aircraft Surface temperature (Inboard) K (°C)				Aircraft Surface temperature (Outboard) K (°C)			
		Wing Lower Surface	**Flaps**	**Nacelle**	**Fuselage**	**Wing Lower Surface**	**Flaps**	**Nacelle**	**Propeller**
1.	**Case 1:** Ground Static **(Start Cycle)**	350 (77)	350 (77)	350 (77)	323 T_{amb} (50)	350 (77)	350 (77)	350 (77)	334 (61)
2.	**Case 2:** Ground Static Forward Thrust Condition **(Idle Condition)**	348 (75)	348 (75)	348 (75)	348 (75)	348 (75)	348 (75)	348 (75)	328 (55)
3.	**Case 3:** Ground Static Forward Thrust Condition **(Take-off Condition)**	332 (59)	332 (59)	362 (89)	332 (59)	332 (59)	363 (90)	362 (89)	340 (67)
4.	**Case 4:** Ground Static Reverse Thrust Condition **(Reverse Condition)**	380 (107)	400 (127)	350 (77)	412 (139)	349 (76)	349 (76)	350 (77)	334 (61)
5.	**Case 5:** Ground Static Forward Thrust Condition **(Take-off Condition)** Complete Aircraft	341 (68) (LH & RH)	341 (68) (LH & RH)	341 (68) (LH & RH)	341 68 (LH) 389 116 (RH)	341 (68) (LH & RH)	341 (68) (LH & RH)	341 (68) (LH & RH)	345 72 (LH) 341 68 (RH)

4.3 Numerical studies: Nacelle Zone and Bay temperature estimation

The resulting contour is plotted after evaluating the proper development of the flow around the nacelle by considering mass balance and energy balance at the domain entry and exit. Figure 4.12 shows the section location over which the temperature contours will be plotted in the results. The plane results show the fluid's behaviour inside the nacelle. Critical cases such as, case 3, 4, 6, 7, and 8 are discussed in this section and case 1, 2, and 5 results are tabulated in Table 4.2.

Y-Z cut plane	Distance (m) from X=0
1	1
2	2.25
X-Z cut plane	Distance (m) from Y=0
3	0.1

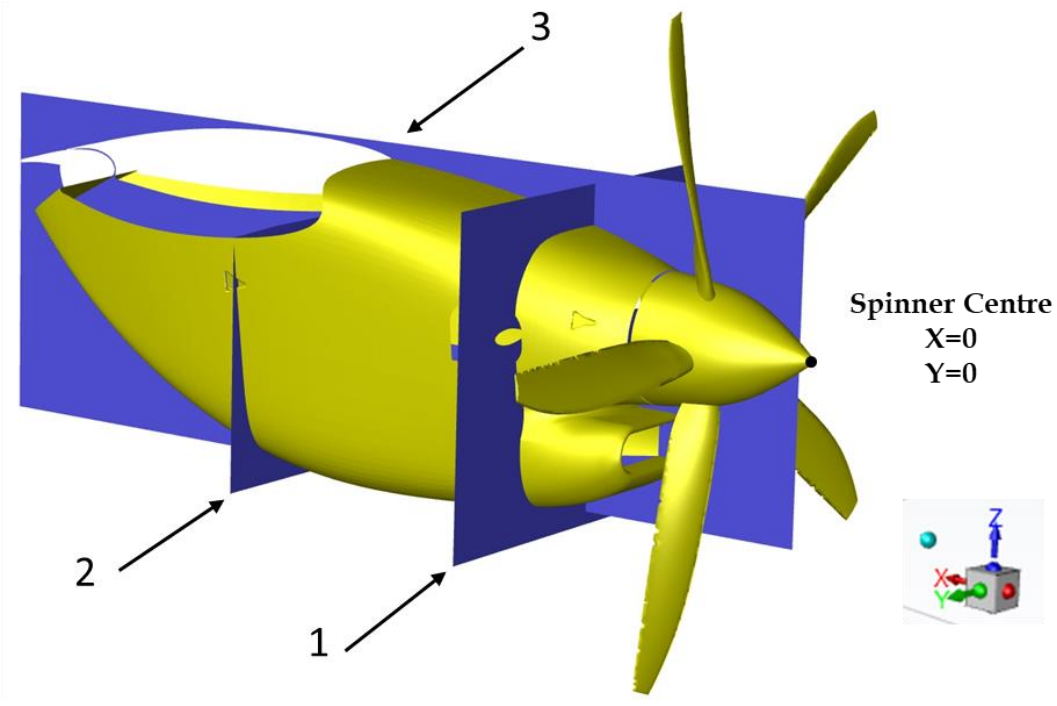

Figure 4.12 Cross-section planes where engine surface temperature was taken

Case 3. (Max. Cruise): In this case, the aircraft's altitude is 25,000 feet, and the free stream total pressure and ambient temperature for the corresponding altitude are 43743 Pa and -34.5°C (238.65K), respectively. The aircraft's speed is 0.47 Mach (159.94 m/s) with a propeller speed of 1700 rpm.

The Engine surface temperature at different plane locations is shown in Figure 4.13. The total temperature and static pressure contour on the nacelle surface are shown in Figure 4.14 and Figure 4.15, respectively.

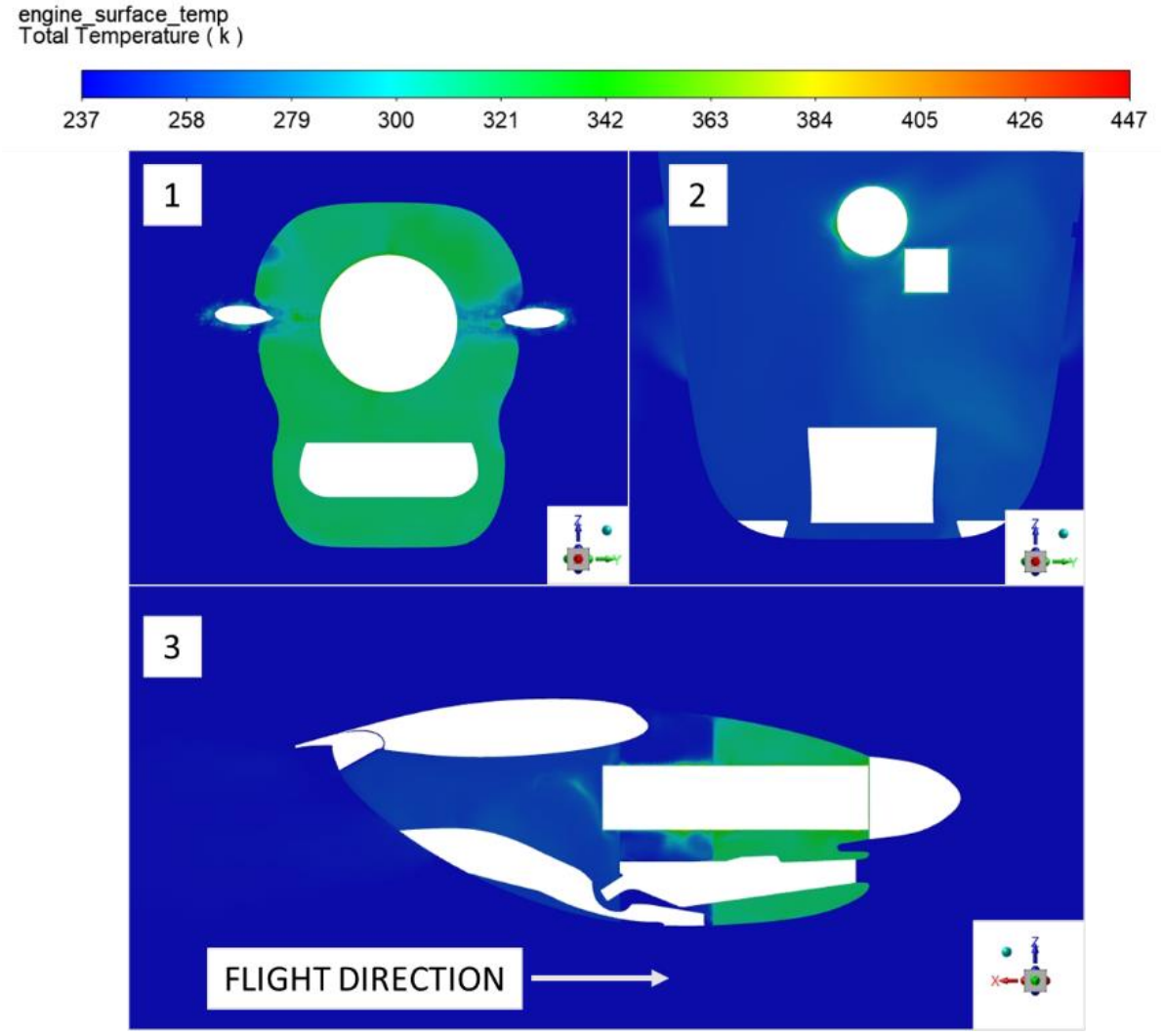

Figure 4.13 Engine surface temperature

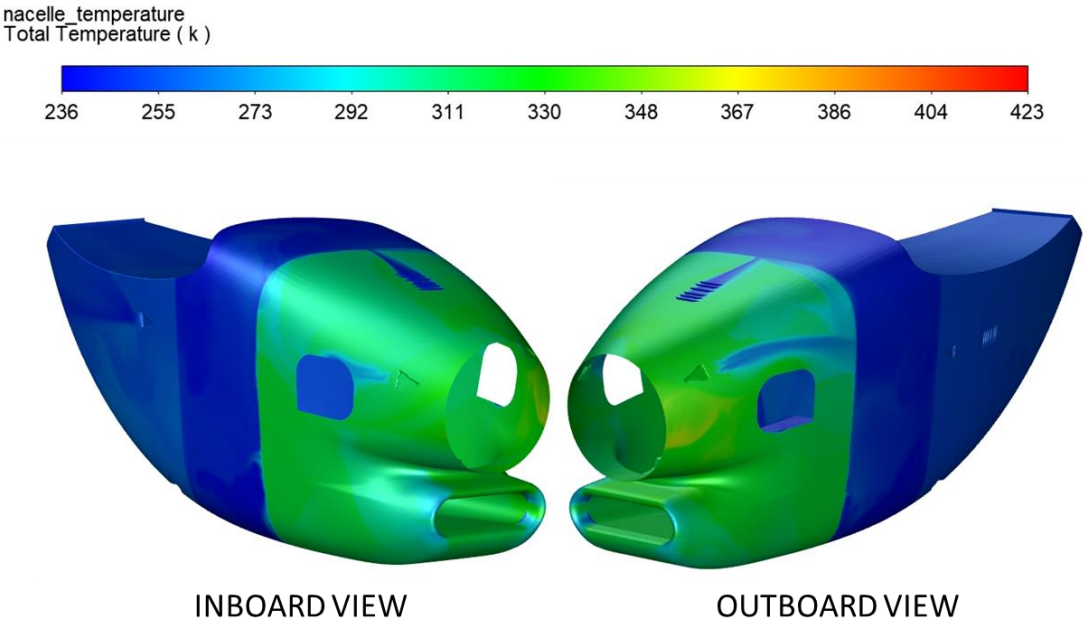

Figure 4.14 Total temperature contour on Nacelle Surface

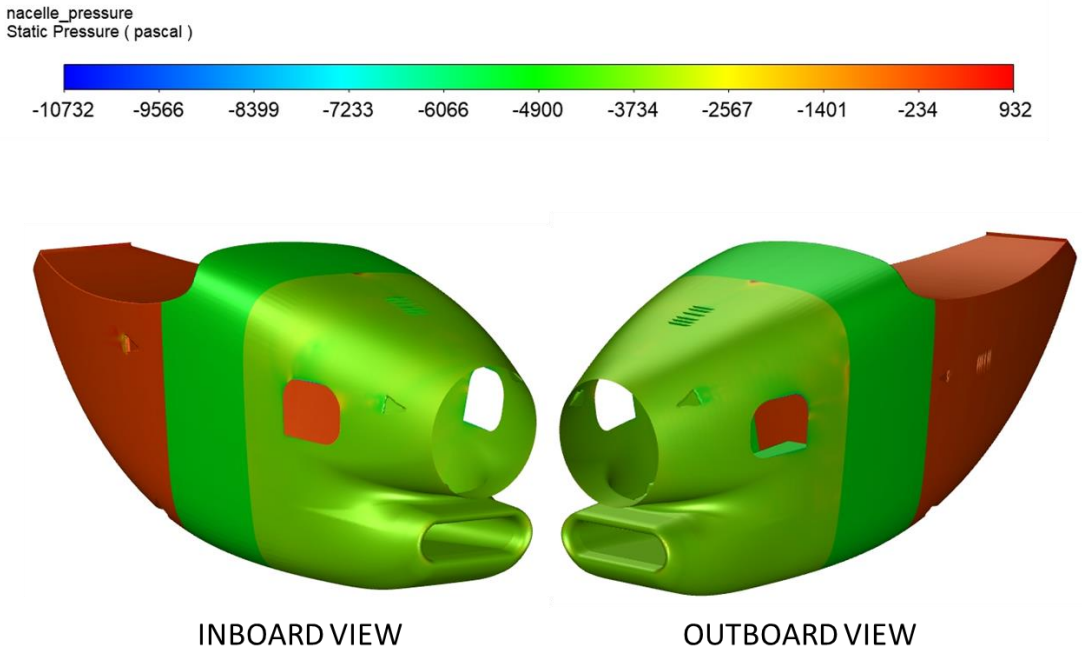

Figure 4.15 Static pressure contour on the Nacelle Surface

Case 4. (Economy Speed Cruise) (Altitude = 25000 ft): In this case, the altitude of the aircraft is 25,000 feet, the free stream total pressure and ambient temperature for the corresponding altitude is 41983 Pa and -34.5°C (238.65K) respectively. The aircraft's speed is 0.4 Mach (136.2 m/s) with a propeller speed of 1700 rpm.

The Engine surface temperature at different plane locations is shown in Figure 4.16. The total temperature and static pressure contour on the nacelle surface are shown in Figure 4.17 & Figure 4.18, respectively.

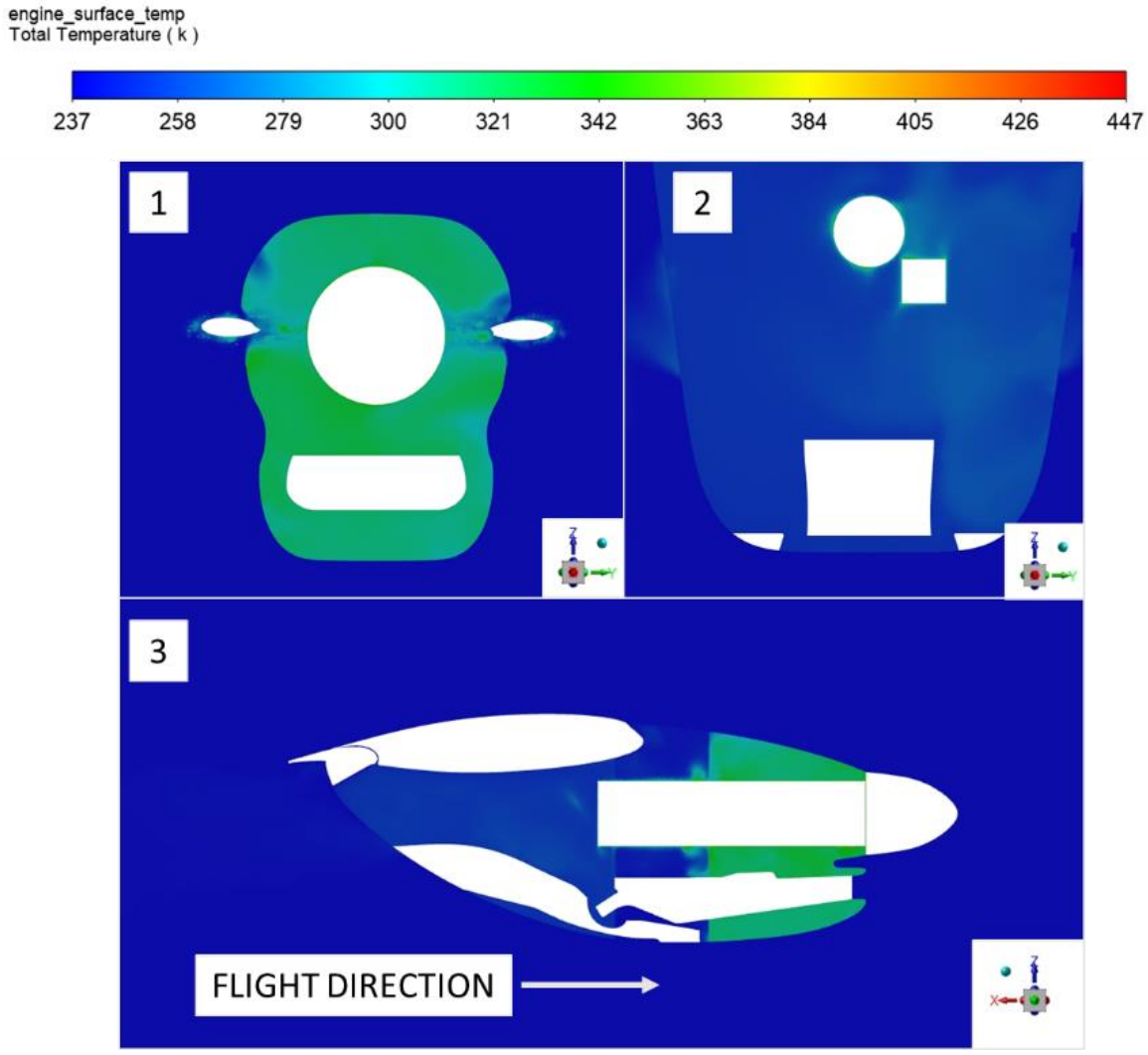

Figure 4.16 Engine surface temperature

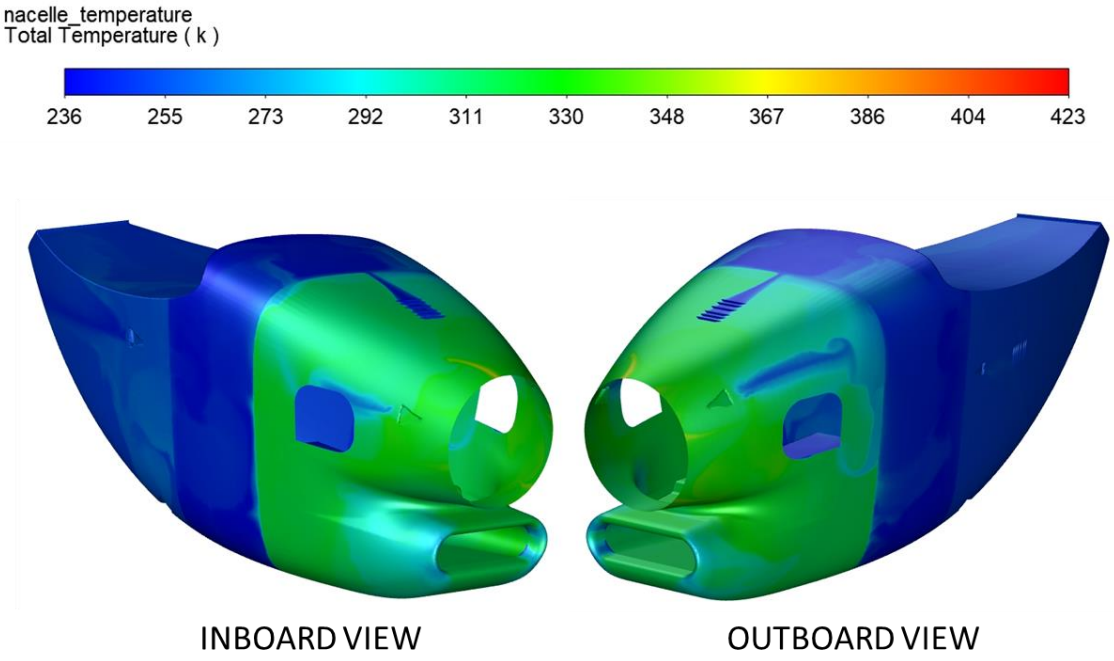

Figure 4.17 Total temperature contour on Nacelle Surface

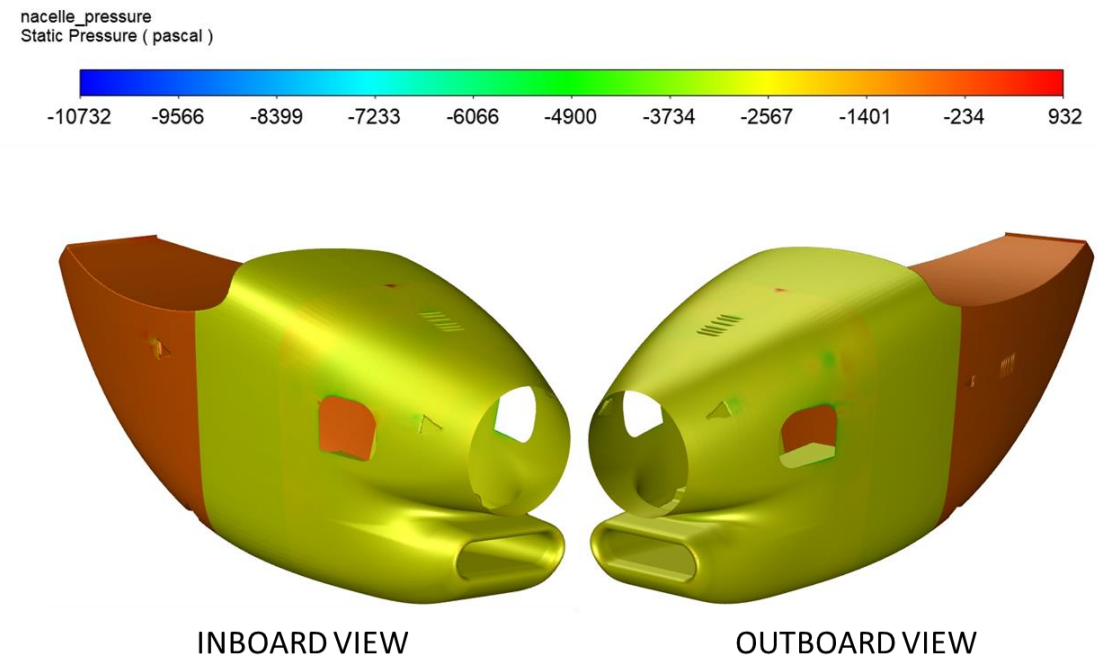

Figure 4.18 Static pressure contour on the Nacelle Surface

Case 6. Ground Run (Take-off Condition): In this case, the aircraft's altitude is 3,000 feet, and the free stream total pressure and ambient temperature for the corresponding altitude are 91709 Pa and 34°C (307.15K), respectively. The aircraft's speed is 0.02 Mach (6.8 m/s) with a propeller speed of 1700 rpm.

The Engine surface temperature at different plane locations is shown in Figure 4.19. The total temperature and static pressure contour on the nacelle surface were shown in Figures 4.20 & Figure 4.21, respectively.

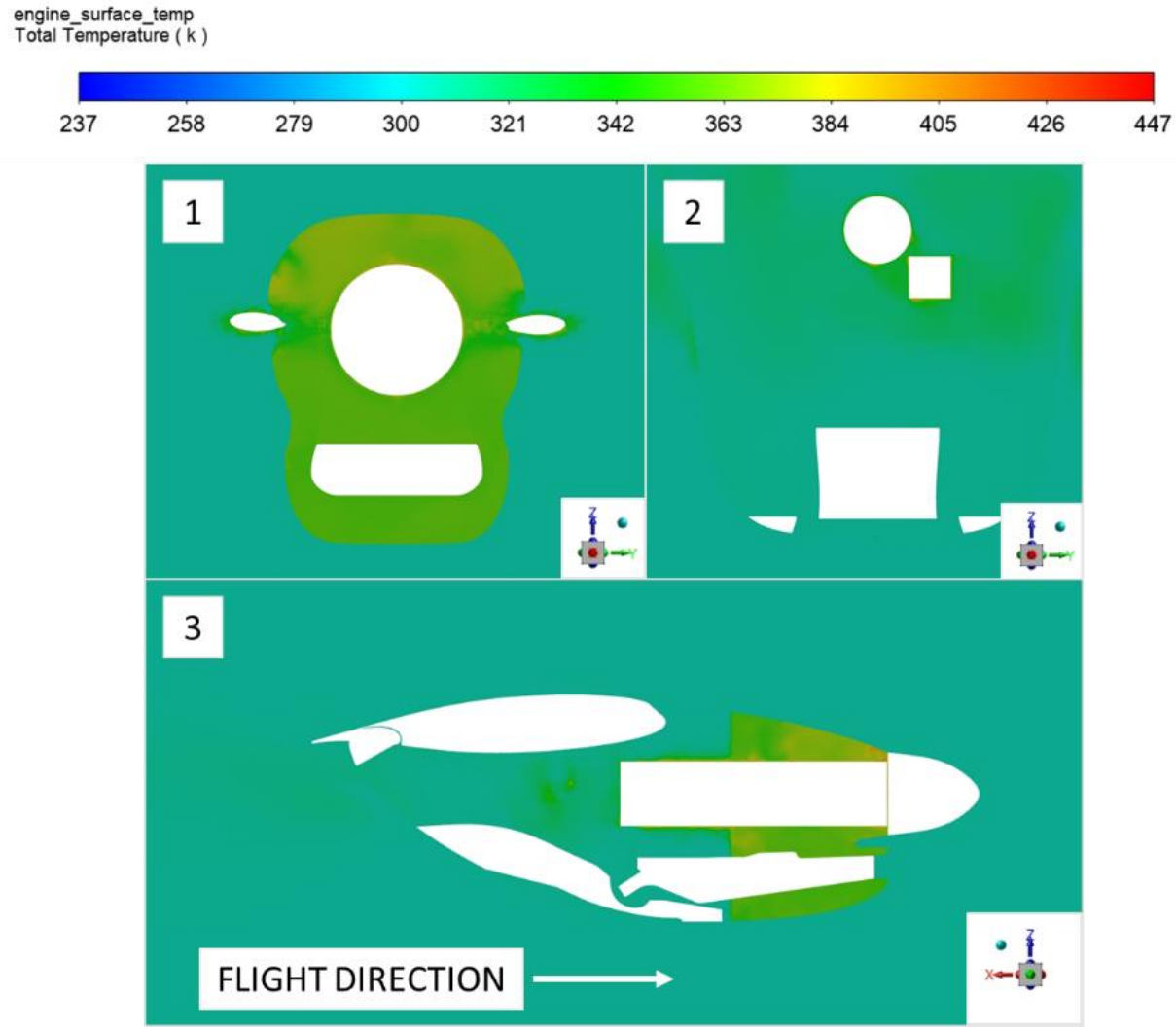

Figure 4.19 Engine surface temperature

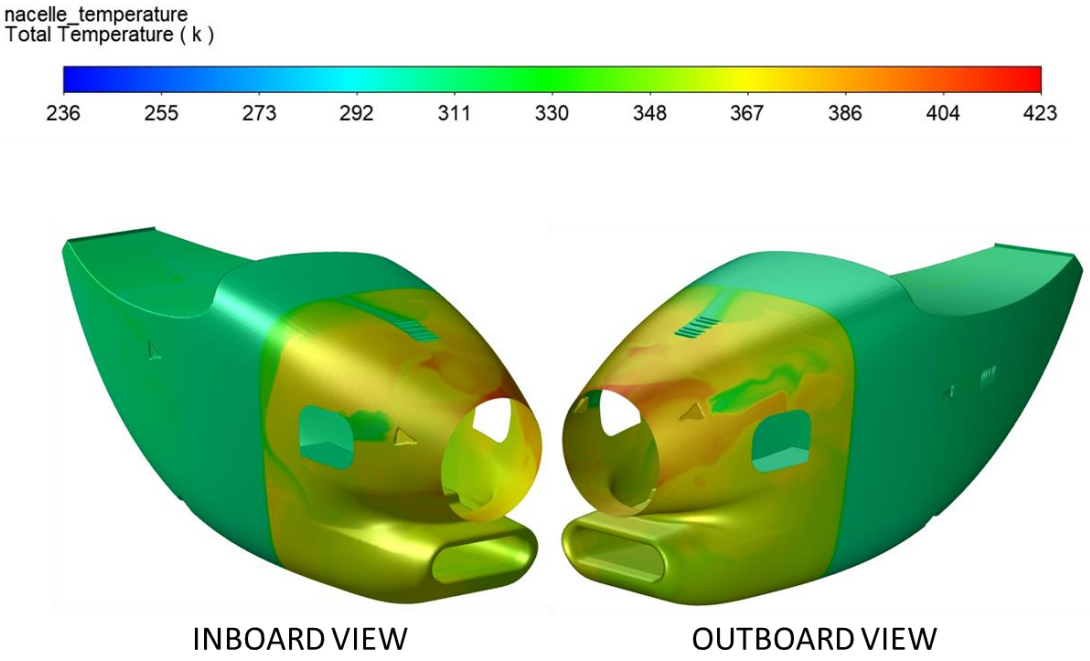

Figure 4.20 Total temperature contour on Nacelle Surface

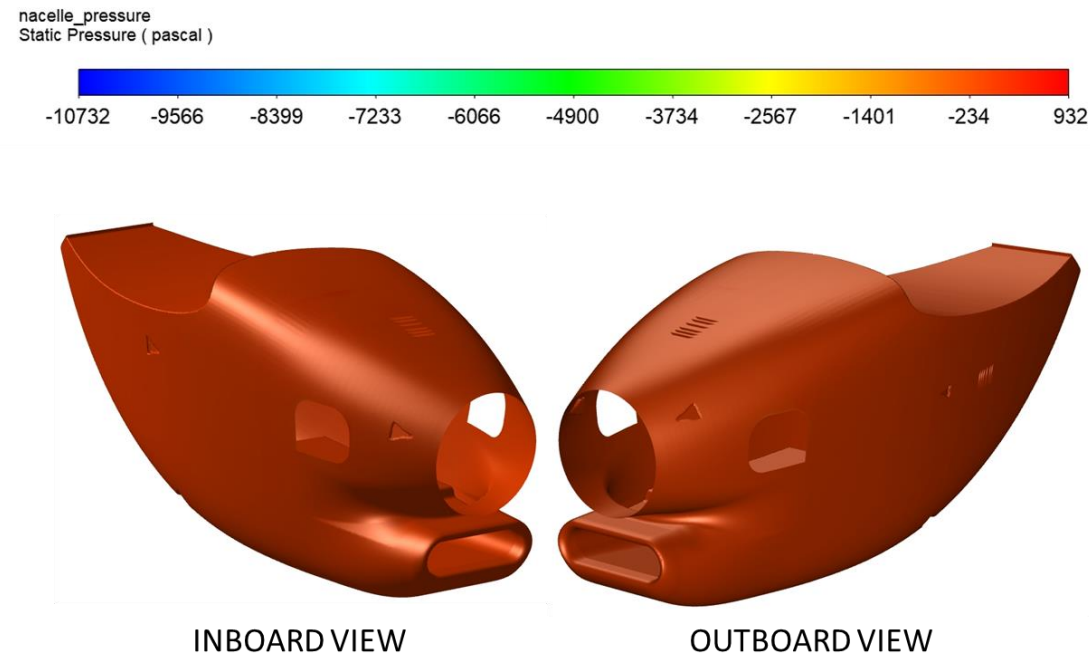

Figure 4.21 Static pressure contour on the Nacelle Surface

Case 7. (Flight Idle Condition): In this case, the aircraft's altitude is 3,000 feet, and the free stream total pressure and ambient temperature for the corresponding altitude are 91709 Pa and 34°C (307.15K), respectively. The aircraft's speed is 0.02 Mach (6.8 m/s) with a propeller speed of 1700 rpm.

The Engine surface temperature at different plane locations is shown in Figure 4.22. The total temperature and static pressure contour on the nacelle surface are shown in Figures 4.23 & Figure 4.24, respectively.

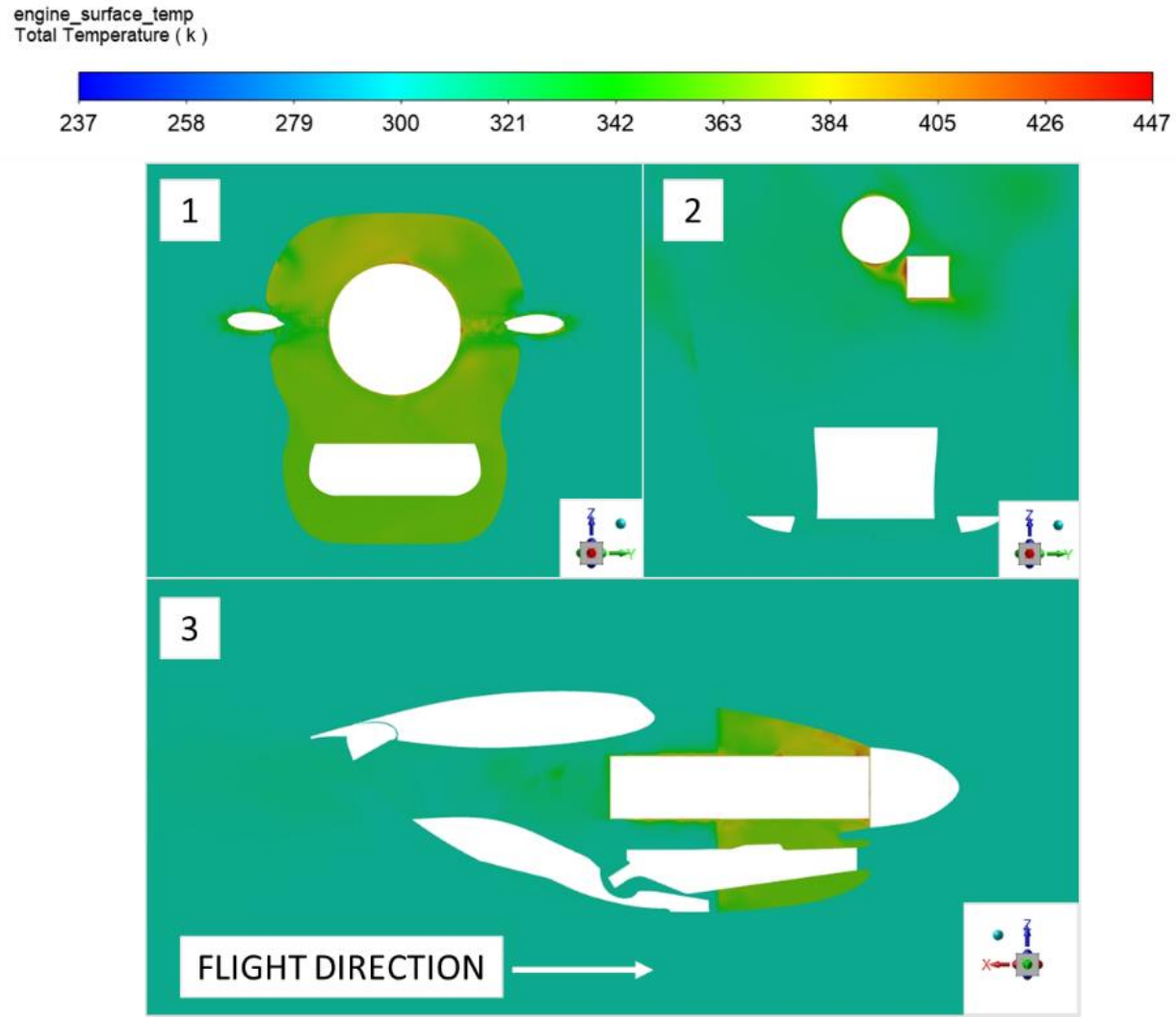

Figure 4.22 Engine surface temperature

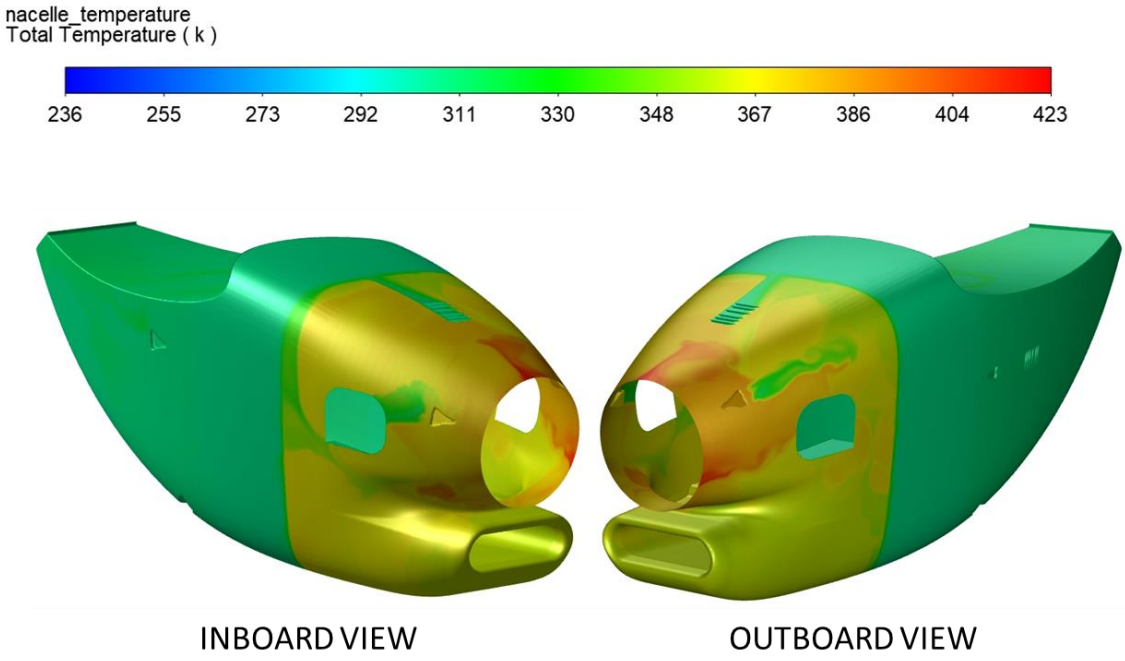

Figure 4.23 Total temperature contour on Nacelle Surface

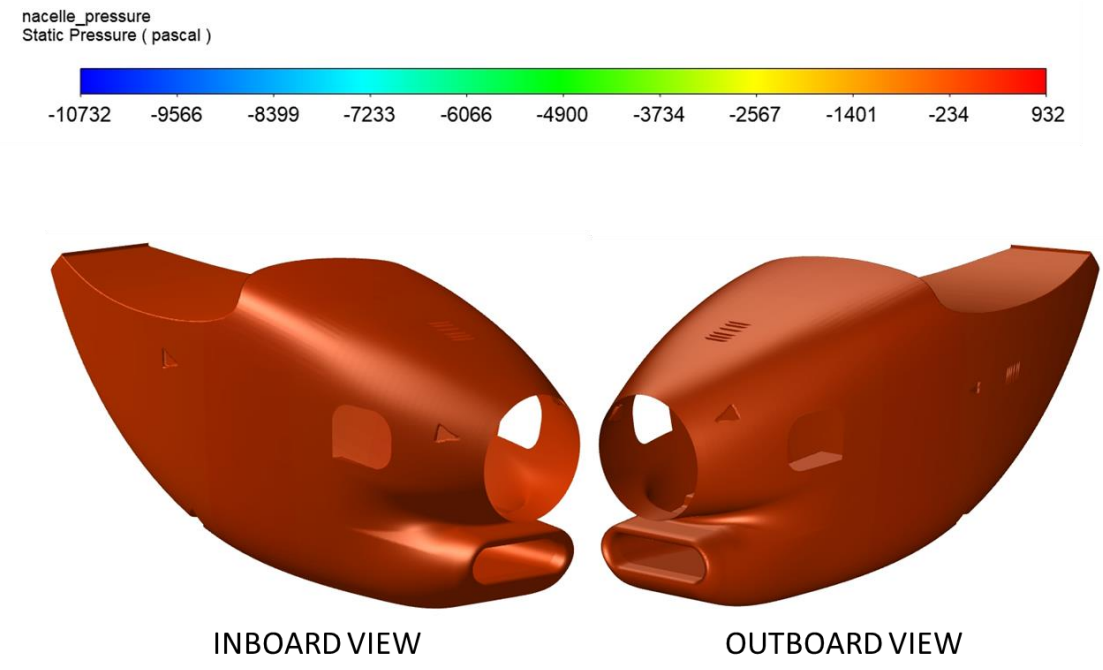

Figure 4.24 Static pressure contour on the Nacelle Surface

Case 8. (Ground Static Take-off Condition): In this case, the aircraft's altitude is 3,000 feet, and the free stream total pressure and ambient temperature for the corresponding altitude are 91709 Pa and 50°C (323.15K), respectively. The aircraft's speed is 0.02 Mach (6.8 m/s) with a propeller speed of 1700 rpm.

The Engine surface temperature at different plane locations is shown in Figure 4.25. The total temperature and static pressure contour on the nacelle surface are shown in Figure 4.26 & Figure 4.27, respectively.

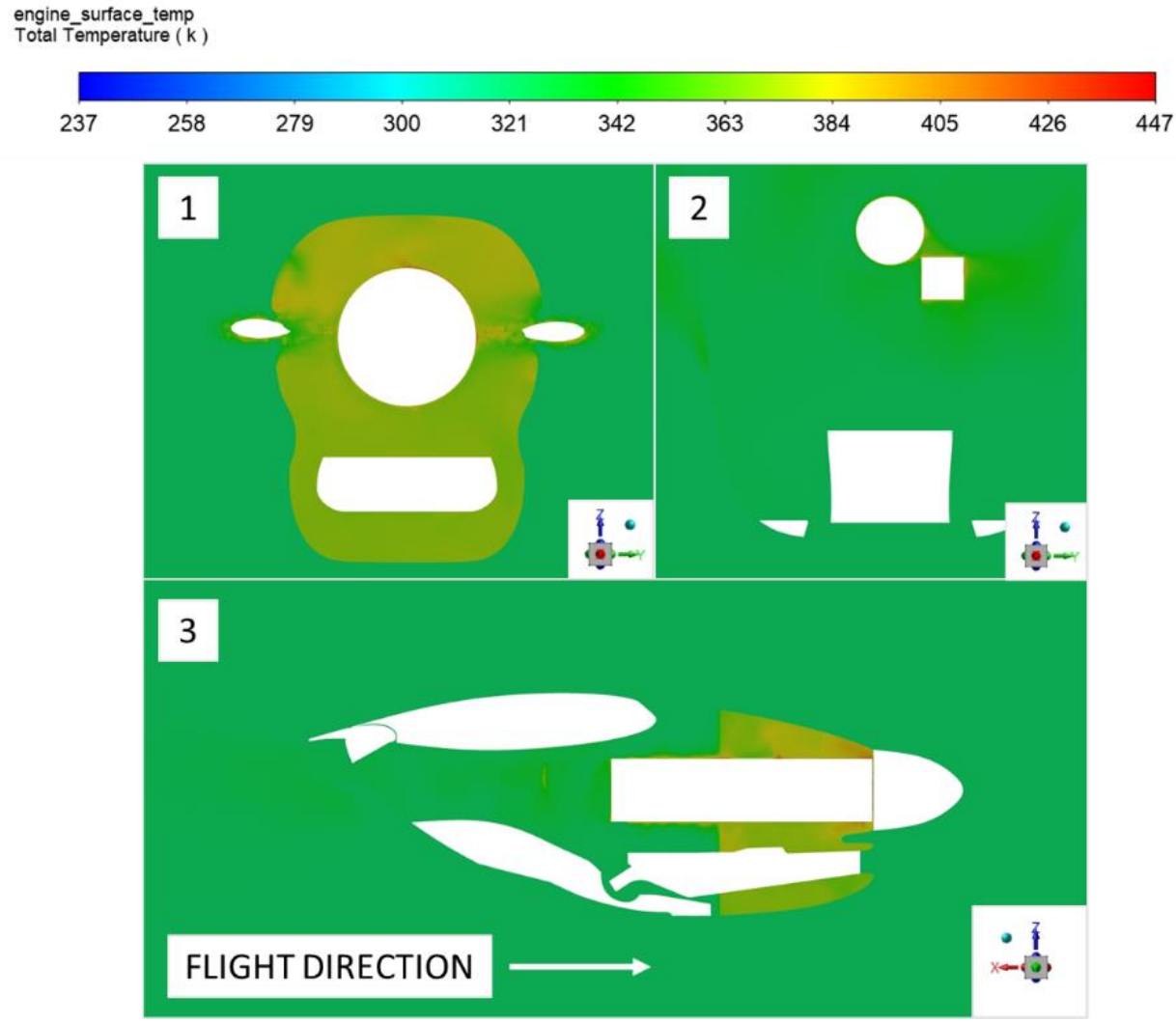

Figure 4.25 Engine surface temperature

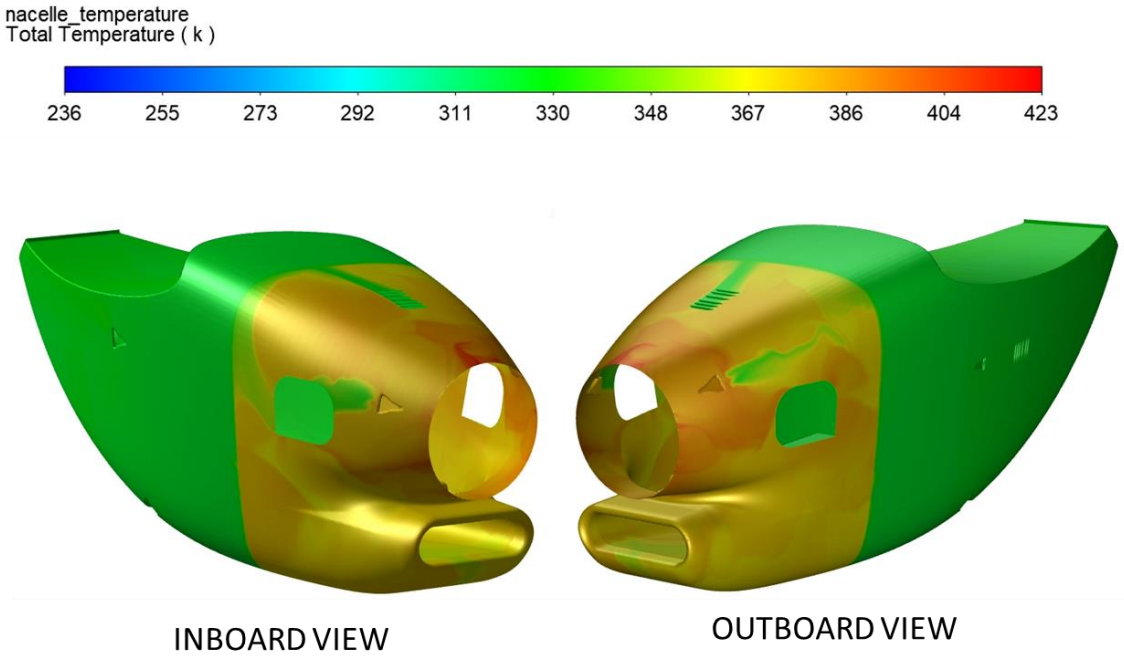

Figure 4.26 Total temperature contour on Nacelle Surface

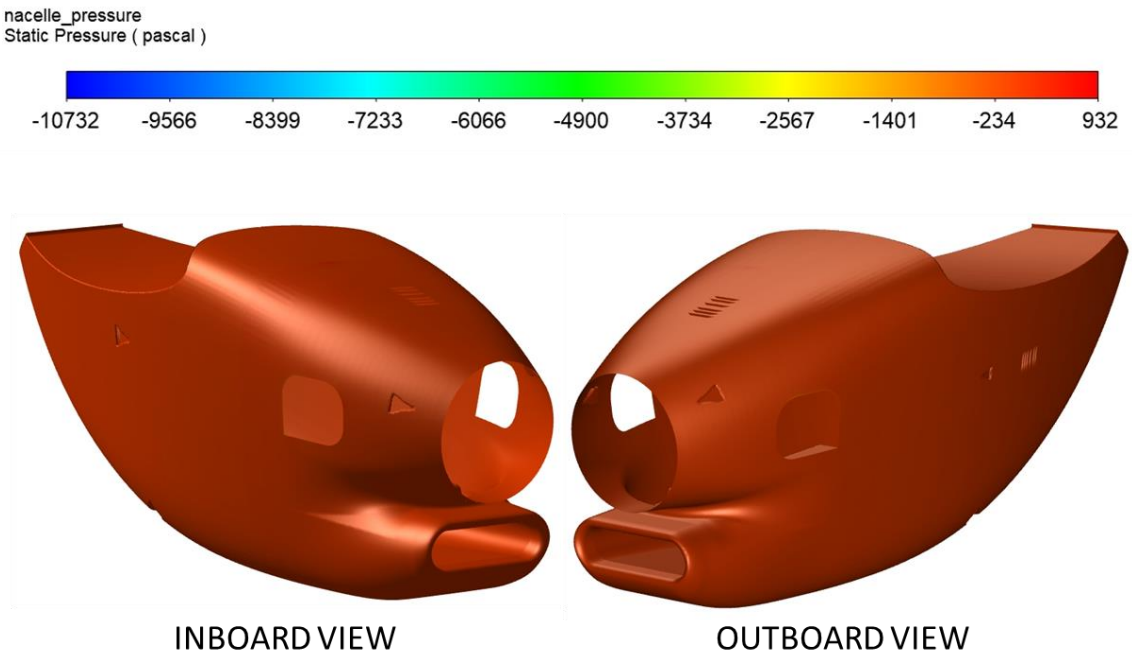

Figure 4.27 Static pressure contour on the Nacelle Surface

Table 4.2 Estimated temperatures data at different locations.

Case No.	Flight Cases	Propeller Speed, RPM	Outside Air Temperature, °C (K)	Speed, m/s (M)	Free Stream Total Pressure, Pa	Temperature observations			
						Hot Section (Front Nacelle) °C (K)		Plenum Section (Centre Nacelle) °C (K)	Inlet Section (Rear Nacelle) °C (K)
						Max	Average		
1	Case 1 (Min. Climb)	1700	6.1 (279.25)	71.46 (0.21)	88578	110.36 (383.51)	69.6 (342.75)	8.43 (281.58)	13.8 (286.95)
2	Case 2 (Best Rate of Climb)	1700	9.75 (263.4)	88.47 (0.26)	66222	115.72 (388.87)	56.21 (329.36)	-6.08 (267.07)	-0.34 (272.81)
3	Case 3 (Max. Cruise)	1700	-34.5 (238.65)	159.94 (0.47)	43743	85.79 (358.94)	41.92 (315.07)	-27.61 (245.54)	-16.36 (256.79)
4	Case 4 (Economy Speed Cruise)	1700	-34.5 (238.65)	136.2 (0.4)	41983	104.38 (377.53)	40.04 (313.19)	-27.70 (245.45)	-18.86 (254.29)
5	Case 5 (Economy Speed Cruise)	1700	-14.5 (258.45)	112.3 (0.33)	61661	112.83 (385.98)	54.69 (327.84)	-10.09 (263.06)	-3.04 (270.11)
6	Case 6 Ground Run (Take off Condition)	1700	34 (307.15)	6.8 (0.02)	91709	137.62 (410.77)	87.68 (360.83)	34.46 (307.61)	36.23 (309.38)
7	Case 7 (Flight Idle Condition)	1020	34 (307.15)	6.8 (0.02)	91709	148.88 (422.03)	91.96 (365.11)	34.68 (307.83)	36.26 (309.41)
8	Case 8 (Ground Static Take-off Condition)	1700	50 (323.15)	6.8 (0.02)	91709	149.9 (423.05)	100 (373.43)	50 (323.1)	50 (323.1)

4.4 Experimental results and validation

Thermal imaging is carried out during the engine profile ground run to capture the exhaust gas temperature effect on the propeller and fuselage surfaces. The Infrared Thermal (IR) Camera SC5500 captured the propeller and aft fuselage surface temperature. The tests were carried out following flight test guidelines for the certification of commuter aircraft. The flight testing was carried out with static ground conditions, with an altitude of 3000 ft. AMSL and OAT 28°C. The experimental results obtained during the engine ground run are shown in Table 5. The recorded IR temperature data is plotted along with the engine parameters at the reverse Tq/thrust test point (reverse 5% Tq), as shown in Figure 4.28. The model designated with the proposed exhaust stub is computed numerically and experimentally. The present CFD simulation results are validated with the experimental data (Temperature Stickers and IR Thermal Imaging) for static reverse conditions. The computational results are validated and presented in Table 4.3 and Table 4.4.

Table 4.3 Validation of numerical and experimental data

Condition	**CFD results (°C)**	**Temperature Stickers (°C)**	**IR Thermal Imaging (°C)**
Ground St. Reverse Tq/Thrust Condition	73	77	71

Table 4.4 Propeller Blade Surface Temperature (°C) on both LH & RH Engine

Sl. No.	Temperature stickers (from hub to tip)	LH Engine	RH Engine
1.	T1	43	54
2.	T2	49	60
3.	T3	54	60
4.	T4	59	60
5.	T5	60	60
6.	T6	71	66
7.	T7	77	66
8.	T8	71	60
9.	T9	62	54

However, to estimate the reliable exhaust jet temperature gradient along the aircraft surfaces, an effort was made to capture jet temperature along with the exhaust stub and exit plane using a non-contact infrared camera. The IR Imagining data are compared and validated with the CFD results. The measured temperature along the stub and stub exit to the propeller plane is shown in Figure 4.29 and Figure 4.30, respectively. The present numerical and experimental results are presented, and the effects of turboprop engine flue gas impingement on propeller blades are discussed. The temperature profiles of the propeller blade are compared and validated with CFD code.

A good correlation between experiments and numerical results is observed from the results. Also, the estimated propeller blade temperature is within the acceptable limit as the propeller manufacturer prescribes. The comprehensive study shows that ambient temperature, propeller speed, Power/Thrust variation (Propeller Blade Angle), the direction of crosswind, and aircraft speed are sensitive and have implications on the surface temperature. Aircraft forward speed has a more significant influence as the forward speed increases, and blade/surface temperature reduces considerably. Hence, the critical condition for the entire flight operating regime is ground static reverse

torque/thrust operation and aircraft landing conditions where reverse torques will be applied at lower speeds. However, the experimental and computational results agree, and the methodology can be adopted for similar complex challenges faced in aerospace applications. Also, the estimated propeller blade temperature is within the acceptable limit as prescribed by the propeller OEM.

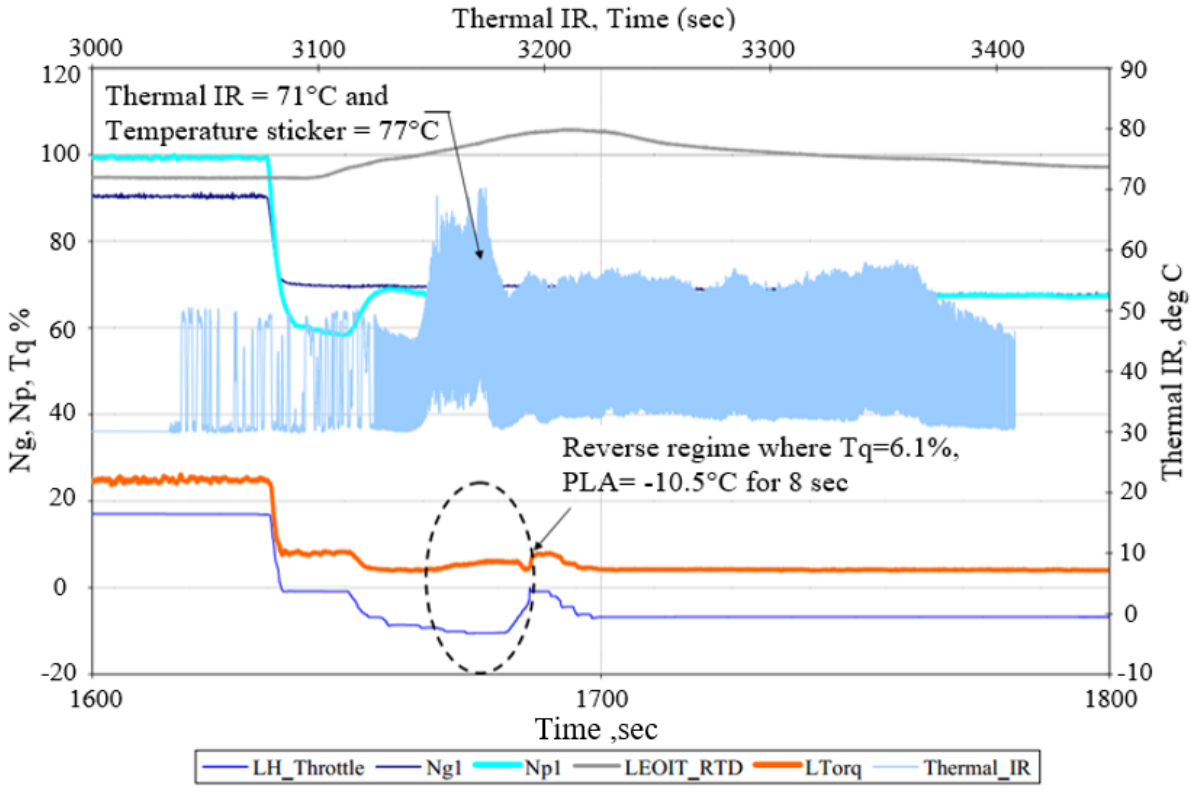

Figure 4.28 Thermal IR data of propeller blade surface temperature plotted against the engine parameters

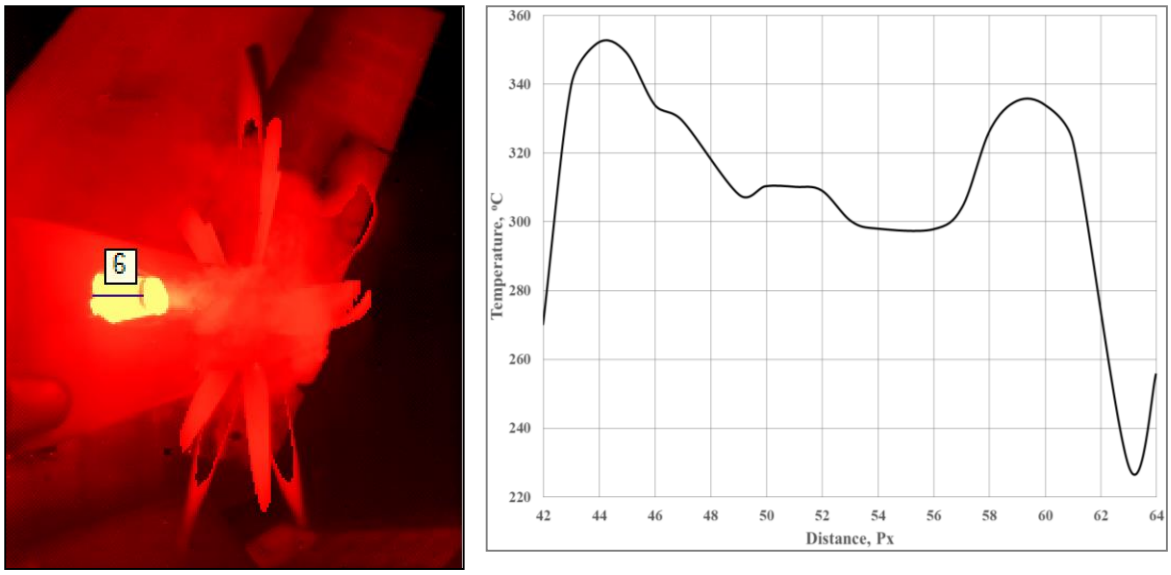

(a) Thermal IR temperature along the plane 6 LH view

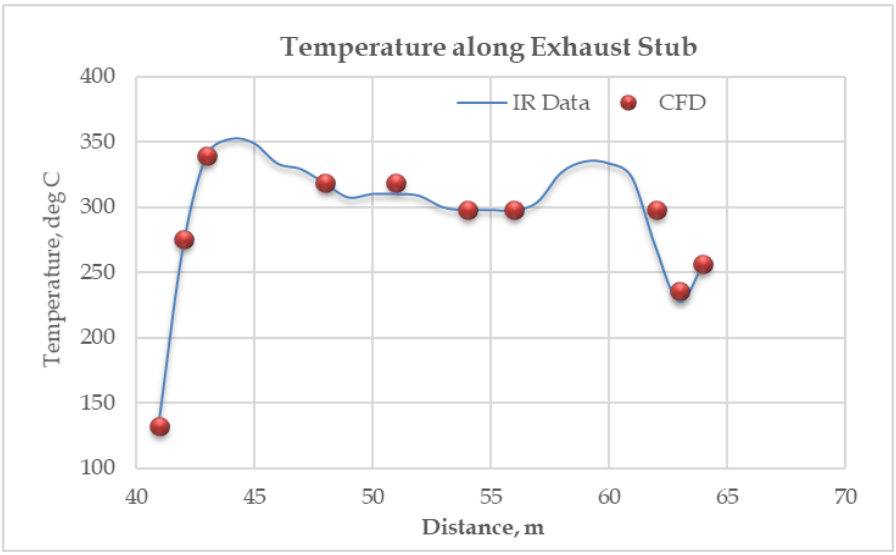

(b)

Figure 4.29 (a) IR Temperature measurement along exhaust stub (b) Comparison of IR temperature and CFD data along the exhaust stub

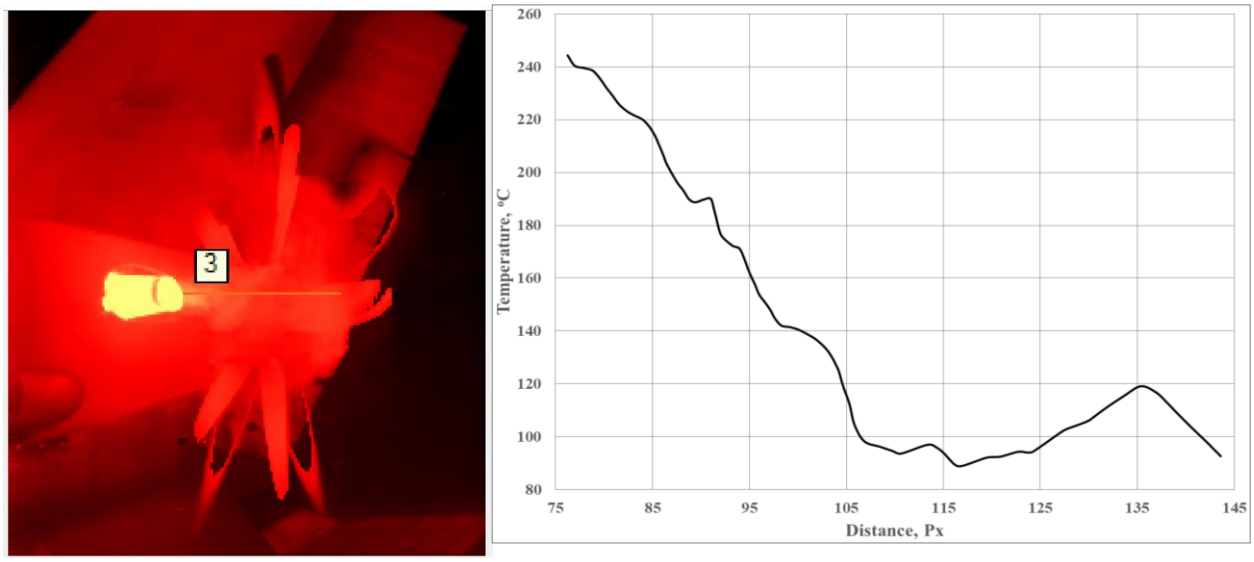

(a) Thermal IR temperature along the plane 3 LH view

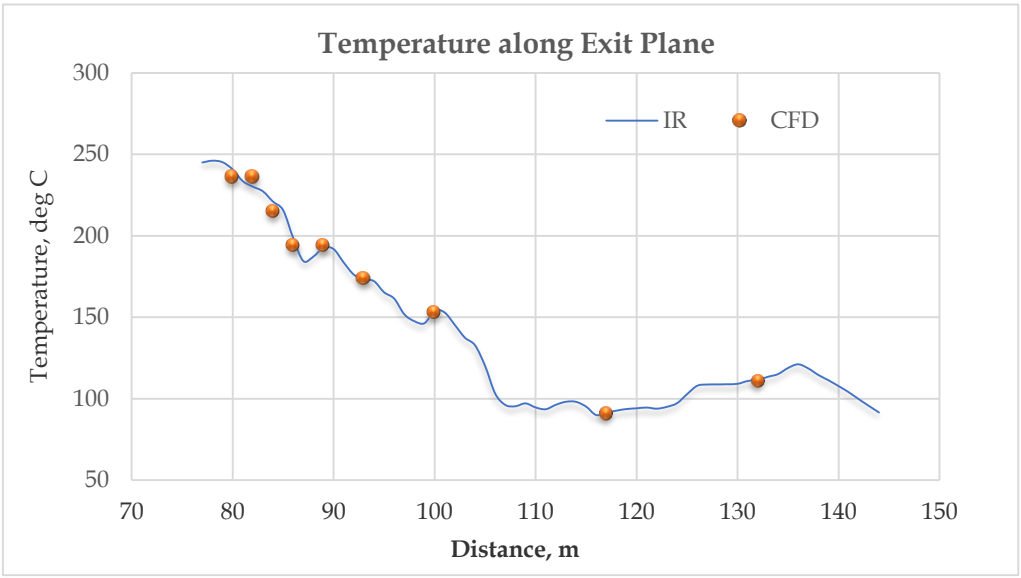

(b)

Figure 4.30 (a) IR Temperature measurement at stub exit to propeller plane. (b) Comparison of IR temperature and CFD results along the stub exit to propeller plane in X-direction

The computational validation of the zonal and bay ventilation methodology and its effectiveness over the nacelle surface temperature distribution is carried out in the study. SST k-ω turbulence model is utilized to numerical study the internal flow of air through the inlets and outlets over the nacelle surface.

As we mentioned, the nacelle is made of aluminium alloy sheets, and intake ducts are made of composite materials. This Aluminum alloy's tensile yield strength (Fty) is

sensitive to temperature variations. With the temperature rise from 477K(204°C) to 594K(276°C), the Tensile Yield Strength of the material drops from 60% to 40% (shown in Figure 4.31) of Fty (100% Fty considered at room temperature).

From the temperature distribution over the nacelle, it can be observed that the peak temperature is not higher than the material yield temperature shown in Table 4.2. Thus, the bay ventilation scheme effectively reduces the heat transferred from the engine to the nacelle.

However, the overall validation is quite reliable with the present numerical model and setup. Hence the present numerical method can be used for various flight operating conditions like taxi, take-off, and cruise. Further improvement can be made by including the radiation model in the CFD solver.

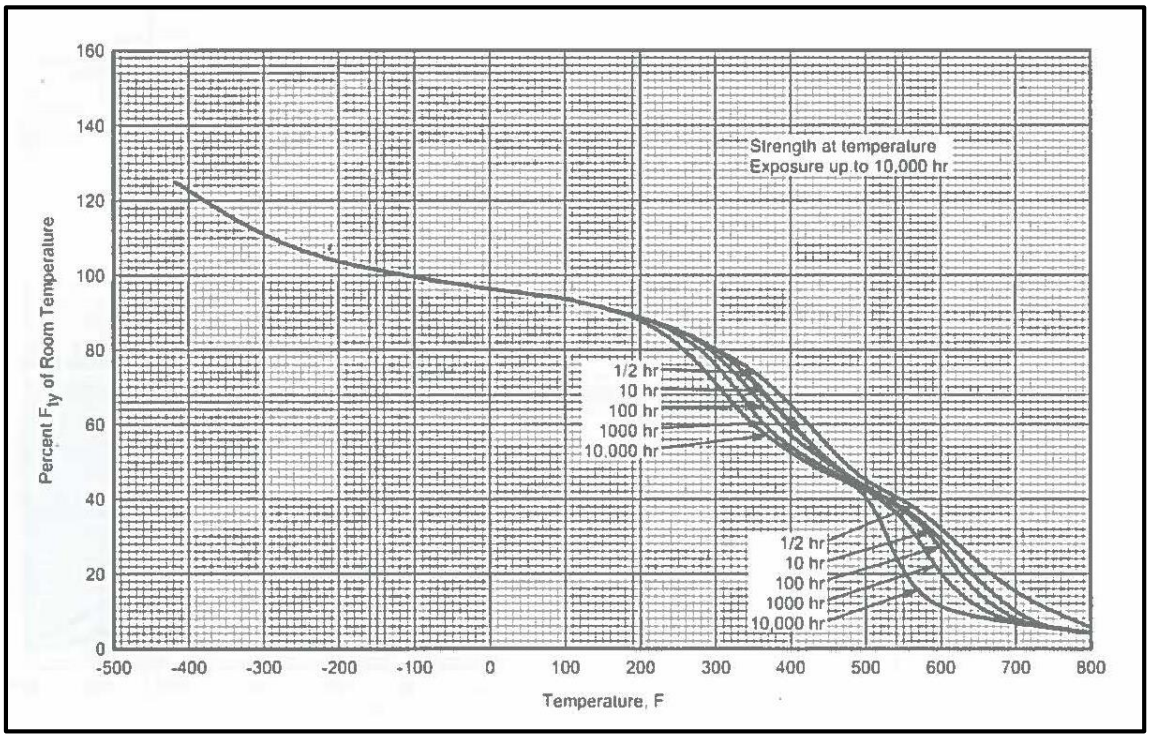

Figure 4.31 Effect of temperature on the tensile yield strength (F_{ty}) of 2219-T81 aluminium alloy sheet and 2219-T851 aluminium alloy plate.

4.5 Effect of Exhaust Stub Design on Engine Performance

The impact of change in exhaust stub angle on the jet thrust at various operating conditions, like at high altitude airports with specified MORA (Minimum Off-Route Altitude) and cruise performance, is estimated using the engine performance estimation deck provided by engine OEM for tractor configuration aircraft as per section 3.5. The jet thrust is estimated for stub angles 20° and 35.5° at different ISA conditions for 0.25M, and the results of the high-altitude airports MORA condition are shown in Table 4.5. The jet thrust is similarly estimated for cruise conditions at different ISA conditions for 0.4M, and the results are shown in Table 4.6. However, the exhaust stub angles are inferred as per Figure 4.32, representing the exhaust stub orientation in Figure 3.8.

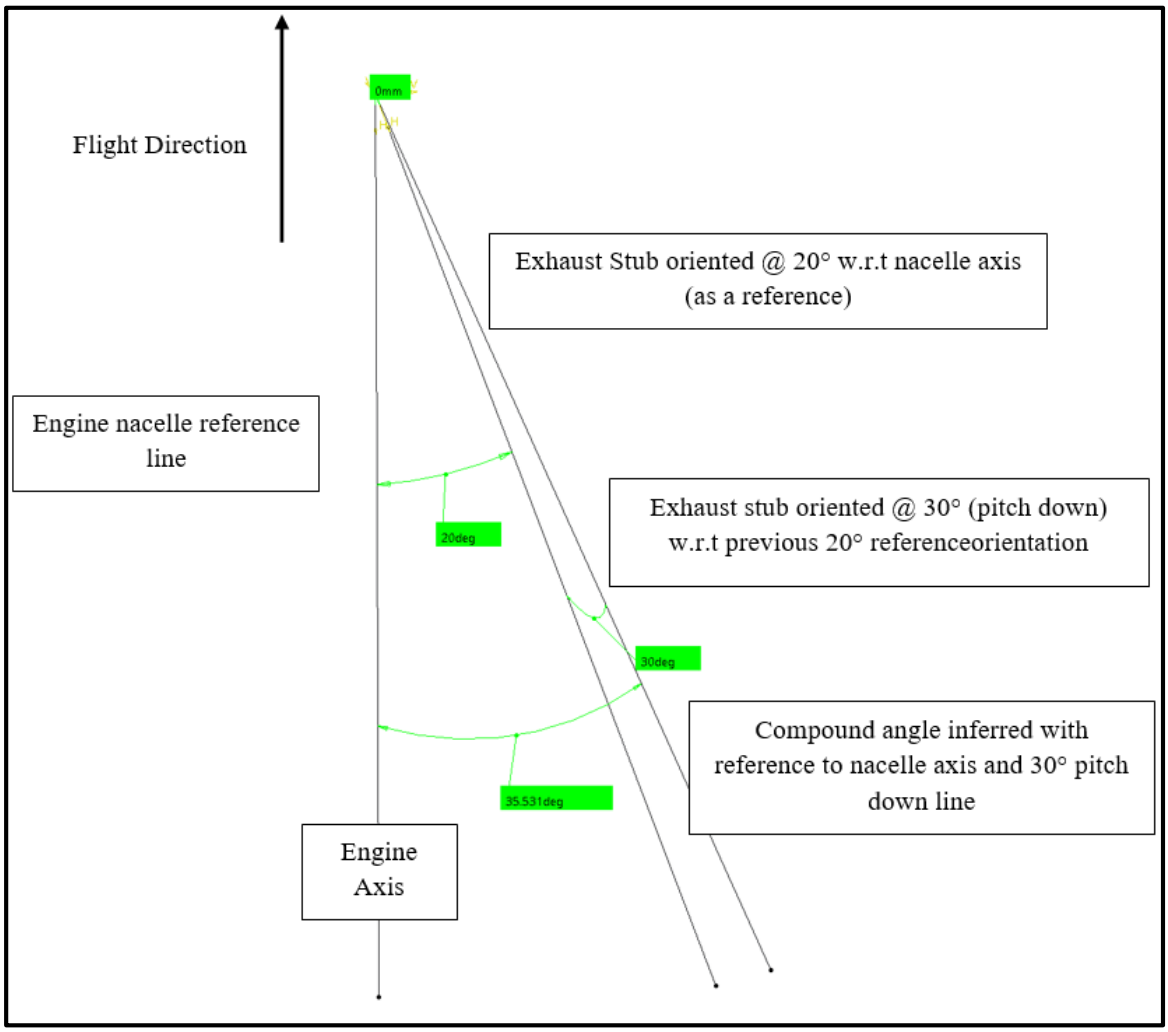

Figure 4.32 Orientation of Exhaust Stub Angle

Table 4.5 Jet Thrust Available for MCOR

ISA	Jet thrust (kg), MCOR, M = 0.25, Exhaust Angle = 20° from engine CL				Jet thrust (kg), MCOR, M = 0.25, Exhaust Angle = 35.5° from engine CL			
	Altitude m (ft.)				Altitude m (ft.)			
	0 (0)	1524 (5000)	3048 (10000)	6279 (20600)	0 (0)	1524 (5000)	3048 (10000)	6279 (20600)
0	41.3	44.5	48.2	46.0	30.4	33.8	37.5	36.8
20	39.7	42.8	45.0	**37.5**	29.1	32.4	34.8	**29.6**
35	37.1	36.7	35.3	29.5	26.9	27.3	26.7	22.9

Table 4.6 Jet Thrust Available for Max Cruise Condition

ISA	Max Cruise, M = 0.4, Exhaust Angle = 20°				Max Cruise, M = 0.4, Exhaust Angle = 35.5°			
	Altitude m (ft.)				Altitude m (ft.)			
	0 (0)	1524 (5000)	4572 (15000)	7620 (25000)	0 (0)	1524 (5000)	4572 (15000)	7620 (25000)
0	-3.1	0.7	7.8	9.7	-9.5	-5.4	2.0	5.0
20	-3.8	0.0	5.2	5.4	-10.0	-5.9	0.0	1.6
35	-4.7	-1.9	1.2	1.6	-10.7	-7.4	-3.1	-1.4

It is observed from Table 4.5 that the jet thrust available at ISA+20, 0.25 M, OEI for high altitude MORA (20600 ft.) condition for 20° exhaust angle is 37.5 kgf and for 35.5° exhaust angle is 29.6kgf. With tilt in the exhaust stub from 20° to 35.5°, the jet thrust is dropped by 8 kgf. Subsequently, concerning the change in exhaust stub angle, no significant impact is observed during cruise conditions at a higher Mach number as per Table 4.6. From this, it is clear that a change in stub angle has significant effects on performance during MORA conditions and the results of the jet thrust are sensitive to changes in exhaust stub angle.

CHAPTER 5

CONCLUSION

From the analytical, numerical and experimental studies following conclusions are drawn:

- A new engine exhaust stub has been designed and fitted on the aircraft with a 30° pitch down. The final exit area of the stub chosen is 93 Sq.in. The thermal effects of exhaust flue gas impingement on the propeller blades and aircraft structures are numerically studied and analyzed analytically.
- In addition, numerical simulation was extended to understand the temperature distribution in different zones of the nacelle and suggest ventilation methodology and its effectiveness.
- The engine stub exit temperature calculated is 640°C and 582°C for aircraft static and cruise conditions, respectively, and results show good agreement with numerical and experimental studies.
- For the pusher configuration, numerical simulations were carried out for flight and ground operating conditions to determine the temperature distribution on the propeller blade and nacelle surfaces.
- For the most critical case of ground static reverse thrust, the temperature estimated on the composite propeller blade surface is 73°C, whereas, experimentally measured is 71°C.
- For the reverse torque case with a forward aircraft speed of 20-40 knots, aluminum aft-fuselage surface temperature estimated is 108°C within the allowable limits of aluminum material. This shows that the designed stub (with 30° pitch down installation) is satisfactory as the temperature on the propeller and aft-fuselage surface is within the allowable limits.
- For the tractor configuration, the propeller is not in the critical path of the exhaust. However, the airframe design needs major attention due to the direct impingement of hot exhaust. For this configuration, the same stub design with asymmetric installation with 20° inboard and 10° outboard for RHE and with 10° inboard and 20° outboard for LHE has been adopted with pitch down.

- The numerical analysis of the zonal and bay ventilation methodology and its effectiveness over the nacelle surface temperature distribution is carried out. The effect of exhaust gas temperature is studied for a ground static condition for both forward (20° blade angle, fine pitch) and reverse thrust (-9° blade angle) with standard and rotated stub angles.
- In the static reverse conditions for asymmetric stubs, the estimated maximum propeller blade temperature is 334K (61°C), and the fuselage surface temperature is 412K (139°C). Compared to the pusher configuration temperature estimated is 10°C and 31°C lesser on the propeller and fuselage surface respectively. Thus, asymmetric installation of the stub is justifiable.
- Using the estimated engine performance program, the engine-propeller performance for different flight conditions is estimated for the tractor configuration. It is observed with the proposed stubs there is a loss of jet thrust by 8 kgf in MORA (20600 ft.), which is within acceptable limits.

Recommendation and future Scope of work for tractor aircraft:

- Based on the numerical, experimental and engine performance studies, the newly designed stub with asymmetric installation has been recommended for installation.
- Aerodynamically and structurally sensitive areas such as nacelles, wings, fuselage, control flaps, etc., exposed to hot exhaust gases, can be reinforced with suitable material selections and thermal barrier coatings.
- To carry out detailed nacelle bay ventilation studies to optimize the cooling inlet and outlet channels to ensure the adequacy of cold air supply and exit of hot air.

CHAPTER 6

REFERENCES

Ajoy Kumar Kundu (2010). “Aircraft Design”, *Cambridge University Press, New York.*

ANSYS FLUENT (2019). “Fluent Theory Guide”, *ANSYS Inc*, USA.

ANSYS ICEM CFD (2019). “ICEM CFD Theory Guide”, *ANSYS Inc*, USA.

Balland, Morgan, Olivier Verseux, and Marie-Josephe Esteve. (2005), "Aero-Thermal Computations with Experimental Comparison Applied to Aircraft Engine Nacelle Compartment." *Turbo Expo: Power for Land, Sea, and Air, Vol. 47268.*

Bhaskar Chakravarthy (2009). “Report on LTA PSA: Nacelle Layout Design”, *CSIR-National Aerospace Laboratories*, Bangalore, India.

Han. B, R. J. Goldstein, "Jet Impingement Heat Transfer in Gas Turbine Systems", *University of Minnesota, Minneapolis, MN55455, USA.*

Buonomo, G., et al. (2013), "Aerothermal analysis of an aircraft nacelle in the framework of a fully coupled approach." *Proceedings of the Italian Association of Aeronautics and Astronautics, XXII Conference, Napoli.*

Changduk Kong, et all. (2000), "Propulsion system Integration of turboprop aircraft for basic trainer." *Aircraft Engineering and Aerospace Technology Volume 72. Number 6 (2000): 524-536.*

Chudy P, Filakovsky K and Friedl J (2004). “Aerodynamic Analysis of Turboprop Engine Air Intake”, *Acta Polytechnica Vol.44 No. 3/2004*, Czech Republic.

Colina Y, Aupoixb B, Boussugea J F and Chanez P (2007). “Numerical Simulation and Analysis of Crosswind Inlet Flows at Low Mach numbers”, *CERFACS, ONERA DMAE and SNECMA, France, Proceedings of the 8th International Symposium on Experimental and Computational Aerothermodynamics of Internal Flows, ISAIF8-0058,* Lyon.

Director, CSIR-NAL, “About NAL”, http://www.nal.res.in, Mar. 18, 2013.

Federal Aviation Regulations, "Federal Aviation Administration." Washington, DC (1990).

Fluent, Ansys. "12.0 User’s Guide, April 2009." Ansys Inc., Lebanon, NH, USA (2019), p.4-26.

Ganesan S, (2011). “Presentation on Computational Fluid Dynamics”, *Gas Turbine Research Establishment,* Bangalore, India.

Greco et. al., "Spinner Ducted Exhaust for Pusher Turboprop Engines", *Patent No. 4892269, Jan 9, 1990.*

Guilherme L. Oliveira, Luis C. C. Santos, André L. Martins, Gilberto G. Becker, Marcus V. F. Reis, Nicolas Spogis and Rodrigo F. A. F. Silva (2008). “A Tool for Parametric Geometry and Grid Generation for Aircraft Configurations”, *ICAS 2008, Embraer – Empresa Brasileira de Aeronáutica, Brazil, ESSS - Engineering Simulation and Scientific Software,* Brazil.

Iwaniuk, Andrzej, Witold Wiśniowski, and Jerzy Żółtak (2016). "Multi-disciplinary optimisation approach for a light turboprop aircraft-engine integration and improvement." *Aircraft Engineering and Aerospace Technology: An International Journal 88/2 (2016):348-355.*

Jianping Yin and Arne Stuermer, "Aerodynamic and Aeroacoustics Analysis of installed Pusher-Propeller Aircraft Configurations", *Journal of Aircraft, Vol. 49, No. 5, Sep. 2012.*

J.M. Mergin and N.J. Verona, "Propeller temperature Control Means", *Patent No. 2627927, May 29, 1947.*

Jiyuan Tu, Guan Heng Yeoh and Chaoqun Liu (2008). "Computational Fluid Dynamics: A Practical Approach", *First Edition, Elsevier,* USA.

K. V. S. Phani, et all. (2021). "Design and Analysis of Composite Propeller Blades for Aircraft". *Journal of Engineering Sciences. Vol 12, Issue 06, June/2021.*

Kwanchai Chinwicharnam and Chinnapat Thipyopas (2016). "Comparison of wing-propeller interaction in tractor and pusher configuration". *"International Journal of Micro Air Vehicles". January-March (2016): 3–20.*

Łapka, Piotr, et al. (2014), "Simplified thermo-fluid model of an engine cowling in a small airplane." Aircraft Engineering and Aerospace Technology: *An International Journal, Vol. 86. Number 3. 2014. 242-249.*

Łapka, P., M. Seredyński, and P. Furmański (2019). "Investigation of thermal interactions between the exhaust jet and airplane skin in small aircrafts." *Progress in Computational Fluid Dynamics, an International Journal 19.1 (2019): 35-43.*

Mahesh S. Mali, Vinay C A, Sanjay V. Kadam, "Numerical Analysis of Propeller Blade Temperature for Optimized Stub of Pusher Configured Turboprop Aircraft", *IJIRSET, Vol.7, Issue 4, April 2018.*

Menter, F.R (1992). "Improved Two-Equation k-ω Turbulence Models for Aerodynamic Flows", *NASA TM-103975, 1992.*

Olejnik, Aleksander, Adam Dziubiński, and ŁukaszKiszkowiak. (2021), "CFD simulation of engine nacelle cooling on pusher configuration aircraft". *Aircraft Engineering and Aerospace Technology, Vol. 93. Number 9. 2021. 1421-1429.*

Prem Kumar. PS, Dr. S. Elangovan and Bhaskar Chakravarthy (2013), "Optimizing Oil-Cooler Duct Position for a Pusher Type Turboprop Aircraft" *AIAA AVIATION Forum, Aviation Technology, Integration, and Operations Conference, Aug 2013.*

Radhakrishnan P, Cmde (Retd) Murthy Y V S and Vinay, (2013). "Ground Test Schedule for LTA Powerplant System" *CSIR-National Aerospace Laboratories,* Bangalore, India.

R. J. GoldStein, K. A. Sobolik, W. S. Seol, "Effect of Entrainment on the Heat Transfer to a Heated Circular Air Jet Impingement on a Flat Surface", *Journal of Heat Transfer, 112, 608-11, 1990.*

Ruchała and Paweł (2017). "Aerodynamic interference between pusher propeller slipstream and an airframe: literature review." *Journal of KONES 24 Vol. 24, No. 3 (2017).*

Segal, Corin. (1997), "Aircraft engine bay cooling and ventilation: design and modeling." *Journal of Aircraft, Vol. 34.1,141-144.*

Suherman Mukti1, Fadli C. Megawanto, Hari Artha (2020). "Exhaust temperature analysis of UAV propeller materials". *M.I.P.I. Vol.14, No 2, August 2020 - (93-98).*

Versteeg H K and Malasekera W (2007). "An Introduction to Computational Fluid Dynamics: The Finite Volume Method", *Second Edition, Pearson Education,* UK.

Vinay C A, G. N Kumar., et.al (2022). "Experimental and numerical investigation on the effect of turboprop engine exhaust gas impingement on pusher aircraft". *International Journal of Turbo and Jet Engines, 2022.* https://doi.org/10.1515/tjj-2022-0011.

Vinay C A and G. N Kumar (2022). "Aero-thermal investigation of thermal interactions between turboprop engine exhaust and selected parts of the airplane skin for tractor

configured aircraft". *Aircraft Engineering and Aerospace Technology.* DOI 10.1108/AEAT-03-2022-0082.

Wienczyslaw Stalewaki, "Design and Optimization of Exhaust System of Light Turboprop Airplane", J. *Kones, Jan 2016.*

Wilcox, D.C. and Alber, I.E (1993) "A Turbulence Model for High Speed Flows", *Proceedings of the 1972 Heat Transfer and Fluid Mechanics Institute, Stanford Univ. Press, Stanford, CA, 1972, pp.231- 252.y*

Wilcox, D.C (1993). "A Two-Equation Turbulence Model for Wall-bounded and Free-Shear Flows," *AIAA Paper 93-2905, Orlando, FL. 1993.*

Wilcox, D.C (1998). "Turbulence Modelling for CFD, 2nd Edition, *DCW Industries, Inc., La Canada, CA, 1998.*

Zeus Numerix Pvt Ltd (2009). "ZN Tutor-CFDTM Version 2.0", http://www.zeusnumerix.com, *IIT Bombay*, Mumbai, India.

Zhidong Wang, Meihong Zhang and Junhong Wang (2006). "A Study On Aerodynamic Design Integration of the Supercritical Wing and Rear mounted Engine Configuration", *ICAS 2006, First Aircraft Design and Research Institute*, Shanghai, China.

Zong-Hong Xie and Shi Wu, "Thermal Effect Analysis of Engine Exhaust Jet Flow on the Structures of a Carrier-based Airborne Early-Warning Aircraft", *IASEM Conference, ACEM16.*

CFD Results for Different Stub Angles

Before arriving at the final design of exhaust stubs, some post-design work was anticipated, and an adequate number of design iterations were carried out. Numerical simulations were carried out with these models, and the propeller and nacelle surface temperature were estimated. The results are shown below.

Case No.	Propeller Speed	Flap angle	Stub Angle (Both I/B & O/B)		Nacelle surface temperature (°C)		Wing lower surface temperature (°C)		Flap Temperature		Fuselage temperature (°C)	Propeller temperature (°C)	Conditions	Remarks
			I/B	O/B	I/B	O/B	I/B	O/B	I/B	O/B				
1.	1020	40°	0°	0°	70	70	70	127	102	250	50	55	Static forward idle condition	In the design process following aspects were considered: • Effect of propeller rotation on LHS & RHS was studied. • The implication of asymmetry between the inboard & outboard stubs for varying pitch up/down conditions was studied. • The effect of Flap deployment for various positions was studied. • Bevel cut of stub exit planes was studied (30°&36°) to assess the bevel angle cut effects on the exhaust exit, which is typically adopted in Acoustics studies. • These studies studied thermal effects on various surfaces, and the design target was maximum utilization of exhaust jet thrust with minimum implication on the aircraft surfaces due to exhaust temperature. • Allowable material limits for Composite is 130°C continuous operation. For Aluminium alloy 150°C.
2.	1020	40°	0°	0°	123	123	123	92	185	157	60	60	Static reverse condition (15-20% Tq)	
3.	1020	40°	0°	0°	75	75	151	105	151	105	75	79	Max reverse condition with A/C speed 40 kts (Landing)	
4.	1700	40°	0°	0°	60	92	60	157	92	254	92	67	Static max forward take-off condition	
5.	1020	40°	30° pitch down	30° pitch down	75	75	75	75	105	105	59	59	Static forward idle condition	
6.	1020	40°	30° pitch down	30° pitch down	136	136	75	75	106	106	65	65	Static reverse condition (15-20% Tq)	
7.	1700	40°	30° pitch down	30° pitch down	87	87	108	78	110	108	78	71	Static max forward take-off condition	
8.	1700	40°	30° pitch down	30° pitch down	92	92	61	61	61	123	61	70	Max forward condition with A/C speed 40 kts	
9.	1020	40°	30° pitch down	30° pitch down	77	77	77	77	77	77	107	64	Max reverse condition with A/C speed 40 kts (15-20% Tq)	
10.	1020	0°	0°	0°	75	98	75	110	75	120	75	59	Static forward idle condition	
11.	1700	0°	0°	0°	57	88	57	104	57	197	57	77	Static max forward take-off condition	
12.	1700	40°	0° (bevel stub)	0° (bevel stub)	90	90	59	59	120	214	59	67	Static max forward take-off condition	
13.	1020	40°	60° pitch Down	30° pitch down	79	79	164	74	134	102	104	57	Static forward idle condition	
14.	1700	40°	60° pitch down	30° pitch down	109	108	77	77	77	77	76	60	Static reverse condition	

LIST OF PUBLICATIONS AND CONFERENCES

International Journals:

- Vinay C A, G. N Kumar, and Giridhara Babu. Y (2022). “Experimental and numerical investigation on the effect of turboprop engine exhaust gas impingement on pusher aircraft”. *International Journal of Turbo and Jet Engines, 2022.* https://doi.org/10.1515/tjj-2022-0011. (SCI indexed, IF:0.9)

- Vinay C A and G. N Kumar (2022). “Aero-thermal investigation of thermal interactions between turboprop engine exhaust and selected parts of the airplane skin for tractor configured aircraft”. *Aircraft Engineering and Aerospace Technology.* https://doi.org/10.1108/aeat-03-2022-0082. (SCI indexed, IF:1.539)

Conference List:

- Vinay C.A., G.N. Kumar, Venkat Iyengar S and Pugazhendhi T (2022). “Aero-thermal investigation on commuter category turboprop aircraft engine nacelle”. *9th International and 49th National Conference on Fluid Mechanics and Fluid Power (FMFP-2022),* IIT-Roorkee, Springer, Paper No. FMFP2022-8170.
- Vinay C.A., G.N. Kumar and Giridhara Babu Y (2022). “Engine exhaust stub sizing for turboprop powered aircraft”. *9th International and 49th National Conference on Fluid Mechanics and Fluid Power (FMFP-2022),* IIT-Roorkee Springer, Paper No. FMFP2022-5766

CSIR-National Aerospace Laboratories
Bangalore

E-mail: vinay.ca@nal.res.in
Phone: 91-9986069565

BIODATA

Vinay C.A

EDUCATION

2013 **M.Tech-Thermal (CGPA 9.0) in Mechanical Engineering Dept., National Institute of Technology-Surathkal, Karnataka, India**

2006 **B.E (First Class with Distinction and University Rank Holder) in Mechanical Engineering University Visvesvaraya College of Engineering (UVCE), Bangalore, Karnataka. India**

WORK EXPERIENCE

Apr. 2008 - Present **Pr. Scientist at National Aerospace Laboratories (NAL), Bangalore, India**

- ***Design and development of NAL's Light Transport Aircraft:*** Aircraft Powerplant and Fuel System.

- System design, integration and testing of Aircraft Powerplant and Fuel System.
- Engine installed and uninstalled performance analysis and health monitoring. Engine vibration measurement and trend analysis.
- Formulating system qualification and flight test procedures for compliance.
- Design and selection of instrumentation for Powerplant and Fuel system.
- CFD analysis: Engine Air Intake; Nacelle; Aircraft ECS Ram Air system; Turbofan engine intake icing studies and super cooled water droplet trajectories study; pusher configured engine-propeller blade surface temperature analysis;
- Real time telemetry monitoring of ground/taxi/flight tests of NAL's Light Transport Aircraft.
- Powerplant & fuel system design, function and operating procedure trainer to test pilots and test engineers.
- Feasibility study and configuration design of Powerplant & Fuel System for Microlight Aircraft for 450 kg class.

Feb 2007 – Apr. 2008 Senior Engineer at QuEST-Rolls Royce Pvt. Ltd., Bangalore, India

- ***Externals design engineer in Technical Support & Operation***

- High bypass turbofan engine external component designs such HP/IP bleed valve support, engine mount design mods, fuel supply injector rework.

- Worked onsite in Rolls-Royce Plc, Derby, UK on component design for Trent 500 and Trent 700 engines.

Apr 2002 – Feb 2007 Technical Officer at GTRE, DRDO, Bangalore, India

- ***Design and Development of Aero Engine Gearbox.***

- Design and stress analysis of critical components of engine gearbox.

- Design, modelling and generation of manufacturing drawings of gears, oil injectors, spiral bevel gears.

- Providing conceptual and salvage schemes based on functional requirements.

- Designed gearbox assembly procedure and assembly tools and fixtures.

PUBLICATIONS

1. Vinay C.A, Kumar G N, Bhaskar Chakravarthy, Venkat Iyengar and HNV Dutt. "CFD Analysis of Turbo Prop Engine Air Intake under Icing Conditions" in proceedings of Symposium on Applied Aerodynamics and Design of Aerospace Vehicle (SAROD 2013), Vol II, PP 626-632, Hyderabad, India (2013).
2. Vinay C.A, Kumar G N, Bhaskar Chakravarthy, Venkat Iyengar and HNV Dutt. "CFD Analysis of Engine Air Intake for a Pusher Type Light Transport Aircraft" in proceedings of International Conference on Computer Aided Engineering (ICAE-2013), pp 395-401, IIT-Madras, India (2013).
3. Vinay C A, M L Shankar and Bhaskar Chakravarthy. "Aero-thermodynamic Design of Jet Pump for A Turboprop Aircraft Engine in Pusher Configuration" published in Springer as proceedings of 5th International and 41st National Conference on Fluid Mechanics and Fluid Power (FMFP-2014), FMFP-E-68, IIT-Kanpur, India (2014).
4. Vinay C A and Bhaskar Chakravarthy. "Aero-thermal Analysis of Insulation to Protect Exhaust Ducts of A Pusher Turbo Prop Engine Aircraft" published in Springer as proceedings of 5th International and 41st National Conference on Fluid Mechanics and Fluid Power (FMFP-2014), FMFP-E-403, IIT-Kanpur, India (2014).
5. Vinay C A and M L Shankar. "Environmental Control System Testing and Performance Evaluation of a Transport Aircraft" Recent Trends in Aerospace Systems Integration and Testing (ASET 2015), Proceedings 3B-1, Page 482, by AeSI, Thiruvanathapuram, IPRC (ISRO), Mahendragiri, India (2015).
6. Vinay C A, S Jayagopal and M L Shankar "Heat Transfer Analysis and Experimental Validation of Halon Bottle of Aircraft Fire Extinguishing System", Indian Society of Mechanical Engineers (ISME) 17th ISME Conference on Advances in Mechanical Engineering, ISME-D-003, Page 1, October 3-4, 2015, IIT-Delhi.

7. Wilbur G Fernandes, Vinay C A and Divijesh P "Turboprop Engine Vibration Measurement and Trend Analysis for Transport Aircraft", Indian Society of Mechanical Engineers (ISME) 17th ISME Conference on Advances in Mechanical Engineering, ISME-T-007, Page 47, October 3-4, 2015, IIT-Delhi.
8. Wilbur G Fernandes, Vinay C A and Priyadarshini L, "Aero Engine Vibration Measurement, Analysis and Trend Monitoring" Proceedings of 2nd International and 17th National Conference on Machines and Mechanisms(iNaCoMM) 2015-70, Page 18, IIT-Kanpur.
9. Vinay C A, Hrishikesh Gadage, M.L Shankar and Padmanathan P, "Numerical Study of Ram Air Intake for Heat Exchanger of Environmental Control System of Light Transport Aircraft", Proceedings of the 23rd National Heat and Mass Transfer Conference and 1st International ISHMT-ASTFE Heat and Mass Transfer Conference, IHMTC2015 17-20, LPSC-ISRO, Thiruvanathapuram.
10. Somanna Gouda P Patil, Vinay C A, Jayagopal S, & Vincent D'Souza, "Performance Analysis and Design Modification of Engine Power Control Cable Routing of Light Transport Aircraft", International Journal of Innovative Research in Science, Engineering and Technology, Volume 5, Special Issue 9, May 2016, NMAM-NITTE, Karkala, Udupi
11. Rahul Mohan.P, Vinay C A, M L Shankar, Sathish D G, Shivaprasad K V, "Environmental Control System Modeling for Configuration Selection for a Light Transport Aircraft", International Journal of Aerospace & Mechanical Engineering, Volume 3 – No.3, June 2016,
12. Abhijeet B Chougule, Vinay C A and Suresh R, "Pusher Configured Turboprop Engine Oil Cooler Ejector Performance: CFD Analysis and Validation, 6th International and 43rd National Conference on Fluid Mechanics and Fluid Power, FMFP2016-Paper No. 35, MNNITA, Allahabad, U.P., India
13. Rajashekharareddy H G, Jayagopal S, Vinay C A, Dr. Basawaraj, "Configuration Selection, Design and Computational Investigation of Cowling System for Microlight Aircraft", International Journal of Innovative Research in Science, Engineering and Technology, Vol. 6, Issue 8, August 2017.
14. Mahesh Mali, Vinay C A, Abhijeet Chougule and Sanjay Kadam, "CFD Study of Propeller Blade Temperature For Pusher Configured Turbo-Prop Engine", 5th International Conference on Computational Methods for Thermal Problems(ThermaComp-2018), IISC Bangalore.
15. Jibin T Joseph, Vinay C A, and Ravikiran Kamath, "Configuration Selection and Fuel System Design for Microlight Aircraft", INTERNATIONAL CONFERENCE ON EMERGING TRENDS IN ENGINEERING, ICETE, Paper ID 247- Special Issue of NMAMIT Annual Research Journal (2017).
16. Joyal Varghese, M L Shankar, Vinay C A, Sathish D G, Shivaprasad K V, "Aircraft Emergency Environmental Control System Modeling, Configuration Design & Analysis", International Journal of Aerospace & Mechanical Engineering (IJAME), ISSN (O): 2393-8609, Volume 3 – No.3, June 2016.
17. Abhijeet B Chougule, Vinay C A and Dr. Saleel Ismail, CFD Analysis of Oil Cooler Duct for Turboprop Aircraft Engine in Pusher Configuration", INTERNATIONAL CONFERENCE ON EMERGING TRENDS IN ENGINEERING, ICETE-2016, Page 771, DOI:10.15680/IJIRSET.2016.0505628 ISSN(Print)-2347-6710, IJIRSET, NMAM-NITTE, Karkala, Udupi.
18. Sachin Khot, Jayagopal S, Vinay C A and C S Venkatesha, "Throttle Sensitivity and Dynamic analysis of Power Control system of a Light Transport Aircraft Engine", INTERNATIONAL CONFERENCE ON EMERGING TRENDS IN ENGINEERING, ICETE-2016, Page 791, DOI:10.15680/IJIRSET.2016.0505628 ISSN(Print)-2347-6710, IJIRSET, NMAM-NITTE, Karkala, Udupi.
19. Saurabh Kalia, Vinay C A and Suresh M Hegde, " CFD analysis of turboprop engine oil cooler duct for best rate of climb condition, International Conference on Advance Materials and Manufacturing Applications (IConAMMA' 16), IOP Conf. Series: Materials Science and Engineering 41 (2016) 012001 doi:10.1088/1757-899X/130/1/012001.
20. Saurabh Kalia and Vinay C A, "Numerical Analysis of Pusher Configured Turboprop Engine Oil Cooler Duct in Flight Operation", 6th International and 43rd National Conference on Fluid Mechanics and Fluid Power (FMFP-2016), FMFP-2016 ISBN 978-93-5267-408-4, FMFP2016-Paper No. 288.

21. Vinay C A. Mahesh S. Mali, Sanjay V. Kadam, “Numerical Analysis of Propeller Blade Temperature for Optimised Stub of Pusher Configured Turboprop Aircraft”, Vol. 7, Issue 4, April 2018, Pages 8, DOI:10.15680/IJIRSET.2018.0704035.

22. Vinay C. A.and Bhaskar Chakravarthy S, “Validation of Numerical Analysis Results for Pusher Configured Turboprop Engine Air Intake”, SAROD-2018, TAAI & SAROD proceedings -2018, Paper ID 29, CP 102.

23. Vinay C. A.Mahesh S Mali and Bhaskar Chakravarthy S, “CFD Study on the Effect of Turboprop Engine Exhaust Stub Angle on Propeller Blade Surface Temperature”, 7th INTERNATIONAL and 45th NATIONAL CONFERENCE ON FLUID MECHANICS AND FLUID POWER (FMFP-2018), FMFP2017–PAPER NO.190.

24. Vinay, C. A, Et al., “Experimental and numerical investigation on the effect of turboprop engine exhaust gas impingement on pusher aircraft”, International Journal of Turbo & Jet-Engines, Online: https://www.degruyter.com/document/doi/10.1515/tjj-2022-0011/html.https://doi.org/10.1515/tjj-2022-0011.

25. Vinay, C. A, Et al., “Aero-thermal investigation of thermal interactions between turboprop engine exhaust and selected parts of the airplane skin for tractor configured aircraft”, Aircraft Engineering and Aerospace Technology (SCI Journal), Volume 95, Number 4, 2023, Pp 594-606. https://doi.org/10.1108/aeat-03-2022-0082, Sept 2022.

26. Vinay, C. A, Et al.” Aero-thermal investigation on commuter category turboprop aircraft engine nacelle” 9th International and 49th National Conference on Fluid Mechanics and Fluid Power (FMFP), Paper No. FMFP2022-8170, IIT-Roorkee.

27. Vinay, C. A, Et al., “Engine exhaust stub sizing for turboprop powered aircraft” 9th International and 49th National Conference on Fluid Mechanics and Fluid Power (FMFP), Paper No. FMFP2022-5766, IIT-Roorkee.